5-2011

PARTICLE BEAM GLOW DISCHARGE SPECTROSCOPY AS A TOOL FOR SPECIATION AND METALLOMICS ANALYSIS

Charles Quarles jr
Clemson University, dq.storm@gmail.com

PARTICLE BEAM GLOW DISCHARGE SPECTROSCOPY AS A TOOL FOR SPECIATION AND METALLOMICS ANALYSIS

A Dissertation
Presented to
the Graduate School of
Clemson University

In Partial Fulfillment
of the Requirements for the Degree
Doctor of Philosophy
Chemistry

---

by
Charles Derrick Quarles Jr
May 2011

Accepted by:
R. Kenneth Marcus, Committee Chair
Julia L. Brumaghim
Ken Christensen
George Chumanov

ABSTRACT

Metallomics is a growing field of interdisciplinary research that investigates metals in biological and environmental systems. One of the major problems in detecting metals in biological systems is the instrumentation required to analyze these complex biological samples. Typically, an inductively coupled plasma-optical emission spectrometer or –mass spectrometer (ICP – OES or – MS) is used for elemental analysis and an electrospray ionization-mass spectrometer (ESI-MS) is used for molecular information. In almost all cases, the sample introduction matrix is different for each instrument, which can affect the physiological conditions of the sample and change its properties. Particle beam/hollow cathode-optical emission spectroscopy (PB/HC-OES) and liquid chromatography-particle beam/glow discharge mass spectrometry (LC-PB/GDMS) are presented as tools for obtaining both elemental and molecular species information without changing sample preparation.

The PB/HC system was coupled to a high resolution Jobin-Yvon polychromator and optimized with respect to operational parameters using a metal mixture of Ag, Ni, and Pb to display the ability of the PB/HC-OES system as a simultaneous multiple element detector. Additionally, a commercially available Hewlett Packard 5973 gas chromatography-mass spectrometer (GC-MS) was converted to a LC-PB/GDMS capable of providing comprehensive speciation (both atomic and molecular) information.

The PB/HC-OES method is presented as a tool for determining metal binding characteristics involving Tf. Transferrin (Tf) is an iron transport protein that is essential for cellular survival, providing Fe^{3+} to cells via receptor mediated endocytosis. Transferrin is ~ 40 % Fe^{3+}-loaded, leaving roughly 60 % of Tf with free binding sites that can potentially bind other metal ions. Validation of the PB/HC-OES method for quantitative analysis was provided by comparing loading percentages of Fe^{3+} into apo-Tf with UV-VIS absorbance measurements. The PB/HC-OES method was used to determine metal loading of Ni^{2+} and Zn^{2+} into the *C*- and *N*-lobes of apo-Tf and binding of Ag^{+} to the surface methionines of Tf. The monitoring of Cr^{3+} loading into apo-Tf by PB/HC-OES and ICP-OES/UV-VIS absorbance methods are presented as further validation for the use of the PB/HC-OES method. Finally, the PB/HC-OES method was used to monitor the direct metal (Fe^{3+}, Cr^{3+}, and Ni^{2+}) competition for transferrin binding under physiological relevant concentrations.

DEDICATION

This dissertation is dedicated to my family (Summer, Ray, Harriett, Rick, and Elizabeth) and friends that supported me during my time at Clemson University.

ACKNOWLEDGMENTS

First I must thank my advisor Dr. R. Kenneth Marcus for believing in me and giving me the opportunity to be part of his research laboratory. I want to thank him for the many opportunities he has provided to me, such as attending multiple conferences and working on collaborations with GAIA Herbs and the Pacific Northwest National Laboratory. These experiences have been very valuable and helped mold my professional career.

I also need to give a very big thank you to Dr. Julia L. Brumaghim, who helped point me in the right direction when I was at my lowest point of graduate school. With her help and guidance I was able to find excitement and joy in my research. She opened the door to issues involving the field of bioinorganic chemistry which has helped me flourish in the field of metallomics.

A thank you must also go out to the Marcus Research Group, both past and present members, Christine Straut, Joy Castro, Jennifer Pittman, Manoj Randunu, Ben Manard, and Carolyn Quarles for their support, friendship, and guidance throughout my graduate degree. Additionally, I would like to thank my undergraduate advisor, Dr. Eric J. Zuckerman, for his encouragement to pursue a graduate degree. Also, I want to thank Brynna Laughlin and Brad Winn for their friendship and support during my time at Clemson University.

Financial support from the Clemson University Institute of Nutraceutical Research and GAIA Herbs is greatly appreciated.

TABLE OF CONTENTS

Page

Table of Contents (Continued) Page

LIST OF TABLES

List of Tables (Continued)

Table Page

List of Tables (Continued)

Table Page

LIST OF FIGURES

List of Figures (Continued)

Figure Page

List of Figures (Continued)

Figure Page

List of Figures (Continued)

Figure Page

List of Figures (Continued)

Figure Page

List of Figures (Continued)

Figure Page

List of Figures (Continued)

Figure Page

List of Figures (Continued)

Figure Page

CHAPTER ONE

INTRODUCTION

METALLOMICS

Understanding the role of metals in biological and environmental systems is a growing area of interest and importance to the scientific community. This is supported by the creation of the interdisciplinary journal *Metallomics*, which began in 2009. Understanding how metals interact within biological systems requires instrumentation that provides both elemental and molecular species information.[1] Typically elemental analysis is achieved using an atomic spectroscopy method such as inductively coupled plasma-optical emission spectroscopy (ICP-OES) or mass spectrometry (ICP-MS).[2] Analysis using an ICP provides quantification and identification of the metal(s) that may be present in a given system. However, ICP does not provide the ability to acquire molecular information and thus molecular detectors are required.[1] Matrix assisted laser desorption ionization (MALDI) or electrospray ionization mass spectrometry (ESI-MS) provide unique molecular information that can be used in a complementary fashion with the ICP to obtain the entire quantitative and qualitative picture of a metal containing species in a biological system.[3, 4]

One of the major drawbacks to using two separate instruments is the sample introduction requirements (i.e. organic solvents or nitric acid) that differ for each instrument. This can cause disruptions to the physiological conditions of the biological system (resulting in denaturing or loss of metal cofactor).

However, an instrument that provides both elemental and molecular species information on a single platform instrument would be of great use for Metallomics research. This dissertation describes the use of glow discharge spectroscopy as a single platform instrument capable of providing both elemental and molecular species information for metal-binding proteins that are important to the metallomics community.

GLOW DISCHARGE

Glow discharge (GD) has been used as a spectroscopic source since the early 1900's, but until the 1960's GDs were not widely used in analytical chemistry.[5] In 1967 W. Grimm presented the first known direct current (dc) GD optical emission source for solids analysis.[6] Eventually, improvements were made to the Grimm type source by Duckworth and Marcus in 1989 that utilized radio frequency (rf) power to analyze non-conductive samples, which were not possible using dc powering modes.[7] GD devices can be used for mass spectrometry or optical emission spectroscopy.[8, 9] GD devices are widely used today for the analysis of all types of samples (solid, liquid, and gas). The following sections will discuss the kinetic processes, geometries, and operational modes for glow discharge sources.

Kinetic Processes

Applying a high voltage (ranging from ~ 100 V to several kV, at currents in the mA range) across two electrodes in the presence of an inert gas causes the

breakdown of the gaseous medium, resulting in electron-ion pairs and allowing current to flow between the electrodes.[10, 11] Current flowing through a gaseous medium is considered a discharge or plasma. Figure 1.1 represents the fundamental processes taking place in a GD source. The positively and negatively charged species will flow towards the respective cathode and anode of the system. When ions with sufficient energy (>30 eV) bombard the surface of the cathode, atoms will be ejected or "sputtered" away from the surface of the cathode.[5] This process of cathodic sputtering is responsible for atomizing the sample into the negative glow where a series of potential and kinetic energy transfers take place. Helium and argon are the typical gases used for glow discharge sources due to their high metastable level energies (He 20.6 and 19.8 eV, Ar 17.7 and 11.5 eV) and ionization potentials (He 24.5 eV and Ar 15.8 eV).[12] The inelastic collisions of metastable atoms, ions, and electrons with atoms that reach the negative glow region can result in the excitation and ionization of these atoms.[5] The major mechanisms responsible for excitation and ionization are:

(Eq. 1.1) Electron Impact: $M + e^- \rightarrow M^* + e^-$
$M + e^- \rightarrow M^+ + 2e^-$

(Eq. 1.2) Penning Ionization: $M + Ar_m^* \rightarrow M^* + Ar$
$M + Ar_m^* \rightarrow M^+ + Ar + e^-$

(Eq. 1.3) Charge Exchange: $Ar^+ + M \rightarrow M^+ + Ar$

It must be made clear that these processes are dictated by kinetics, and not thermodynamics. The ions formed and photons released in the negative glow can be analyzed by mass spectrometry and optical emission spectroscopy, respectively. The rates and the extents of the fundamental kinetic processes that

take place in the plasma are governed by the operating conditions and the physical configuration of the glow discharge source.

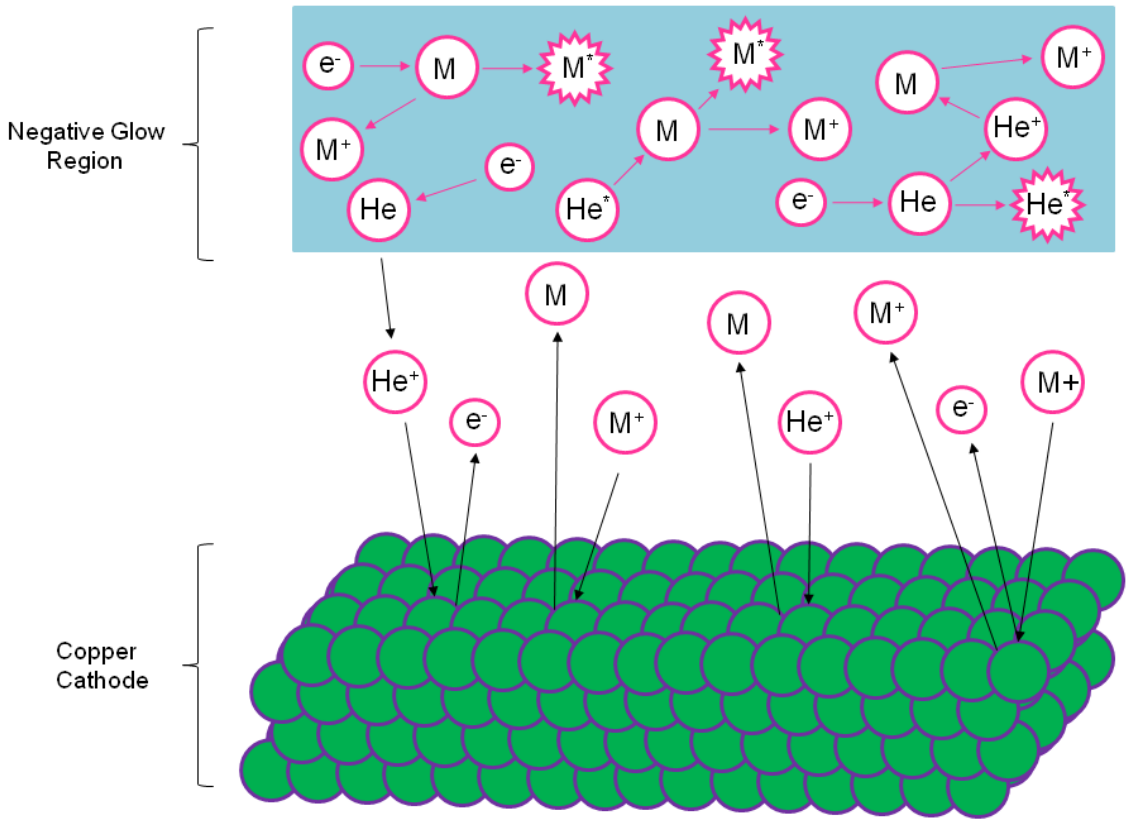

Figure 1.1 Fundamental processes occurring in a glow discharge plasma. M = sputtered neutral, He* = argon metastable, He^+ = argon ion. Note that Ar or He can be used in this process.[13]

Glow Discharge Geometries

The basic design of a glow discharge source must include an anode and a cathode (which most commonly is the analytical sample). The most important aspect with a glow discharge design is that the geometry allows for efficient sample interchange, reproducible sputtering and effective ion and/or photon

production/extraction.[14] The most common configurations found in the literature are the coaxial cathode, planar diode, Grimm-type, and hollow cathode geometries (Fig. 1.2). Typical operating conditions for the different geometries can be found in Table 1.1. The coaxial cathode (Fig. 1.2a) is the most common configuration, found principally in commercial GDMS instruments. This configuration allows for pin-like or disc shaped samples to be placed into the end of a direct insertion probe that acts as the cathode, while the source housing is the anode. The end of the samples is exposed to the discharge for sputtering and the ions are sampled through an ion exit aperture to the mass analyzer region.

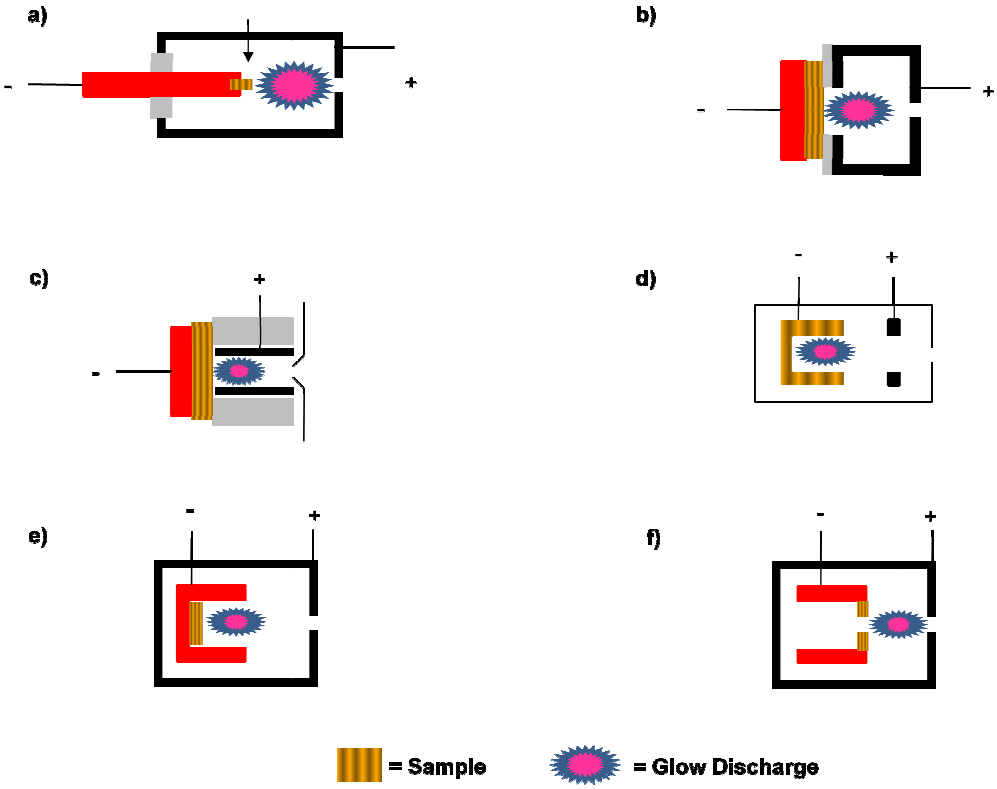

Figure 1.2 Diagrammatic representations of the various GD source configurations: **a)** coaxial cathode **b)** planar diode **c)** Grimm-type **d)** hollow cathode lamp **e)** hollow cathode **f)** hollow cathode plume.[13]

The ability to form samples into pin-like or disc shapes can be problematic in some cases. Therefore, the planar diode geometry (Fig. 1.2b) was designed to analyze large flat samples. Note, this configuration is just a variation of the coaxial cathode design. The flat sample (cathode) is placed parallel to the anode in a closed cell. The housing is made up of the anode and the cathode mount, and the ions are introduced into the mass analyzer in the same manner as in the coaxial design. This geometry allows for depth profiling of flat samples.

The next configuration of note is the Grimm-type (Fig. 1.2c), which is typically used for atomic emission spectroscopy,[15] but can be applied to mass spectrometry under the right operation conditions.[10] This configuration is similar to the planar diode, but has an additional pumping system very close to the sample that prevents redeposition of sputtered atoms. The anode is placed less than one dark space from the cathode resulting in a very stable, restricted discharge. Surface and depth-resolved analyses are possible due to the restricted glow discharge, the additional pumping system near the cathode allows for operation at higher pressures than the other geometries.

The last geometry of importance is the hollow cathode. When two cathodes are located close to each other, their discharges will coalesce into one single negative glow region.[15] This phenomenon makes the hollow cathode an attractive geometry due to the increased sensitivity which results from the increased sputtering, excitation and ionization rates in comparison to the previously mentioned configurations. The hollow cathode lamp (Fig. 1.2d) is the most common of the hollow cathode configurations; it can be used as an ion or

photon source. Typically hollow cathode lamps are used in atomic absorption spectrometry due to the ability to emit sharp and stable spectral lines.[5] There is a cylindrical hollow cathode design (Fig. 1.2e) that allows for samples to be introduced into the cavity and then atomized and excited/ionized. The last variation is the hollow cathode plume (Fig. 1.2f), which allows for the sample to be placed at the end of a cylindrical tube with a small opening put into the middle of the sample, resulting in the plasma being pushed through the orifice.[16]

Table 1.1 Typical glow discharge geometries and operating parameters.

Geometries	Detection	Operating Parameters
Coaxial cathode[14]	Ions	Up to 1000 V 1-5 mA ~ 2.0 Torr Ar
Grimm-type source[14]	Ions or photons	Up to 1500 V 1-5 mA Up to 6.0 Torr Ar
Hollow cathode[14]	Ions or photons	~400 V 10-60 mA ~2.0 Torr Ar (or He)

Glow Discharge Operational Modes

Glow discharge sources can be operated in direct current (dc), radio frequency (rf), or pulsed powering modes. The sample type, detection method, and conditions will dictate which method is used. The direct current (dc) mode is the simplest of the three operational modes. This mode creates a stable, steady state source of ions/photons, which is easily amendable to any type of analyzer.

Because the sample acts as the cathode in all of the configurations shown above, only electrically conductive samples can be analyzed using the dc mode. Detection limits for conductive samples using the dc mode are typically found to be below 1 ng g^{-1} for high resolution mass analyzers.[10]

Not being able to analyze non-conductive samples led to the use of radio frequency (rf) powering schemes, that provide the ability to directly analyze non-conductive glass, ceramic, and polymer samples. When using rf powers (13.56 MHz), no charging takes place at the sample (cathode) because of the oscillation of positive and negative charges that bombard the "cathode" which neutralize each other, so that the net charge is neutral.[17] In the 1970's, Coburn and Kay as well as Harrison and co-workers published the first work with rf-GDMS sources.[8, 9] In 1989, Marcus and Duckworth began the main exploration into the use of the rf-GDOES and MS as an analytical tool.[7] Radio frequency power supplies cost somewhat more than dc power supplies, but offer the advantage of analyzing non-conductors.[18] In addition to analyzing non-conducting samples, rf plasmas offer greater electron energies and plasma potentials compared to dc power supplies.[19] For these reasons, all commercial GDOES instruments use rf power supplies.

Another operational mode that has been drawing a good deal of interest is the pulsed power mode. It operates by applying high amounts of short-term (millisecond) power (either rf or dc) to the cathode. This pulsed mode has improved sensitivity due to the enhanced sputtering that allows for increased analyte excitation and ionization.[20] When operating a glow discharge source with

the pulsed mode, the discharge gas ions are created in the pre-peak and analyte ions are created in the post-peak.[21] Thus, with the use of a time-gated detector, it is possible to have time-resolved detection, resulting in an improved signal-to-noise ratios and greater spectral simplicity as background gas species are not observed.

LIQUID SAMPLE INTRODUCTION INTO GLOW DISCHARGE PLASMA

While glow discharges have been extensively applied to solids analysis, it has a growing appeal to be used as an ionization/excitation source for the analysis of liquid samples due to its ability to provide elemental and molecular species information when operated in an inert atmosphere. However, the introduction of liquid solvent at flow rates from 0.1 – 2.0 mL min^{-1} (typical for liquid chromatography) suppresses the plasma energetics.[22] The first efforts to analyze liquid samples by GD started with drying the solution based analyte onto the cathode, leaving a residue on the surface to be later sputtered from the surface for analysis.[5] This analysis only works for single samples and is not adaptable to on-line sampling via liquid chromatography (LC). These challenges were first accomplished by using the “moving belt” and later the “particle beam” technology to introduce and analyze liquid samples using glow discharge devices.

Moving Belt Interface

The “moving belt” works by depositing small liquid droplets onto stainless steel beads that are part of a conveyor chain, this chain then moves into a reduced pressure drying tube that heats and desolvates the sample leaving the dried analyte on the chain.[23, 24] The chain (with the dried sample residue) comes into contact with the cathode of the GD, resulting in sputtering of the residue from the stainless steel bead.[23, 24] The “moving belt” is capable of working at flow rates up to 200 µL min^{-1}, but requires plasma powers of > 25 W for stable operation and the power required is the limiting factor for maximum flow rates.[25] This is a convenient method to introduce liquid flow into a GD source, but the “moving belt” has two major flaws; memory effects and different species-specific response characteristics for multiple elements. These flaws limited the use of the “moving belt” as an interface for delivering liquid into glow discharge plasmas.

Particle Beam Interface

The limited use of the “moving belt” apparatus in LC-MS as a whole led to the exploration of new liquid sampling interface systems. In 1984 the particle beam interface, initially named the monodisperse aerosol generation interface for coupling (MAGIC) LC-MS,[26] was invented in an effort to turn liquid analyte into gas phase analytes for use with electron ionization. The advantage of this method derives from the ability to work across a wide ranges of solutions and flow rates that may be used in LC, while delivering dry analyte particles into a low pressure source.[25] The PB apparatus (Fig. 1.3) has 3 major parts: a nebulizer

that creates an aerosol spray from the liquid flow, a desolvation chamber to desolvate the droplets, and a momentum separator to remove solvent vapors and nebulizer gases. The PB interface can handle liquid flow rates up to ~ 2.0 mL min^{-1}. Marcus and co-workers have used this PB technology to introduce liquid samples into a glow discharge source coupled with an optical emission or mass spectrometer detector for a wide range of applications.[25, 27-35]

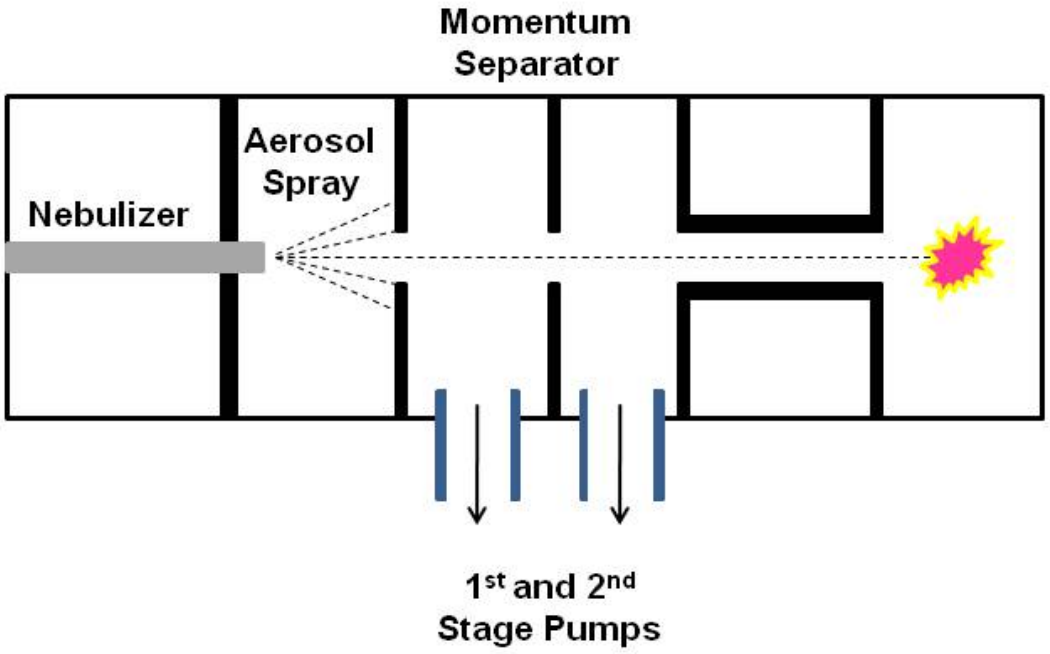

Figure 1.3 Schematic diagram of the particle beam interface

LIQUID CHROMATOGRAPHY PARTICLE BEAM GLOW DISCHARGE

Two types of PB/GD instruments are employed throughout the work presented here. The first is a particle beam/hollow cathode-optical emission spectroscopy (PB/HC-OES) system and the second is a liquid chromatography-

particle beam/glow discharge mass spectrometry (LC-PB/GDMS) system. In both cases the glow discharge source is operated in dc mode at voltages up to 1 kV and currents as high as 60 mA.

The PB apparatus used for the PB/HC-OES system consists of a thermoconcentric nebulizer, a desolvation chamber, and a two-stage momentum separator. Use of the PB enables liquid samples to be introduced as dry analyte particles into the hollow cathode glow discharge source without residual vapors that would quench the plasma energetics. Also, no spectral interferences are encountered since residual vapors are removed and operation of the source is under inert atmosphere. The optical emission spectrometer employed is a high resolution polychromator with 26 photomultiplier tubes that was once part of the JY RF-5000 system used for analyzing solids. Use of this polychromator allows for detection of multiple elements simultaneous, which is different from past experiments using the PB/HC-OES system that employed a simple monochromator. Operating the hollow cathode glow discharge source under inert atmosphere allows for detection of both non-metals (e.g. C, H, N, and O) and metals (e.g. Ag, Cr, Fe, Ni, and Zn) simultaneously. The ability to detect and quantify non-metals and metals provides the ability to calculate stoichiometric ratios across a wide range of samples. In particular the monitoring of metal-binding studies involving transferrin using the PB/HC-OES method will be discussed in great detail in the subsequent chapters.

For the LC-PB/GDMS system the PB interface utilizes a concentric nebulizer rather than thermoconcentric nebulization, with the desolvation

chamber and two-stage momentum separator similar to the PB/HC-OES system above. The mass spectrometer chamber is from a Hewlett Packard 5973 GC-MS, which had the GC removed and replaced with the PB interface. The EI source was removed and a copper cathode with a geometry similar to the direct insertion probe (coaxial cathode) was inserted. Utilizing a mass spectrometer as the detector for the glow discharge source allows for atomic and molecular species information to be obtained simultaneously using a single platform instrument. This is important since there is no available instrument that provides this type of analytical information on a single platform instrument.

SUMMARY

This chapter described the glow discharge kinetics, geometries, and operating conditions that are used for analytical chemistry. The section on glow discharge was published in *The Encyclopedia of Spectroscopy and Spectrometry*, 2nd Edition (C. D. Quarles Jr., J. Castro, R. K. Marcus, 2010, Elsevier, pp. 762-769). Chapters 2 and 3 describe the optimization of operating conditions for the PB/HC-OES and LC-PB/GDMS systems, respectively, and outline future applications. Chapter 2 involves the coupling of a high resolution JY-5000 polychromator, which allows simultaneous detection of multiple elements, as the detector for the PB/HC system and was published in the Journal of *Spectrochimica Acta Part B* (C. D. Quarles Jr., R. K. Marcus, 2009, vol. 64, pp. 1185-1193). Chapter 3 describes the conversion of a commercial HP5973 GC-MS to a LC-PB/GDMS capable of obtaining elemental and molecular species

simultaneously and was published in the Journal of *Analytical Atomic Spectroscopy* (C. D. Quarles Jr., S. Niemann, R. K. Marcus, 2010, vol. 25, pp. 1780-1786). Chapters 4 – 6 deal with applying the PB/HC-OES system as a tool for Metallomics based research with emphasis in the monitoring of metal loading into transferrin. Chapter 4 was published in *Metallomics* (C. D. Quarles Jr., J. L. Brumaghim, R. K. Marcus, 2010, vol. 2, pp 154-161) and involves the validation of the PB/HC-OES method for detecting Fe^{3+} loaded Tf with that of a common UV-VIS absorbance method, and describes the potential that the PB/HC-OES system has in monitoring other metal ions that can be loaded into Tf. Chapter 5 was published in *Metallomics* (C. D. Quarles Jr., J. L. Brumaghim, R. K. Marcus, 2010, vol. 2, pp. 792-799) and describes the comparison of the PB/HC-OES method with an ICP-OES/UV-VIS absorbance method for the monitoring of Cr^{3+} loading into apo-Tf. Chapter 6 has been submitted to the *Journal of Biological Inorganic Chemistry* (C. D. Quarles Jr., R. K. Marcus, J. L. Brumaghim, submitted January 2011) and investigates the direct competition of Fe^{3+}, Cr^{3+}, and Ni^{2+} under physiological concentrations for binding into apo-Tf.

REFERENCES

1. A. Sola-Vazquez, J. M. Costa-Fernandez, R. Pereiro and A. Sanz-Medel, *Analyst*, 2011, **136**, 246-256.

2. A. Sanz-Medel, M. Montes-Bayon and M. L. F. Saanchez, *Anal. Bioanal. Chem.*, 2003, **377**, 236-247.

3. C. N. Ferrarello, M. R. Fernandez de la Campa and A. Sanz-Medel, *Anal. Bioanal. Chem.*, 2002, **373**, 412-421.

4. J. Szupanar, *Analyst*, 2005, **130**, 442-465.

5. R. K. Marcus, *Glow discharge spectroscopies*, Plenum Press Publishing Corporation, New York, 1993, 7.

6. C. J. Belle and J. D. Johnson, *Appl. Spect.*, 1973, **27**, 118-124.

7. D. C. Duckworth and R. K. Marcus, *Anal. Chem.*, 1989, **61**, 1879-1886.

8. J. W. Coburn and E. Kay, *Appl. Phys. Lett.*, 1971, **18**, 435-438.

9. D. L. Donohue and W. W. Harrison, *Anal. Chem.*, 1975, **47**, 1528-1531.

10. N. Jakubowski, R. Dorka, E. Steers and A. Tempez, *J. Anal. At. Spectrom.*, 2007, **22**, 722-735.

11. F. L. King and W. W. Harrison, *Glow Discharge Spectrosc.*, 1993, 175-214.

12. E. Nasser, *Fundamentals of gas ionization and plasma electronics*, Wiley Interscience, New York, 1972.

13. C. D. Quarles Jr, J. Castro and R. K. Marcus, *Glow discharge mass spectrometry in The Enclyclopedia of Spectroscopy and Spectrometry*, 2nd edn., Elsevier, 2010.

14. W. W. Harrison, C. Yang and E. Oxley, *Glow Discharge Plasmas in Analytical Spectroscopy*, 2003, 71-96.

15. D. Fang and R. K. Marcus, *Glow Discharge Spectrosc.*, 1993, 17-66.

16. R. K. Marcus and W. W. Harrison, *Anal. Chem.*, 1986, **58**, 797-802.

17. A. Bogaerts and R. Gijbels, *Spectrochim. Acta Part B: Atomic Spectroscopy*, 1998, **53**, 1-42.

18. C. R. Shick, Jr., A. Raith and R. K. Marcus, *J. Anal. At. Spectrom.*, 1994, **9**, 1045-1051.

19. M. R. Winchester and R. Payling, *Spectrochim. Acta Part B*, 2004, **59**, 607-666.

20. C. Yang, K. Ingeneri and W. W. Harrison, *J. Anal. At. Spectrom.*, 1999, **14**, 693.

21. J. A. Klingler, C. M. Barshick and W. W. Harrison, *Anal. Chem.*, 1991, **63**, 2571-2576.

22. P. H. Ratliff and W. W. Harrison, *Spectrochim. Acta, Part B*, 1994, **49**, 1747-1757.

23. J. M. Brackett and T. J. Vickers, *Spectrochim. Acta Part B*, 1983, **38**, 979-985.

24. J. M. Brackett and T. J. Vickers, *Spectrochim. Acta Part B*, 1984, **39**, 837-841.

25. T. M. Brewer, J. Castro and R. K. Marcus, *Spectrochim. Acta, Part B: Atomic Spectroscopy*, 2006, **61B**, 134-149.

26. R. C. Willoughby and R. F. Browner, *Anal. Chem.*, 1984, **56**, 2626-2631.

27. T. M. Brewer, B. Fernandez and R. K. Marcus, *J. Anal. At. Spectrom.*, 2005, **20**, 924-931.

28. T. M. Brewer and R. K. Marcus, *Anal. Chem.*, 2007, **79**, 2402-2411.

29. W. C. Davis, J. L. Venzie, B. Willis, R. L. Coffee, Jr., D. P. Arya and R. K. Marcus, *Rapid Comm. Mass Spectrom.*, 2003, **17**, 1749-1758.

30. M. A. Dempster and R. K. Marcus, *J Anal. At. Spectrom.*, 2000, **15**, 43-48.

31. T. E. Gibeau and R. K. Marcus, *Anal. Chem.*, 2000, **72**, 3833-3840.

32. F. Jin and R. K. Marcus, *J. Anal. At. Spectrom.*, 2003, **18**, 589-595.

33. J. L. Venzie, W. C. Davis and R. K. Marcus, *J. Anal. At. Spectrom.*, 2004, **19**, 1309-1314.

34. J. You, M. A. Dempster and R. K. Marcus, *J. Anal. At. Spectrom.*, 1997, **12**, 807-815.

35. J. You, P. A. Depalma, Jr. and R. K. Marcus, *J. Anal. At. Spectrom.*, 1996, **11**, 483-490.

CHAPTER TWO

SIMULTANEOUS MULTIELEMENT DETECTION IN PARTICLE BEAM/HOLLOW CATHODE-OPTICAL EMISSION SPECTROSCOPY

INTRODUCTION

Metals account for less than 2% of the total body weight in the human body, but contribute to crucial roles such as structural/stabilization of compounds/proteins, binding substrates for regulation, enzyme catalysis, oxygen transport, signal transduction, and controlling redox reactions.[1-4] Current challenges are ongoing in the determination of metal content, speciation, localization, and use within organisms to give a better understanding to the factors that govern metal binding and selectivity within them.[1, 4] Unlike metals in the earth's crust, the abundance of metals in the human body is on the trace level (≤ ng mL^{-1}).[3] The ability to detect and identify trace amounts of metals within a given compound is a primary goal of metal speciation, but this only tells a small part of the story. The ability to analyze and detect not only the metal, but also to deduce the entire make-up of the compound or protein based on the total elemental composition, is the more relevant information regarding the function of the compound/protein. This laboratory refers to this type of methodology as “comprehensive speciation”.

Typically, metal speciation is performed using high-performance liquid chromatography (HPLC) or capillary electrophoresis (CE) coupled with inductively coupled plasma-optical emission or mass spectrometry (ICP-

OES/MS).[5, 6] These techniques lack the ability to detect non-metals such as carbon, hydrogen, nitrogen, and oxygen with high sensitivity due to constant backgrounds in/from the plasma,[7, 8] particularly when they are present in the chromatographic mobile phases. Common tools in proteomics, matrix assisted laser desorption ionization (MALDI) and electrospray ionization MS (ESI MS) provide fundamental information as it applies to proteins, but these techniques only give the molecular information and do not readily yield the inorganic/elemental information needed to gather a full picture of the protein–metal interaction.[9] Relative to atomic spectroscopy methods, they suffer from poor sensitivity and quantification power due to the complex matrix effects from biological samples/buffer systems. Techniques supplying both molecular and atomic information would be very powerful contributors in the field of metallomics.

This laboratory has previously developed a liquid chromatography-particle beam/hollow cathode-optical emission spectrometer (LC-PB/HC-OES) that can analyze inorganic and/or organic samples, providing empirical formulas based on element ratios (including C, H, N, O, S, and metals), with detection limits on the single ng mL^{-1} level and below.[10-13] The PB/HC-OES system combines the excitation properties of a glow discharge (GD) source with the solvent removal capabilities of the particle beam (PB) to allow dry analyte particles to reach the hollow cathode (HC) GD region.[7] Use of the PB allows work in an inert (discharge gas) atmosphere plasma, in the absence of solvent remnants, which makes it possible to detect “gaseous” elements and non-metals such as C, H, N, O, S, and P with high sensitivity. Previous experiments using monochromator

detection system include determinations of metal salts and organometallic compounds, as well as the non-metal detection of proteins and amino acids based on C and H content.[11-18] Improvements have been made by substituting the monochromator with a polychromator, allowing for simultaneous, multielement detection, thus reducing data collection times, sample sizes, and the dependence on chromatographic retention times to substantiate elemental correlations. In addition, the use of a nitrogen-purged spectrometer permits enhanced detection of many of the non-metal elements at more sensitive transitions that lie in the vacuum-UV region of the spectrum.

Presented here is the evaluation of the PB/HC-OES using the polychromator from a JY RF-5000 as the detector. This instrument was originally operated as an rf-GD-OES instrument used for solids analysis, but the commercial rf-GD source has been removed and the new HC source added in its place. Direct mounting of the PB/HC with the polychromator required changes to the source block geometry; as a result optimization of working parameters was needed. Nitrate salts (silver, lead, and nickel) were chosen for the optimization studies, because they present a range of physical, chemical and spectroscopic properties. The ability to monitor Cu (I) and Ar (I) during analysis provides insights into interesting interelement and matrix effects; effects that were not observed using the monochromator. Spectroscopic and temporal responses of the elemental constituents of different proteins are presented to demonstrate the utility of this approach in metallomics. These studies set the groundwork for using this system as a detector across the breadth of metal speciation. Chapter 2 was

published in the Journal of *Spectrochimica Acta Part B* (C. D. Quarles Jr., R. K. Marcus, 2009, vol. 64, pp. 1185-1193).

EXPERIMENTAL

Sample Preparation and Solution Delivery

High-purity (18.2 MΩ-cm) Barnstead Nanopure (Dubuque, IA) water and HPLC grade methanol (EMD Chemicals, Cincinnati, OH) were used for preparation of metal salt samples and as the mobile phase solutions. Stock solutions (1000 μg mL^{-1}) of lead nitrate, nickel nitrate, and silver nitrate (Sigma-Aldrich, St. Louis, MO) were prepared in 50% HPLC grade methanol and 50% Nanopure water and stored at room temperature in the dark. Protein solutions of hemoglobin, myoglobin, and cytochrome c (Sigma-Aldrich) were prepared in 0.1 % trifluoroacetic acid (TFA) (Fisher Scientific, Fair Lawn, NJ). A Waters (Milford, MA) model 510 high-performance liquid chromatography pump with a six-port Rheodyne 7125 (Rohnert Park, CA) injection valve using a Rheodyne 10 μL injection loop was used for delivery of sample solutions to the PB interface.

Particle Beam Interface

A Thermabeam (Extrel Corporation, Pittsburgh, PA) particle beam interface (Fig. 2.1) was used to introduce the sample into the hollow cathode glow discharge source [7]. This interface consists of a thermoconcentric nebulizer, a desolvation chamber, and a two-stage momentum separator. Liquid flow enters the nebulizer through a fused-silica capillary (100 μm i.d.) positioned inside of a metal tube that has a DC potential applied across its length. This

potential creates thermal energy that is transferred to the coaxial flow of He gas, which passes across the tip of the capillary to affect aerosol generation. This spray enters the desolvation chamber, which is wrapped with heating tape for variable temperature control, to desolvate the aerosol. The particle-containing gas stream is then introduced into a two-stage momentum separator that removes low mass gas molecules (solvent and He nebulizer gas), delivering dry analyte particles (≤ 10 μm size [19, 20]) to the HC source volume.

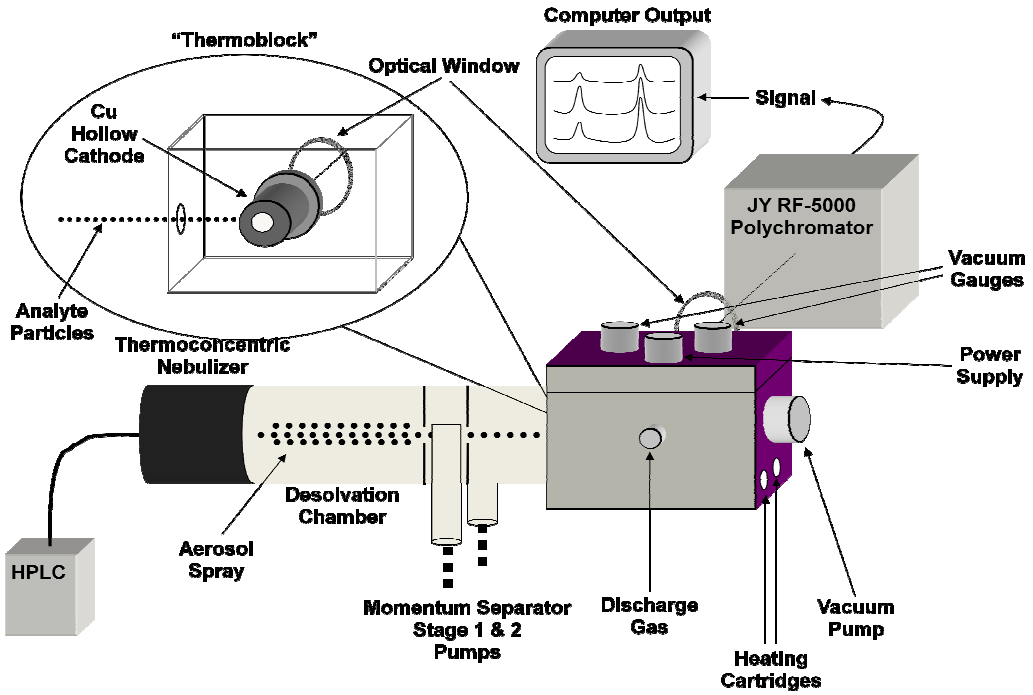

Figure 2.1 Diagrammatic representation of HPLC-PB/HC-OES system

Hollow Cathode Glow Discharge Source

The HC glow discharge design was altered slightly from the one employed in previous works [10-14, 16-19, 21, 22]. The HC was machined from bulk copper rod with an inner diameter of 3.5 mm and a length of 26.5 mm. The discharge gas

passes through the back end of the hollow, toward the optical window, passing the 3.45 mm diameter particle inlet drilled in the side of the cathode, to sweep material into the main portions of the discharge region. The HC is mounted in the center of a “thermoblock” made of stainless steel. The overall dimensions of the steel block were reduced, while keeping optical lengths the same as the old design. The new thermoblock design has a removable top for access to the HC without having to take the source completely apart. The previous design required removal of the HC through the side port having the optical lens mounted to it. In this design, that port is bolted to the instrument in proximity to the spectrometer entrance slit. The cartridge heaters (model SC 2515, Scientific Instruments, Ringoes, NJ) were relocated to the bottom of the block, yielding more uniform heating of the HC, which is required to provide sufficient energy to vaporize the introduced particles. The block temperature is monitored with a W-Re thermocouple and the gas pressure monitored with a Pirani-type vacuum gauge (VRC Model 912011, Pittsburgh, PA). Power is provided to the HC by a Bertan (Model 915-1N, Hicksville, NY) power supply that is operated in constant current mode. Helium (ultra high purity) is used as the discharge gas for the analytical studies, while Ar is used in those studies where the effects of different parameters on excitation conditions are performed.

Optical Emission Spectrometer and Data Acquisition

A JY RF-5000 (Jobin-Yvon, Division of Horiba Group, Longjumea, France) has been modified and applied as the detector for the LC-PB/HC system.

Essentially, the rf-GD source supplied with the spectrometer has been replaced with the PB/HC-OES source. The JY RF-5000 polychromator includes a 0.5-m Paschen-Runge polychromator with an ion-etched holographic grating with 2400 grooves mm^{-1}, providing a practical resolution of ~0.01 nm. The optical path is nitrogen purged to enable optical emission detection across the range of 110-620 nm. The photomultiplier tube for each of the optical channels (26 in total on this instrument) is sampled by the analog-to-digital converter at a rate of 2 kHz. The elemental transitions monitored here are: Ag (I) - 338.28 nm, Ar (I) - 404.44 nm, C (I) - 156.14 nm, Cu (I) - 327.39 nm, Fe (I) - 371.99 nm, Na (I) - 589.59 nm, Ni (I) - 341.47 nm, P (I) - 177.49 nm, Pb (I) – 220.35 nm, and S (I) - 180.73 nm. Spectrometer control and data acquisition were controlled using JY Quantum 2000 version 1.1 software on a Hewlett-Packard Vectra VE computer. Data files were then exported and processed as Microsoft Excel (Seattle, WA) files. Reported analyte responses (peak area, peak height, and peak width) are the average of 3 determinations (i.e. injections) at each set of experimental conditions.

RESULTS AND DISCUSSION

Conditions Effecting Analyte Response

The dry particle delivery to the glow discharge from solution-based samples requires efficient nebulization and desolvation of the analyte, followed by aerodynamic transport through the momentum separator. Once the dry analyte particles enter the HC, they are vaporized and atomized, with the excited

species' emission monitored via the polychromator. To obtain optimal performance, a number of parameters (liquid flow rate, nebulization temperature, desolvation temperature, thermoblock temperature, and the discharge gas pressure and current) were evaluated using injections of the multielement, nitrate salt solutions. The optimization procedure was done methodically beginning with the particle introduction aspects, moving through to the signal generation parameters. In each case, the operation parameters were studied across ranges of that produced meaningful analytical responses. Because of the desire to operate as an HPLC detector, optimization of peak area, peak height, and peak width is necessary to obtain the best analytical response while maintaining the desired chromatographic quality. Responses (peak area, height, and width) of Pb (I) 220.35 nm, Ni (I) 341.47 nm, and Ag (I) 338.28 emission intensities for 10 µL triplicate injections of a multielement solution were collected to determine optimal conditions. Fig. 2.2 represents a single 10 µL injection of the multielement salt solution (50 µg mL^{-1} Ag, 100 µg mL^{-1} Ni, and 250 µg mL^{-1} Pb) under what might be called intermediate operation conditions. The responses for each of the elements in the test mixture follow the same trends as a function of changes in sample introduction conditions, and so only the Ni (I) responses will be presented in the following discussions.

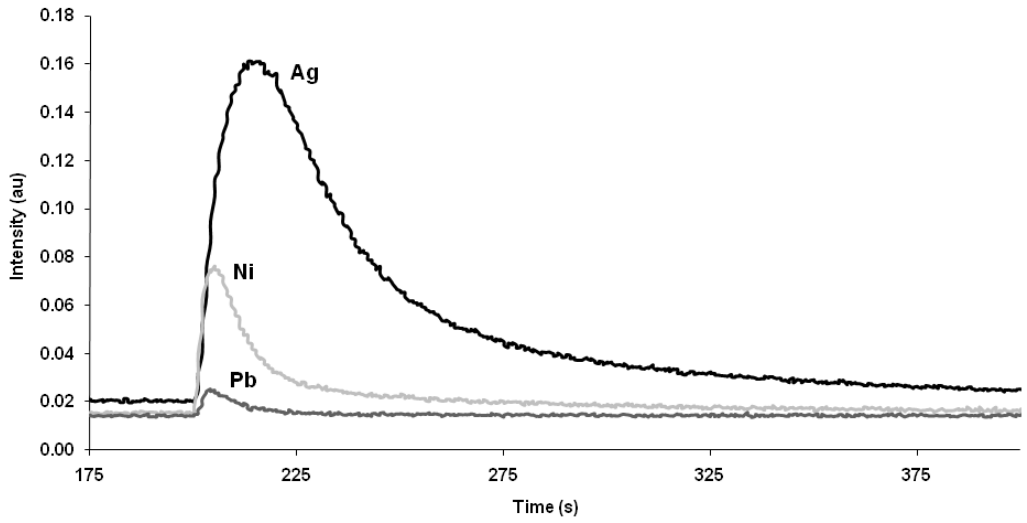

Figure 2.2 Illustration of simultaneous, multielement monitoring of a 10 μL injection containing 50, 100, and 250 μg mL^{-1} of Ag, Ni, and Pb respectively. Solvent = 50:50 water:methanol, nebulizer gas flow rate = ~1400 mL min^{-1} He, nebulizer tip temperature = 110ºC, HPLC flow rate = 0.9 mL min^{-1}, hollow cathode block temperature = 400℃, desolvation chamber temperature = 150℃, discharge current = 60 mA, discharge pressure = 2 Torr He

In order to affect efficient glow discharge excitation, only dry analyte particles should reach the HC volume (i.e. no residual solvent gets into the glow discharge). Residual vapors reaching the glow discharge compete for the fixed amount of plasma energy, effectively quenching the plasma,[23-25] while also contributing elemental and molecular spectral backgrounds. The nebulization of the solvent and analyte into a fine aerosol spray is the first of a two-part process required to produce dry analyte particles; the second being the desolvation step. There is a balance in terms of the amount of thermal energy imparted in the nebulization process (i.e., tip temperature) and the liquid load (i.e., flow rate). It is

important to remember that the data presented here reflects discrete injections of the same amount of sample; it is the bulk solution flow that changes.

As seen in Fig. 2.3a, the analyte response (peak height) of nickel passes through a maximum at ~ 0.9 mL min^{-1}, as solvent flow rate increases at a given nebulizer temperature, leveling to an intermediate response at higher flow rates. An increase in height in this case is likely the result of temporal compression of the sample plug. As expected, the peak heights increase with the nebulizer tip temperature at all flow rates, reflecting more efficient nebulization. Temperatures higher than 120 ℃ result in poor temporal stability and signal suppression due to desolvation occurring within the capillary, eventually resulting in clogging. Peak area response (Fig. 2.3b) is a better reflection of the total analyte transport (and eventual vaporization/excitation efficiency). Here, it can be seen that greater integrated intensities are achieved at higher flow rates than for peak height, though at the highest nebulizer temperatures a local maxima is seen at flow rates that were optimum for peak height measurements. These two sets of responses are interpreted as a trade-off between efficient nebulization (high temperature and low flow rates) and the higher pressure developed in the desolvation chamber at high flow rates, improving transport through the differential pumping in the momentum separator. The importance of the mixing that occurs in the high pressure (~ 0.2 atm) desolvation chamber is highlighted in the response of peak widths (FWHM) at increasing solvent flow rates (Fig. 2.3c). In the absence of mixing, fast flow rates should deliver the analyte plug in a shorter period of time, but what is seen is the opposite effect. The larger solvent/vapor volume in the

spray chamber, which occurs at high flow rates and temperatures, results in pronounced peak broadening. Ultimately, the nebulization conditions must allow for efficient vapor production (high temperature and low flow rate), with a chamber pressure (vapor loading) that yields good aerodynamic transport, without excessive mixing. Based on the overall responses of the three metals the optimal operating conditions are at 0.9 mL min^{-1} flow rate and a nebulization temperature of 110 ℃.

(a)

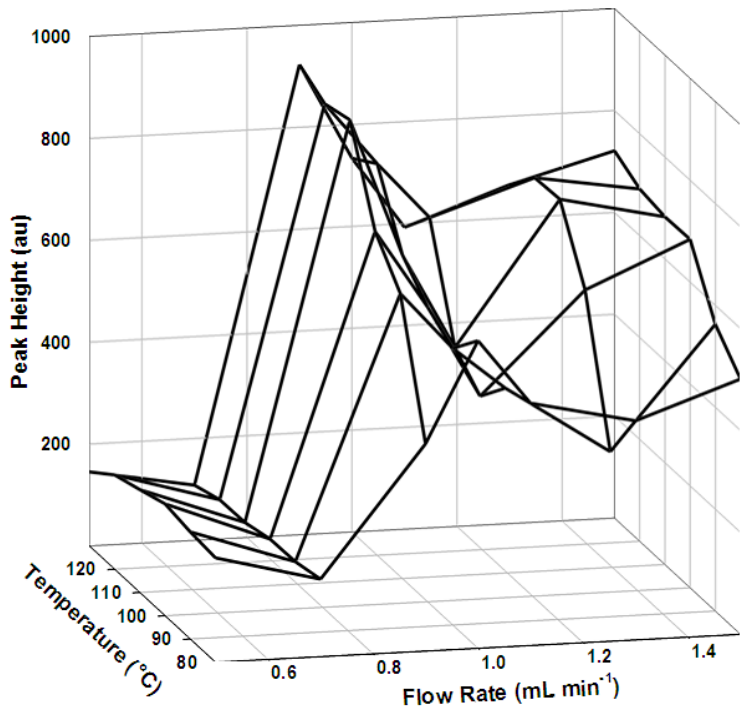

(b)

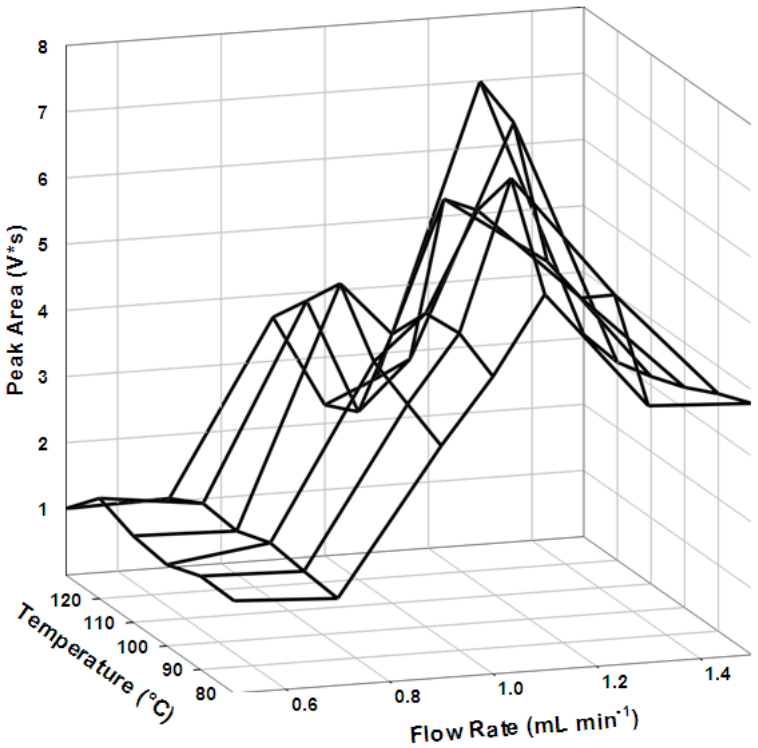
Peak Area (V*s)
8
7
6
5
4
3
2
1
Temperature (°C)
120
110
100
90
80
0.6
0.8
1.0
1.2
1.4
Flow Rate (mL min-1)

(c)

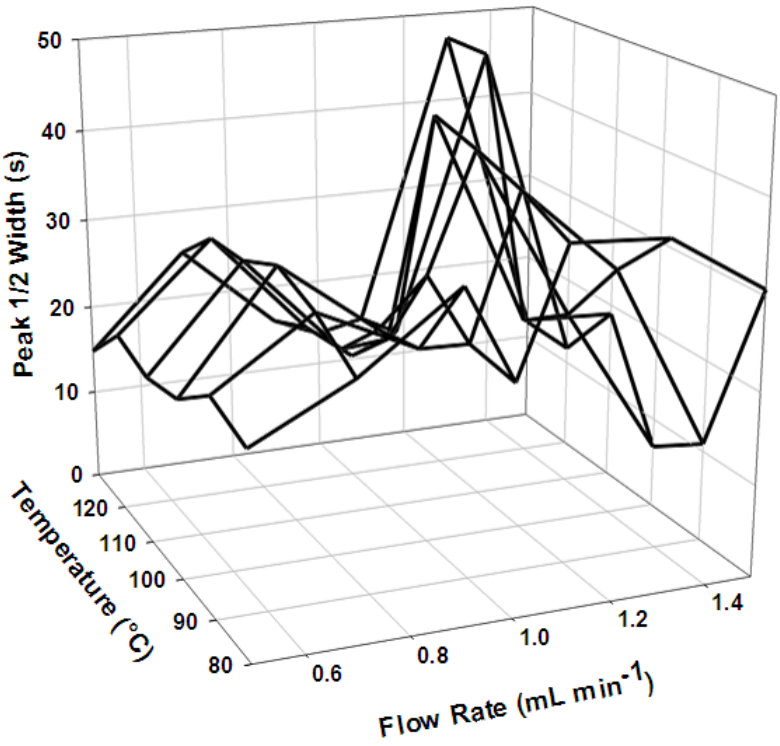
Peak 1/2 Width (s)
50
40
30
20
10
0
Temperature (°C)
120
110
100
90
80
0.6
0.8
1.0
1.2
1.4
Flow Rate (mL min-1)

Figure 2.3 Effect of nebulization conditions on Ni (I) 341.41 nm emission intensity for triplicate injections of nitrate salt solution containing 50 µg mL^{-1} of silver, 100 µg mL^{-1} of nickel, and 250 µg mL^{-1} of lead. **a)** peak height **b)** peak area **c)** peak width. Solvent = 50:50 water:methanol, injection volume = 10 µL, nebulizer gas flow rate = ~1400 mL min^{-1} He, hollow cathode block temperature = 350℃, desolvation chamber temperature = 150℃, discharge current = 60 mA, discharge pressure = 2 Torr He

The desolvation chamber is the second component involved in the process of sample introduction into the HC. An optimum temperature must be maintained to ensure that the aerosol spray is completely desolvated, allowing the analyte to be analyzed as if it was particulate matter introduced into a gas stream. Temperatures from 90–190 ℃ were evaluated. Temperatures below 90 ℃ begin to approach temperatures below the boiling point of the 50:50 water:methanol carrier solvent, causing inefficient solvent removal and condensation within the chamber. This was evident as the emission responses decrease dramatically as the desolvation temperature is below 90 ℃. At temperatures greater than 190 ℃ the emission responses also showed dramatic decreases. This may be caused by vaporization or dissociation of the salts prior to entering the momentum separator, leading to removal of analyte vapor by the momentum separator. The optimal desolvation chamber temperature for analysis was found to be 150 ℃, which was used for each of the remaining studies.

The operational parameters for the GD source (voltage/current, gas identity/pressure) must be optimized to provide proper atomization and excitation. Use of GD sources in direct solids analysis relies on sample

atomization through cathodic sputtering by discharge gas ions, followed by excitation and ionization through gas-phase collisions with electrons and metastable discharge gas atoms.[23, 26, 27] The HC source design employed here relies principally on thermal vaporization of introduced particles for atomization. As such, the principle role of the discharge gas identity is the establishment of suitable excitation conditions. Helium was chosen as the discharge gas due to its high metastable-atom levels (19.77 and 20.55 eV), and coincident higher energy electron populations that can provide energy for molecular species dissociation and excitation.[23] In the optimization of discharge parameters, and potential diagnosis of excitation condition variations, it is valuable to monitor the emission of the discharge gas species. Unfortunately, this instrument is not equipped with a He (I) detection channel, and so excitation conditions within the plasma are monitored using the Ar (I) emission channel in some of the studies that follow.

The peak height, area, and width responses of triplicate injections (10 µL, 100 µg mL^{-1} Ni, Pb, and Ag) as a function of pressure variations between 0.5 and 4.0 Torr, (1 Torr = 133.33 Pa) and current variations between 20 and 70 mA were monitored. Across the entire range of pressures, the intensity was generally proportional to current. This trend is expected because the increase in current results in more electrons within the HC, allowing for more collisions that result in optical emission responses.[23] Pressure is an important parameter because high pressures reduce mean free path and greater collision frequencies, while low pressures result in higher electron energy distributions.[28] The data show a decrease in response at the low and high pressure regions, with the maximum

response seen at 2 Torr. Beyond the observed optical responses, extremes of low currents and high pressures tended to change the plasma location, to occur outside of the geometric constraints of the primary hollow. At the optimal conditions of pressure and current, the plasma exists in the correct position within the hollow cathode, providing for the greatest analytical sensitivity and temporal stability.

In addition to the noted contributions of discharge gas pressure to emission efficiencies (affecting collision frequency and electron energy), there is one other salient aspect to the role of pressure — residence time in the plasma. Peak width increases as discharge gas pressure increases, reflecting the increased amount of collisions that are taking place within the HC. Thus, while higher pressure yields lower electron energies, the atoms remain in the plasma for a longer period of time. One additional aspect that was not anticipated, is the fact that low discharge currents lead to broader peak widths. This would certainly suggest that sputtering of particle residues may play some role in atomization under the thermal conditions in this set of studies. The optimal parameters for the discharge conditions were set at a pressure of 2.0 Torr He and a discharge current of 60 mA. Past operating conditions for the PB/HC-OES system varied from 1.0–2.0 Torr and 40–60 mA depending on the type of analyte being examined,[11, 12, 15, 29] but the general trend is the same as past experiments in this laboratory.[22]

According to Slevin and Harrison,[30] the mode of delivery of atoms from the surface to the gas phase in a HC is affected by the HC temperature. If the

temperature of the HC source is sufficiently low, cathodic sputtering is the major mechanism for atomization. When the temperature of the HC is modest (~100 ℃) both cathodic sputtering and selective vaporization of volatile compounds occur. At higher HC temperatures (> 100 ℃), thermal volatilization is the major source of atomization. It has been previously shown that vaporization from the HC walls is the primary means of generating gas-phase species in the PB/HC-OES system.[17, 19] Optimal HC temperatures have ranged from 200–300 ℃, with higher temperatures leading to pyrolysis of carbonaceous samples.[10, 11, 17, 19, 20] Given the difference in the placement of the heaters and thermocouples in the new design, it was imperative to characterize the role of "measured" temperature on the analyte responses.

In principle, changes in temperature will affect the rate of particle vaporization as well as the overall extent of the vaporization/atomization processes. Fig. 2.4 depicts the peak height, area, and width of the emission responses for Ni (I), Pb (I), and Ag (I) as a function of the measured thermoblock temperature over a range of 250–500 ℃, with a fixed current and pressure of 60 mA and 2 Torr He. Different from the other experimental parameters evaluated to this point, there are differences in the elemental responses related to the vaporization step. For example, the peak height (Fig. 2.4a) response for Ag increases as temperature increases, while the nickel and lead responses remain consistent throughout. By the same token, as the Ag (I) increases so too does its variability among the triplicate injections. These basic trends suggest that, over this temperature range, Ag vaporization is enhanced, while those of Pb

and Ni are not appreciably affected. On a first principle basis, one would consider the various melting points of the metals, though more correctly those of the compounds are relevant. Coincidently, the melting points of the metal salts increase from 56–290 ℃ from Pb to Ni nitrates, while the melting points of the metals range from 327–1455 ℃ from Pb to Ni (Ag valu es lie in between in both cases). It must be remembered that melting points are obtained for what are bulk materials at atmospheric pressure in comparison to micron-sized particles at pressures of ~10^{-3} atm, and so direct correlations are hard to make.

As mentioned above, there are kinetic and thermodynamic aspects to the role of temperature in vaporization. These two points begin to be discerned in the peak area and width responses of the three elements. The peak area (Fig. 2.4b) responses reflect the total vaporization as a function of temperature. For Ag and Pb, the response is consistent over the entire temperature range, while the Ni response increases with higher temperatures. Source block temperatures of > 400 ℃ are seen to increase the overall yield of Ni a toms in the plasma. The peak width (Fig. 2.4c) responses differentiate between the kinetic and thermodynamic aspects. The vaporization of Ag is more rapid with increasing temperatures, and so there is an increase in peak height while the area remains the same. Alternatively, more Ni is being vaporized at higher temperatures, but on a slower time scale. While Ag and Ni show appreciable thermal differences, there is virtually no effect of temperature on the Pb responses. This suggests that the temperatures employed are above any threshold values in the Pb vaporization process.

The optimum temperatures observed here are appreciably higher than previous works (~200 ℃).[10, 11, 17, 19, 20] This difference can be attributed to the source block geometry changes and the size and amount of boron nitride used in the new design of the thermoblock. The actual temperature of the HC walls is likely very comparable in the two designs, with the present measurements probably closer to reality because the thermocouple element is placed much closer to the HC. While it is easy to suggest that higher temperatures would be desirable, temperatures could not exceed 500 ℃ due to melting of the Teflon O-ring used in the top of the HC source block, causing loss of vacuum integrity. In addition, temperatures exceeding 500 ℃ would also be expected to yield a decrease in analyte response for organic species due to pyrolysis.[10, 11, 17, 19, 20] Further refinement may be required to efficiently detect inorganic and organic (metal and non-metal) species simultaneously.

(a)

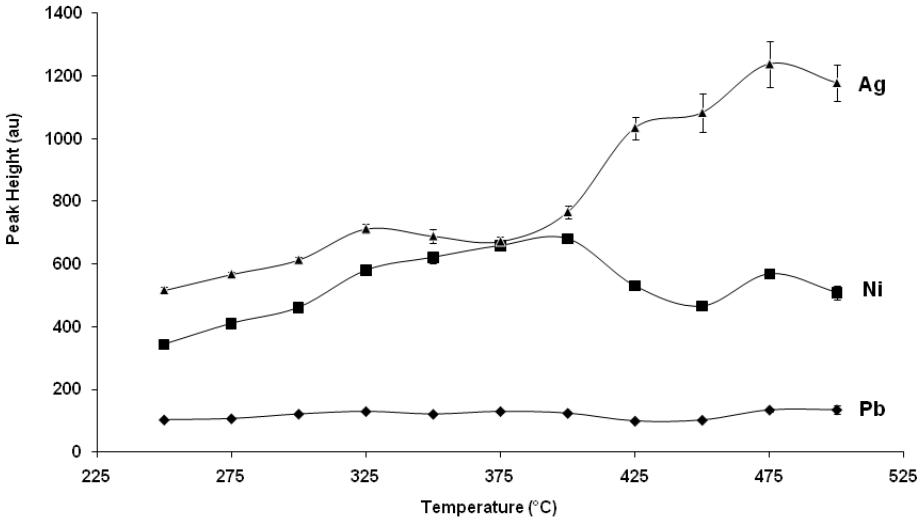

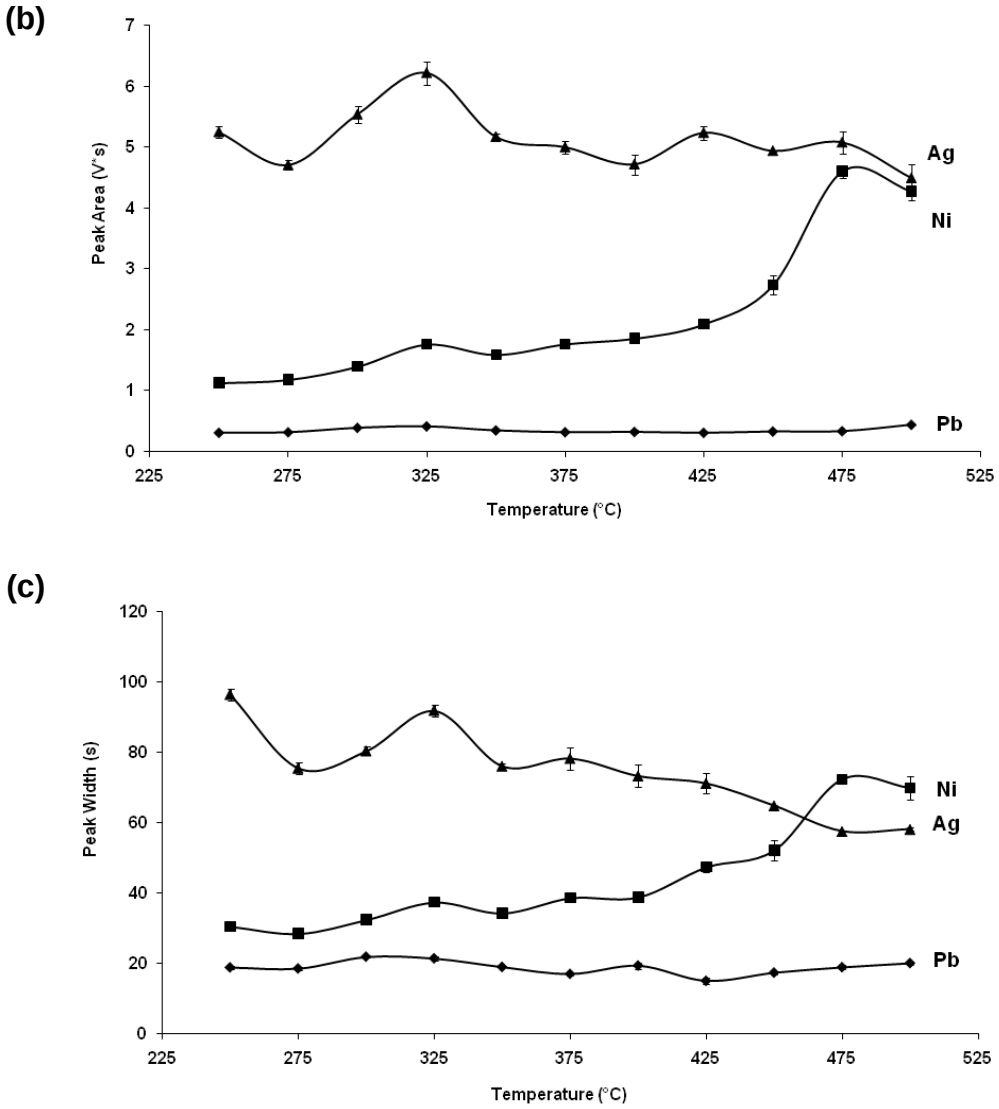

Figure 2.4 Effect of vaporization conditions on Ni (I) 341.41 nm, Pb (I) 220.35 nm, and Ag 338.28 (I) nm emission intensity for triplicate injections of nitrate salt solution containing 50 µg mL^{-1} of silver, 100 µg mL^{-1} of Ni, and 250 µg mL^{-1} of lead. a) peak height b) peak area c) peak width. Solvent = 50:50 water:methanol, injection volume = 10 µL, nebulizer gas flow rate = ~1400 mL min^{-1} He, nebulizer tip temperature = 110℃, HPLC flow rate = 0.9 mL min^{-1}, desolvation chamber temperature = 150℃, discharge current = 60 mA, discharge pressure = 2 Torr He

Characterization of Analytical Responses

Consistently, previous work with the PB/HC-OES on monochromator-based detection systems showed quite good analytical response characteristics, with detection limits in the low μg mL^{-1} to ng mL^{-1} levels,[11, 12, 21] suggesting that it would be possible to analyze biological and environmental samples on the trace element level. Of course, what is more important in speciation applications is to have such capabilities in a simultaneous, multielement mode. Analytical response curves were generated over a concentration range of 0.001 to 400 μg mL^{-1} (each) for the nitrate salt solutions using the peak area of 10 μL triplicate injections. The results of these determinations are presented in Table 2.1. Given the large range of the test solution concentrations (six orders of magnitude), these results are quite compelling. Detection limits were also determined, and are also presented in the table in units of concentration and absolute mass in the 10 μL injection volume. The LODs are in the mid-ng mL^{-1} range with absolute masses at the single-nanogram level for the nitrate salts. The concentration of LODs is somewhat higher than metals by inductively coupled plasma (ICP)-OES.[31, 32] Additionally, previous studies have shown that enhanced sensitivity can be achieved with the PB/HC-OES when using solutions with added carrier salts for example 100 μg mL^{-1} KCl.[16, 20] A comparison of the detection limits for iron using ICP-OES and the PB/HC-OES system found that LODs that were 0.9 ng mL^{-1} and 41.9 ng mL^{-1}, respectively.[14] Generally, the ICP is sampling a steady state of milliliters of sample solution while the PB/HC-OES system analyzes microliter-size samples. In terms of mass (which is of relevance in

chromatographic applications), the PB/HC-OES system is able to detect low nanograms of absolute mass introduced into the HC, whereas this has not been demonstrated with ICP-OES systems using solution nebulization methods.

Table 2.1 Elemental response function characteristics.

Salts	Response Function	Correlation (R^2)	LOD (μg mL^{-1})	Absolute Mass (ng)
$Pb(NO_3)_2$	y = 0.0071x - 0.0193	0.9878	0.216	2.16
$Ni(NO_3)_2$	y = 0.0497x - 0.027	0.9668	0.017	0.17
$AgNO_3$	y = 0.0948x - 0.3397	0.9981	0.019	0.19

Identification of Potential Interelement and Matrix Effects

The key advantage of the new polychromator system is that it allows for simultaneous multielement detection. An interesting change in emission response was noted in early evaluation of this system when the emission transient half-widths became longer when some multielement solutions were introduced into the HC or multiple injections were made in succession. This phenomenon is illustrated in Fig. 2.5, which consists of the transients for sequential single-element injections of Ag, Ni, and Pb (10 μL of 50, 100, and 250 μg mL^{-1} respectively), followed by a single injection of those elements combined (at the same concentrations). Based on the peak heights, the Ag (I) response is somewhat suppressed, while the Ni (I) is moderately enhanced. At the same time the Pb (I) response shows a smaller height with a longer, distorted transient decay. These changes suggest that the energetic conditions within the

HC plasma are being perturbed; effecting atomization rates and/or excitation conditions. These phenomena would not be readily identified when using a monochromator system.

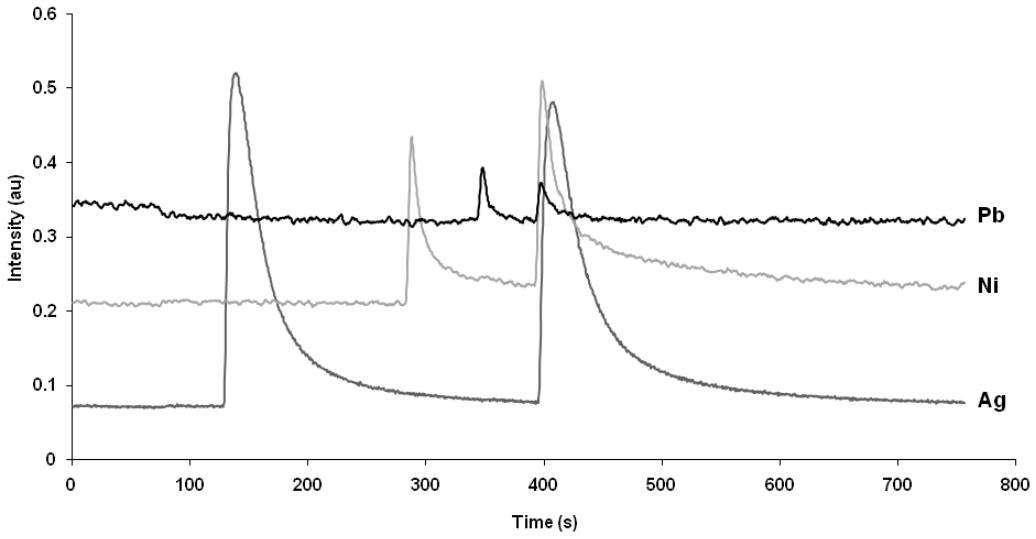

Figure 2.5 Single and multiple element injections of silver, nickel, and lead (50, 100, and 250 µg mL^{-1} respectively). Response and peak shape changes when multiple elements are present in the HC. Solvent = 50:50 water:methanol, injection volume = 10 µL, nebulizer gas flow rate = ~1400 mL min^{-1} He, nebulizer tip temperature = 110℃, HPLC flow rate = 0.9 mL min^{-1}, hollow cathode block temperature = 400℃, desolvation chamber temperature = 150℃, discharge current = 60 mA, discharge pressure = 2 Torr He

In order to evaluate these sorts of multielement interactions, optical and electrical diagnostics can be used in tandem. In addition to target analytes, key species to monitor would be the Cu (I) response as a measure of cathode sputtering, the discharge gas optical emission as a reflection of the excitation

conditions, and the discharge current/voltage to assess the electrical characteristics. Unfortunately, there is no optical channel for He (I) on this instrument to monitor excitation conditions. Alternatively, it is possible to use Ar (I) emission as a surrogate. As an extreme case, Fig. 2.6 shows the effects of a 5× (by mass) excess of Na on the 100 μg mL^{-1} injections of Ag, including the influences on sputtering and excitation conditions as monitored by the Cu (I) and Ar (I) emission lines respectively. Each of the optical channels is monitored continuously during the course of the successive triplicate injections. It is observed that when silver is solely introduced into the plasma no change or effect is seen on the Na (I), Cu (I), and Ar (I) emission channels, however, when adding Na to the solution, the response for silver decreases dramatically and suppression is seen for both Cu and Ar that occurs on the same time scale as the injection transient. Perhaps surprising is the fact that there is very little signal on the Na (I) channel (though proper operation of the channel verified), but it is known that Na is a poor emitter in GD plasmas. Sodium is an easily ionizable element that affects analyte emission signals in other spectrochemical devices.[33, 34] The ready ionization of Na is seen also as a decrease of the discharge maintenance voltage, also corresponding to the time scale of the injection transient. Thus, given the multielement capabilities it is easily deduced that there is decreased sputtering and a lowering of electron temperatures associated with the Na introduction; the GD equivalent to the common EIE effect as seen in arc discharges as well.[34]

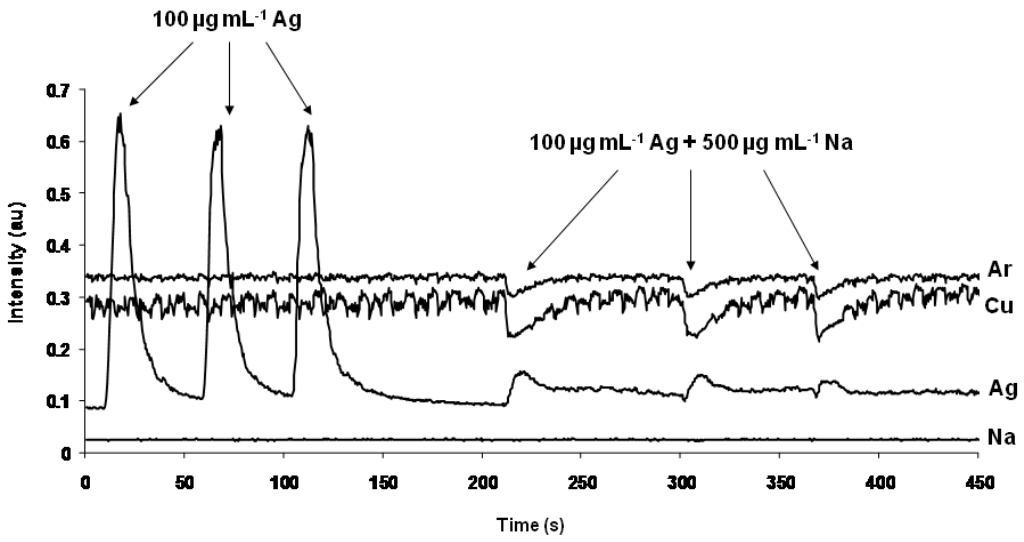

Figure 2.6 Effects of Na on Ag (I) intensities, excitation conditions, and sputtering conditions while monitoring Ar (I) 404.44 nm, Cu (I) 327.39 nm, Na (I) 589.59 nm, and Ag (I) 338.28 nm emission intensities. Solvent = 50:50 water:methanol, injection volume = 10 µL, nebulizer gas flow rate = ~1400 mL min^{-1} He, nebulizer tip temperature = 110℃, HPLC flow ra te = 0.9 mL min^{-1}, hollow cathode block temperature = 400℃, desolvati on chamber temperature = 150℃, discharge current = 60 mA, discharge pressure = 2 Torr He

Simultaneous Monitoring in Protein Determinations

Within the field of metallomics, the ability to determine metals across a vast array of chemical forms is required. As stated previously, it is not sufficient to identify that a chromatographic fraction contains a particular metal, but the precise identity of the compound must be known. The concept of determining empirical formulae based on metal and non-metal responses has been demonstrated using the PB/HC-OES system for various small organometallics

and metalloproteins.[11-14, 18] Previous PB/HC-OES work also illustrated the concept that total protein determinations can be performed based on C (I) emission, with detection limits in the single ng range .[17] In terms of using empirical formulae to identify proteins, iron-containing proteins have been determined based on Fe (I)/S (I) ratios, while also obtaining metal-content LODs on the ng level (using microliter injections).[11] These levels are in fact very competitive on a mass basis with conventional ICP-MS.

Future work on protein determinations coupled with chromatographic separations is projected to be the mainstay of the PB/HC-OES system as a tool for speciation and metallomics. Fig. 2.7 demonstrates the monitoring of simultaneous responses of C (I), Fe (I), S (I), and P (I) for 200 µL injections of protein solutions. The first two sets of peaks represent successive injections of hemoglobin while the last three pairs reflect equal mass concentrations of a mixture of hemoglobin, myoglobin, and cytochrome *c*. The ability to simultaneously observe the metals and non-metal constituents of the proteins is demonstrated, with the use of C as an analyte being unique among other OES systems. Other “gaseous elements” such as N, H, and O could also be determined but are excluded here for simplicity of presentation. Hemoglobin was chosen in this demonstration because it is a middle range molecular weight (68 kDa) protein that is rich with heteroatoms. The first set of optical transient traces (60 mg mL^{-1}) in Fig. 2.7 display double peaks, which may be related to the overloading of the HC. The 1 mg mL^{-1} injections show little more than the C (I) signal (at this scale setting), which shows a single-mode transient as

expected. The transients for the protein mixtures illustrate better the presumed mass overloading phenomenon as the total protein concentrations decrease from 15 to 3 mg mL^{-1}, becoming single-mode at the lower concentration. Also of note is the fact that each of the proteins has a different empirical formula (e.g., only hemoglobin is phosphorylated), which would be seen through the transients of each. Finally, it is interesting that the transient intensities for the C (I) emission for the 1 mg mL^{-1} hemoglobin and the 0.75 mg mL^{-1}protein mixture are nearly equivalent on this scale. This would suggest that the overall atomization and excitation efficiencies of these diverse proteins are quite similar.

It is likely that the PB and GD conditions for proteins will differ from those of the salts. One of the primary challenges in moving forward in the LC sampling is band broadening (extended tailing) of the optical transients that was not seen in the previous source design.[22] The sources of this broadening are either related to eddy currents in the gas flow within the hollow or interactions of analyte species with the cathode surface itself. These two processes will be differentiated through the use of volatile organometallic compounds introduced into the gas phase without a surface vaporization step.

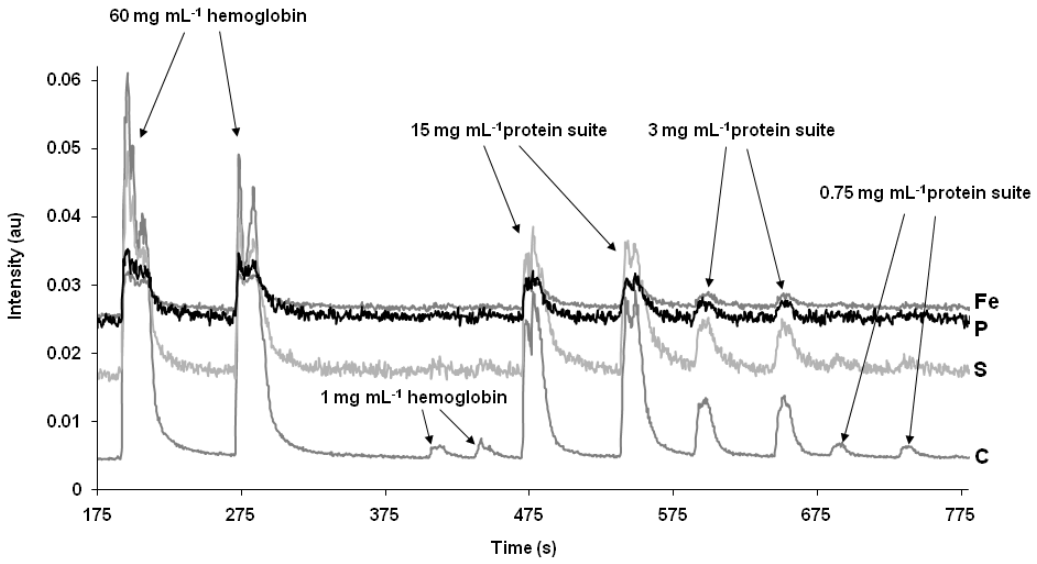

Figure 2.7 Injection of multiple protein solutions. Monitoring C (I) 156.14 nm, S (I) 180.73 nm, P (I) 177.49, and Fe (I) 371.99 nm emission intensities. Solvent = 50:50 water:methanol, injection volume = 200 µL, nebulizer gas flow rate = ~1400 mL min^{-1} He, nebulizer tip temperature = 110℃, HPLC flow rate = 0.9 mL min^{-1}, hollow cathode block temperature = 400℃, desolvation chamber temperature = 150℃, discharge current = 60 mA, discharge pressure = 2 Torr He

CONCLUSION

A JY RF-5000 high resolution polychromator has been implemented with the PB/HC-OES system in order to explore its potential as a simultaneous, multielement detector for applications in metal speciation and metallomics where liquid chromatography is typically applied for species separation. The vacuum polychromator permits the monitoring of optical transitions down to 110 nm, which is most important in the determinations of non-metals such as C, O, and S. Because of the changes in the overall source design, optimization of the

operating conditions (both in terms of the PB interface and the HC) was performed and found to be in general agreement with previous work published on the PB/HC-OES. Detection limits (very low mg mL^{-1} – ng mL^{-1}, without carriers) for nitrate salts (single-nanogram, absolute) are comparable to previous work where a monochromator was used. In addition to its analytical versatility, the multielement capabilities provide a number of interesting possibilities for plasma diagnostics. Matrix and interelement effects not previously explicitly documented within the HC are now possible. Future studies will include using the PB/HC-OES system as a species-specific detector in the general fields of metal speciation and metallomics.

REFERENCES

1. T. Dudev and C. Lim, *Acc. Chem. Res.*, 2007, **40**, 85-93.

2. C. G. Fraga, *Mol. Asp. Med.*, 2005, **26**, 235-244.

3. I. A. Kaltashov, M. Zhang, S. J. Eyles and R. R. Abzalimov, *Anal. Bioanal. Chem.*, 2006, **386**, 472-481.

4. D. J. Thiele and J. D. Gitlin, *Nature Chem. Bio.*, 2008, **4**, 145-147.
5. J. Chamoun and A. Hagege, *Radiochimica Acta*, 2005, **93**, 659-664.

6. M. B. de la Calle Guntinas, G. Bordin and A. R. Rodriguez, *Anal. Bioanal. Chem.*, 2002, **374**, 369-378.

7. T. M. Brewer, J. Castro and R. K. Marcus, *Spectrochim. Acta, Part B: At. Spectr.*, 2006, **61B**, 134-149.

8. J. Szupanar, *Analyst*, 2005, **130**, 442-465.

9. R. Lobinski, D. Schaumloffel and J. Szpunar, *Mass Spectrom. Rev.*, 2006, **25**, 255-289.

10. T. M. Brewer, B. Fernandez and R. K. Marcus, *J. Anal. At. Spectrom.*, 2005, **20**, 924-931.

11. T. M. Brewer and R. K. Marcus, *Anal. Chem.*, 2007, **79**, 2402-2411.

12. M. A. Dempster and R. K. Marcus, *J. Anal. At. Spectrom.*, 2000, **15**, 43-48.

13. F. Jin and R. K. Marcus, *J. Anal. At. Spectrom.*, 2003, **18**, 589-595.

14. T. M. Brewer and R. K. Marcus, *J. Anal. At. Spectrom.*, 2007, **22**, 1067-1075.

15. W. C. Davis, F. Jin, M. A. Dempster, J. L. Robichaud and R. K. Marcus, *J. Anal. At. Spectrom.*, 2002, **17**, 99-103.

16. F. Jin, J. J. Hickman, K. Lenghaus and R. K. Marcus, *Anal. Bioanal. Chem.*, 2004, **380**, 204-211.

17. F. Jin, K. Lenghaus, J. Hickman and R. K. Marcus, *Anal. Chem.*, 2003, **75**, 4801-4810.
18. J. You, M. A. Dempster and R. K. Marcus, *Anal. Chem.*, 1997, **69**, 3419-3426.

19. M. A. Dempster, W. C. Davis, R. K. Marcus and P. R. Cable-Dunlap, *J. Anal. At. Spectrom.*, 2001, **16**, 115-121.

20. J. You, M. A. Dempster and R. K. Marcus, *J. Anal. Atomic Spectrom.*, 1997, **12**, 807-815.

21. J. You, P. A. Depalma, Jr. and R. K. Marcus, *J. Anal. At. Spectrom.*, 1996, **11**, 483-490.

22. J. You, J. C. Fanning and R. K. Marcus, *Anal. Chem.*, 1994, **66**, 3916-3924.

23. D. Fang and R. K. Marcus, *Glow Discharge Spectrosc.*, 1993, 17-66.

24. S. K. Ohorodnik, S. Degendt, S. L. Tong and W. W. Harrison, *J. Anal. At. Spectrom.*, 1993, **8**, 859-865.

25. R. E. Valiga, D. C. Duckworth and D. H. Smith, *Rapid Commun. Mass Spectrom*, 1996, **10**, 305-310.

26. J. A. C. Broekaert, *Glow Discharge Spectrosc.*, 1993, 113-174.

27. F. L. King and W. W. Harrison, *Glow Discharge Spectrosc.*, 1993, 175-214.

28. D. Fang and R. K. Marcus, *Spectrochim. Acta, Part B: At. Spectr.*, 1990, **45B**, 1053-1074.

29. F. Jin, J. J. Hickman, K. Lenghaus and R. K. Marcus, *J. Anal. At. Spectrom.*, 2004, **19**, 1199-1205.

30. P. J. Slevin and W. W. Harrison, *Appl. Spectr. Rev.*, 1975, **10**, 201-256.

31. A. A. Alomary and S. Belhadj, *Environ. Monitor. Assess.*, 2007, **135**, 265-280.

32. C. Hang, B. Hu, Z. Jiang and N. Zhang, *Talanta*, 2007, **71**, 1239-1245.

33. C. T. J. Alkemade, T. Hollander, W. Snellman and P. J. T. Zeegers, *Metal Vapours in Flames*, Pergamon Press, Oxford, 1982.

34. P. W. J. M. Boumans, *Theory of spectrochemical excitation*, Hilger and Watts, London, 1966.

CHAPTER THREE

CONVERSION OF A COMMERCIAL GAS CHROMATOGRAPHY-MASS SPECTROMETER TO A LIQUID CHROMATOGRAPHY-PARTICLE BEAM/GLOW DISCHARGE MASS SPECTROMETER

INTRODUCTION

The lack of a single instrument available to perform comprehensive speciation for both organic and inorganic species has been a topic of discussion at many scientific meeting over the last decade. Most laboratories employ inductively coupled plasma-optical emission spectroscopy or mass spectrometry (ICP-OES or -MS) for elemental analysis and liquid chromatography-mass spectrometry (LC-MS) (*e.g.*, electrospray-MS) to obtain the molecular information.[1] Since, these are both expensive instruments that require skilled operators, a simpler, single platform instrument capable of providing both elemental and molecular information is greatly desired. While such an instrument would likely involve some compromises in ultimate performance, the range of applications that could benefit from these basic capabilities is quite large.

Glow discharges (GDs) have been employed as ionization sources for analyzing solid samples based on their excellent ability to sputter and excite/ionize the analyte.[2, 3] Ionization of analyte species in the gas phase is affected by electron and Penning-type collisions.[4] Glow discharge sources used with MS analyzers provide the ability to obtain both elemental and molecular information simultaneously when coupled with gas and liquid chromatography

(GC and LC) separations.[5-9] While gaseous introduction into a GD source is relatively straightforward, the presence of residual solvents from a liquid originating sample is deleterious to source performance.[10, 11] The ability to directly introduce liquid samples into a GD source is made possible by utilizing particle beam (PB) technology,[12] a transport-type LC-MS interface originally introduced by Willoughby and Browner.[13] This technology has been exploited by Marcus and co-workers to perform comprehensive speciation analysis of botanical extracts using both EI and GD sources.[14, 15]

Gas chromatography-mass spectrometers (GC-MS) are used in many natural products laboratories, but the types of samples that often require speciation analysis are not volatile and lack sufficient thermal stability for separation by GC.[16] Many of these same laboratories employ LC separation strategies for determinations of involatile compounds, most often using UV-Vis absorbance detection. Unfortunately, this approach is virtually useless in the case of the identification of unknowns. Conversion of a GC-MS to an LC-MS would allow for a much wider range of samples to be analyzed on a single platform, providing much needed sensitivity and qualitative powers. Such a conversion can be accomplished using the particle beam interface available from CSS Analytical Inc. (Shawnee, KS) that interfaces directly to commercial GC-MS chambers and utilizes the same EI source typical of a GC-MS instrument. The identification of medicinally active compounds in prairie plants was accomplished by LC-MS using the Genesis II (CSS Analytical) PB interface.[17] This approach provides molecular species' data, but changing the source from an EI to a GD

source would allow generation of molecular and elemental information simultaneously, within a single LC separation.

Described here is the conversion of an existing GC-MS (HP/Agilent 5973 MSD, Santa Clara, CA) into a liquid chromatography-particle beam/glow discharge mass spectrometer (LC-PB/GDMS) system. Various sample introduction and plasma parameters were evaluated using caffeine as the test compound. Analyte particle entry into the source without residual solvent vapors is critical to ion source performance, and thus the nebulization, desolvation, and momentum separator parameters were optimized as a function of flow rates (liquid and gas), desolvation temperatures, and the momentum skimmer gap distances and orifice diameters of the transfer tube. The glow discharge operation space was also evaluated. The analytical responses for caffeine injections using the original EI source were compared to the responses from the GD source. Other organic and inorganic compounds and metals were investigated to understand the instrument performance for a range of analyte types that would be encountered in the realm of comprehensive speciation analysis. Chapter 3 was published in the Journal of *Analytical Atomic Spectroscopy* (C. D. Quarles Jr., S. Niemann, R. K. Marcus, 2010, vol. 25, pp. 1780-1786).

EXPERIMENTAL

Sample Preparation and Solution Delivery

High-purity (18.2 MΩ cm) Barnstead Nanopure (Dubuque, IA) water and HPLC grade methanol (EMD Chemicals, Cincinnati, OH) were used for preparation of the samples and used as the mobile phase solutions. Stock solutions (1000 µg mL^{-1}) of caffeine, creatinine, a tetra-peptide (N-CBZ-PRO-LEU-GLY), selenium-methyl-selenocysteine, lead nitrate, and cesium chloride (Sigma-Aldrich, St Louis, MO) were prepared in 50% HPLC grade methanol and 50% Nanopure water and stored in a cold room (~5 ℃). A Waters (Milford, MA) model 510 high-performance liquid chromatography pump with a six-port Rhedoyne 7125 (Rohnert Park, CA) injection valve, using a Rheodyne 100 µL injection loop, was used for delivery of the sample solutions to the particle beam interface.

Particle Beam Interface

Fig. 3.1 is a diagrammatic representation of the components of this PB/GDMS system. A Genesis II particle beam interface (CSS Analytical Company Inc., Shawnee, KS) was used to introduce the sample into the glow discharge source volume. The interface consists of a nebulizer, a heated desolvation chamber, and a two-stage momentum separator. Fig. 3.1 displays a detailed schematic of this design. Liquid flow enters the capillary of the concentric nebulizer, with high purity helium acting as the sheath gas. The aerosol spray then enters a heated chamber equipped with variable temperature

control to affect the desolvation of these particles. The particle–vapor stream is then introduced into the two-stage momentum separator that removes low-mass gas molecules (*i.e.* solvent and helium nebulizer gas) and delivers dry analyte particles into the glow discharge source. The momentum separator design allows for adjustments to be made on the distance of the 1st and 2nd stage skimmer gaps (d_1 and d_2). The optimum distance of d_1 is dependent upon the nozzle characteristics (*e.g.*, length and aperture diameter) and since these factors were not investigated, the value remained fixed at a distance of 2.4 mm. On the other

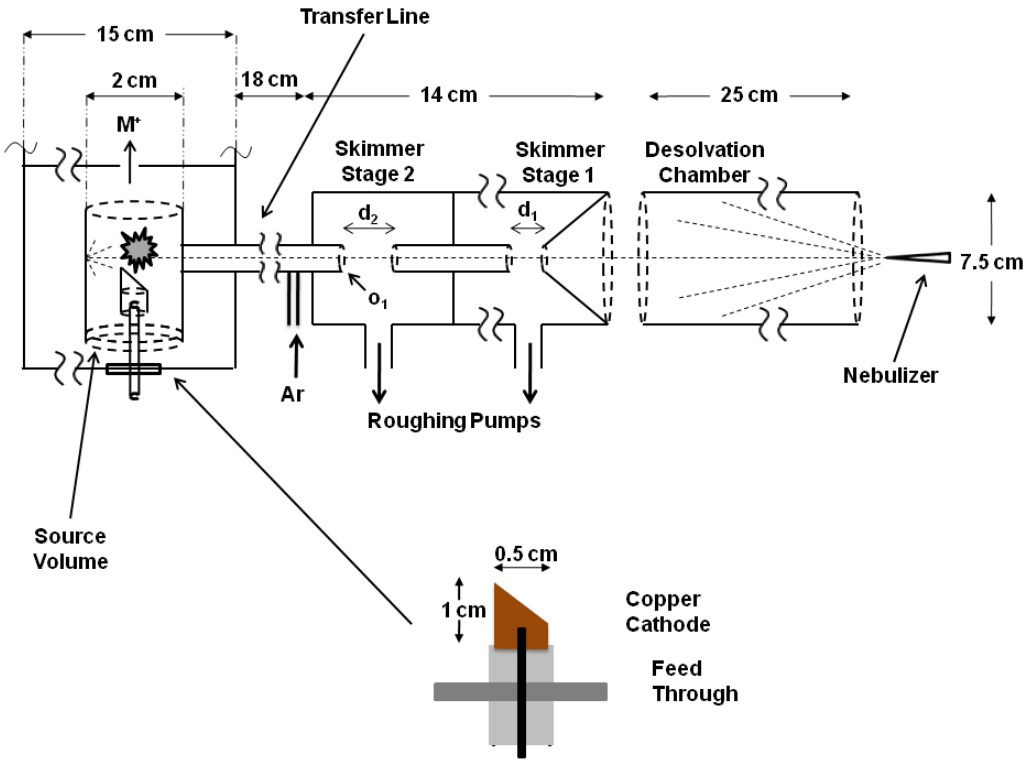

Figure 3.1 Diagrammatic representation of the components of the particle beam/glow discharge mass spectrometer system.

hand, the d_2 distance was varied over a range of 0.6–2.4 cm. Three transfer lines between the momentum separator and the ion volume were constructed, having entrance aperture diameters of 1.0, 1.5, and 2.2 mm.

Glow Discharge Source

The GD source has been designed to fit in the original EI/CI source volume of the Agilent 5973 MSD. The cathode was machined from an oxygen-free, hard copper (OFHC) rod into a cylindrical shape with a 45° angle tip at the end as depicted in Fig. 3.1.[7, 18-20] Other types of metal cathodes have been explored and copper cathodes were found to provide the best sensitivity and offer fragmentations similar to those of EI sources.[20] The cathode assembly is fixed to a standard Agilent CI source body by custom tooling. The GD source is then mounted in the standard analyzer assembly of the Agilent 5973 MSD. The cathode is affixed to the high-vacuum end of a copper feed through (Model 0020103, Insulator seal, MDC Vacuum Products, Sarasota, FL). The GD source is powered through the copper feed through which is welded into the steel plate of 6.4 mm diameter, which mounts directly on the MSD manifold. A Bertan (Model 205A-05R, Hicksville, NY) power supply operated in constant voltage mode provided the discharge power. Argon (ultra high purity) is used as the discharge gas. Heating of the GD source volume is the same as with the original CI or EI source and is controlled by the MSD software. The MSD chamber pressure and Ar pressure into the GD source volume are monitored by a Hewlett Packer (Santa Clara, CA) 5945A Gauge Controller, with the gauge mounted of the aft end of the instrument.

Mass Spectrometer and Data Acquisition

A Hewlett Packard 5973 MSD has been modified with the original GC interface being replaced with the particle beam LC-MS interface, which mounts directly to the MSD chamber. The actual conversion takes 2–4 hours. The MSD consists of a quadrupole with a high-energy dynode (HED, −10 kV) placed perpendicular to the end of the quadrupole. Directly across from the HED is the electron multiplier horn (−2224 V dc) that collects the signal and reports the information through the Agilent MSD ChemStation (version G1701DA) used for instrument operation and data collection/analysis. Microsoft Excel (Seattle, WA) was used to process the data acquired by ChemStation. Reported analyte responses (extracted ion mode) are the average of triplicate determinations (*i.e.* injections) at each set of experimental conditions.

RESULTS AND DISCUSSION

Particle Beam Parameter Optimization

Previous work done in this laboratory employed a heated nebulizer tip for solution delivery,[7, 15, 19, 21-24] but this instrument delivers an aerosol spray based solely on pneumatic nebulization. For this type of nebulization, it is key to have the correct helium pressure to provide liquid dispersion and an aerosol flow of sufficient energy (momentum) to be carried into the momentum separator. Responses of the caffeine parent ion peak ($M^{+\cdot}$ @m/z = 194 Da) over 2.5–5.0 L min^{-1} helium (50–100 psi) at a liquid flow rate of 0.7 mL min^{-1} revealed a maximum analyte response when 3.5 L min^{-1} (70 psi) of helium were supplied to

the nebulizer. Although not studied here, it is thought that as you decrease the solvent flow, that less helium would be required to affect efficient nebulization. The helium flow is important in supplying momentum for the analyte particles to efficiently reach the transfer line regardless of solvent flow rates. On the other hand, there is likely a trade-off at higher helium flow rates/pressures as greater dispersion and turbulence may occur. In addition, higher flow rates may yield smaller droplets that in turn yield small particles that are not effectively transported through the system.

The momentum separator is responsible for removing solvent and nebulizer gas, leaving only dry analyte particles to enter the GD source. The most important design parameters of a momentum separator are the distances between the skimmer orifices (d_1 and d_2), their diameters, and the diameter of the transport line aperture/orifice. A short distance would permit more solvent to enter the 2nd stage skimmer and potentially the GD source, while a long distance would remove more solvent but allow for greater analyte particle dispersion to take place, lowering efficiency. Distance d_2 was adjusted for optimal solvent removal and analyte signal based on changes of the liquid flow rate. In addition, the size of the transfer line skimmer opening (o_1) was varied from 1.0–2.2 mm diameter. Solvent removal was studied by monitoring the intensity of m/z = 18 Da (water), m/z = 32 Da (methanol), and m/z = 92 Da (background) for these experiments.

Fig. 3.2a shows that as distance d_2 is increased, less solvent (0.5 mL min^{-1}) reaches the ion volume, but at distances >1.2 cm the removal of solvent is

not significantly changed. This same study (data not shown) was repeated at a flow rate of 0.7 mL min^{-1} to see if the amount of solvent loading played an important role in solvent removal, the data although at slightly higher levels, revealed the same trends as 0.5 mL min^{-1}. Fig. 3.2b displays the response of caffeine ($M^{+\cdot}$ @m/z = 194) over distances of 0.75–2.25 cm for distance d_2. The data reveal an optimal response for d_2 found at 1.00–1.25 cm with a gradual decrease in response with increasing distances, meaning that the analyte is being pumped away by the momentum separator and not entering the GD source. At distances shorter than 1.00 cm, a substantial drop off in analyte response is seen, which is likely due to overloading of the GD source with solvent. The optimal 2nd skimmer stage gap distance d_2 was determined to be 1.15 cm and fixed to this value for the remainder of the studies.

(a)

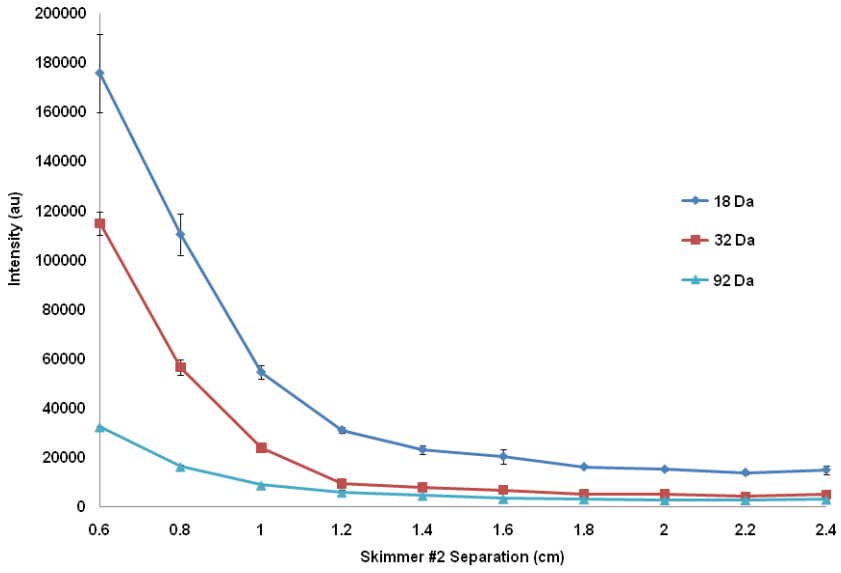

(b)

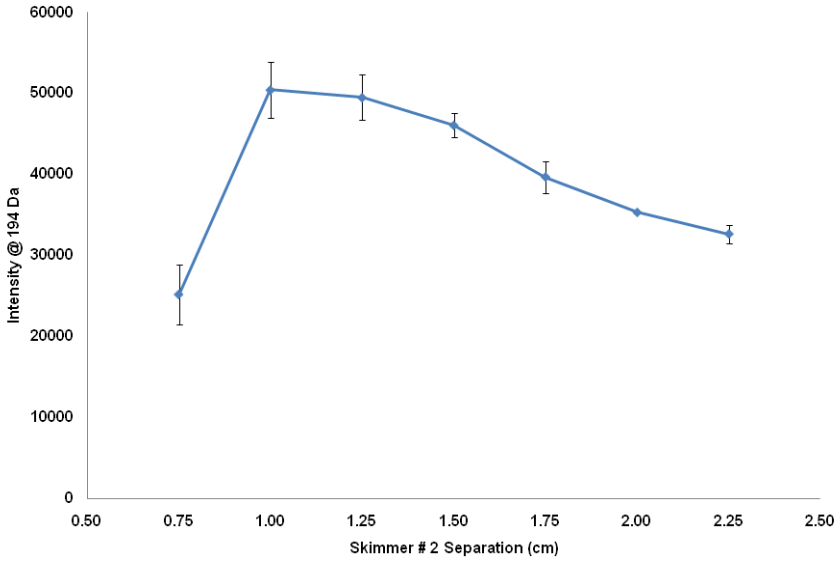

Figure 3.2 Effect of distance d_2 on **a)** solvent loading into the GD source as monitored at m/z = 18, 32, and 92 Da. **b)** the response of caffeine ($M^{+\cdot}$ @ m/z = 194). Transfer line aperture = 1.5 mm diameter, Solvent = 50:50 water:methanol, HPLC flow rate = 0.5 mL min^{-1}, nebulizer helium flow rate = 3.5 L min^{-1} (70 psi), desolvation chamber temperature = 90 ℃, discharge current = 1.0 mA, argon flow = 4.87 mL min^{-1} (MS chamber pressure = 8.5 x 10^{-4} Torr Ar), source temperature = 300 ℃.

Effects of liquid flow rate and size of the transfer line skimmer aperture/orifice diameter (1.0, 1.5, and 2.2 mm) were evaluated and optimized. Fig. 3.3a reflects the abundance of water (*m*/*z* = 18 Da) entering into the GD source for the three skimmer hole sizes over the range of 0.1–0.9 mL min^{-1} at the 1.0, 1.5, and 2.2 mm openings. Up to 0.5 mL min^{-1} only a slight increase in solvent is seen entering the source with increasing flow rates. But at >0.5 mL min^{-1} more solvent enters into the GD source that can lead to higher

backgrounds and less efficient analyte ionization. The amount of solvent getting into the source also increases with the larger transfer line orifice diameters. Interestingly the amount of solvent entering the GD source decreases at 0.9 mL min^{-1} for the smaller diameters, but an increased amount of solvent enters the GD source with the larger diameter hole. At 0.9 mL min^{-1} it is believed that turbulence is causing the decrease in solvent for the 1.0 and 1.5 mm holes. Fig. 3.3b is representative of the increased continuous background (as measured at *m*/*z* = 92 Da) seen with the increased liquid flow rate for the three aperture sizes. As seen with the data in Fig. 3.3b, an increase of background is seen at flow rates >0.5 mL min^{-1} and larger entry holes.

(a)

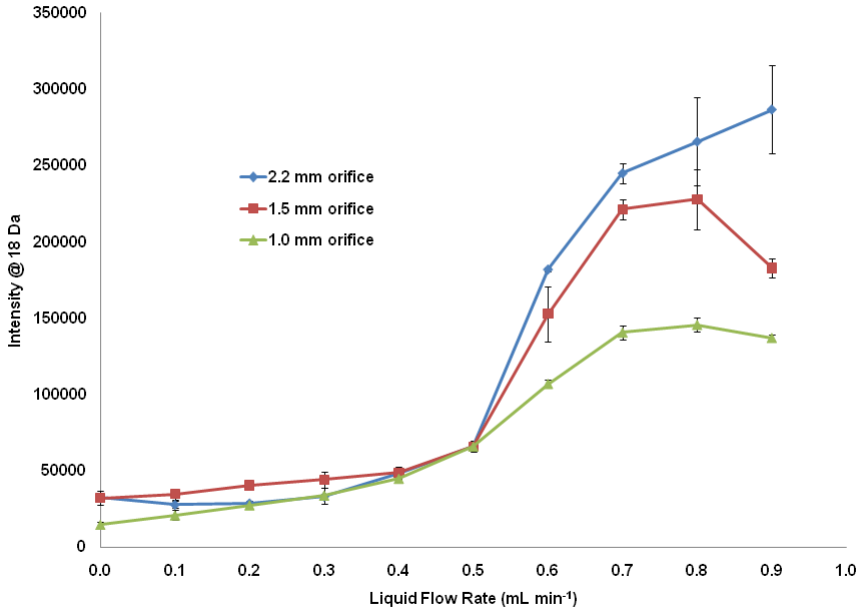

(b)

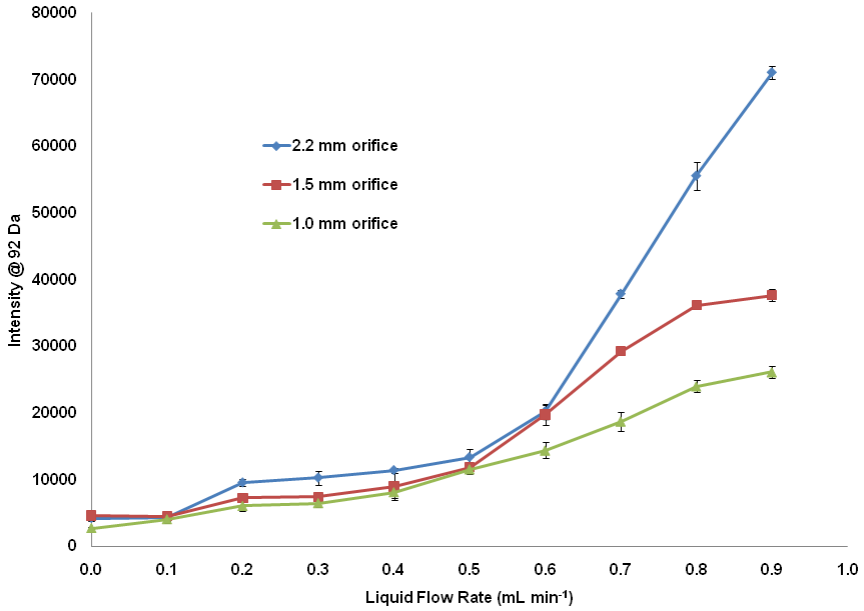

(c)

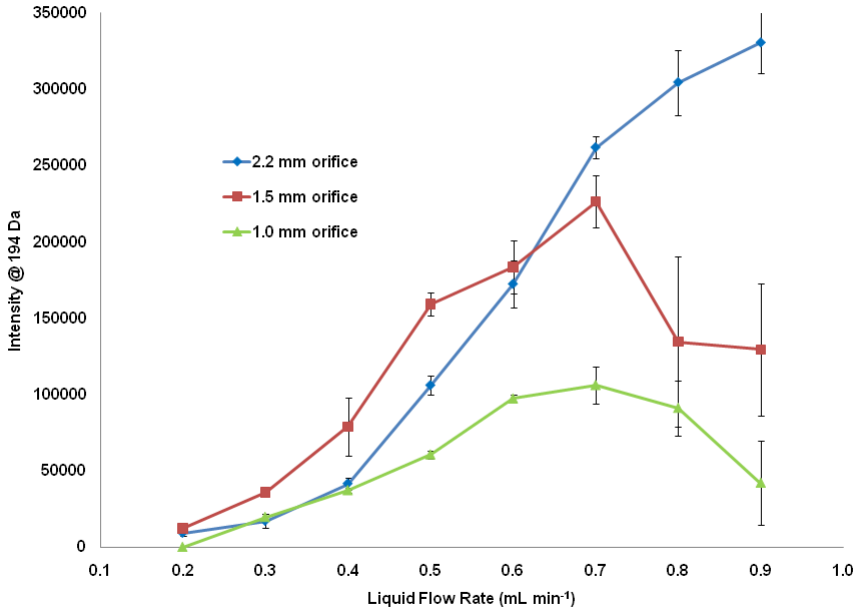

Figure 3.3 Effect of liquid flow rate and transfer line orifice sizes on **a)** solvent loading as monitored at m/z = 18 Da (water) and **b)** m/z = 92 Da (background), and **c)** analyte response of 100 µL triplicate injections of 250 µg mL^{-1} caffeine ($M^{+\cdot}$ @ m/z = 194). Solvent = 50:50

water:methanol, nebulizer helium flow rate = 3.5 L min^{-1} (70 psi), desolvation chamber temperature = 90 ℃, discharge current = 1.0 mA, argon flow = 4.87 mL min^{-1} (MS chamber pressure = 8.5 x 10^{-4} Torr Ar), source temperature = 300 ℃.

In order to determine if the additional solvent entering the GD source affects analyte response, caffeine injections for flow rates of 0.2 to 0.9 mL min^{-1} for each sizes of the transfer line orifice are seen in Fig. 3.3c. The response shows that, for the 1.0 and 1.5 mm openings the optimal signal occurs at 0.7 mL min^{-1}. A substantial decrease in response is seen at flow rates of ≥0.8 mL min^{-1}, this is due to clogging of the entry holes that was evident with the buildup of caffeine at the entry of the transfer line. The largest diameter skimmer hole did not have the same rollover of response and there was no clogging, but an increase in error for the higher flow rates is most likely the result of caffeine sticking to the walls in the transfer line to the GD source. Based on the obtained signal-to-background ratio of the parent ion peak and the adjacent spectral regions, it was determined that the optimal liquid flow rate is 0.7 mL min^{-1} and the optimal transfer line aperture diameter is 2.2 mm.

To ensure that dry particles are entering the GD source, the desolvation chamber temperature must be optimized to allow for the proper amount of energy to desolvate the analyte particles. The response of caffeine ($M^{+\cdot}$ @m/z = 194) over a temperature range of 50–120 ℃ for the desolvation chamber revealed a maximum response is found when the temperature is 60–80 ℃. At temperatures ≥90 ℃, a significant decrease in analyte response is noticed which is most likely

due to higher nebulization efficiency leading to smaller droplets/dry particles which are more susceptible to being skimmed away by the momentum separator.[25] Below 50 ℃ there is a large variation in responses, most likely due to insufficient solvent removal which affects the ionization of the analyte within the glow discharge plasma. Low temperatures will also allow for condensation within the chamber and sticking of particles along the walls of the transfer line leading into the GD source. For the remainder of the studies 80 ℃ was used as the desolvation chamber temperature.

Glow Discharge Source Parameter Optimization

For GD sources, particles have to enter the source volume, and be vaporized to put analyte species in the gas phase for excitation/ionization and subsequent detection.[6, 19, 26] This process can occur by either sputtering off of the cathode surface or vaporization from the heated walls of the source volume. With previous PB/GDMS work, it was thought that the particles were required to hit the cathode,[12] and so this source was designed with this in mind. The analyte response of caffeine ($M^{+\cdot}$ @ m/z = 194) monitored as GD source temperatures were increased from 200–300 ℃ showed a steady increase of ~2.5x, leveling somewhat above 280 ℃. The source volume temperature dependence suggests that vaporization of the particles off of the ion volume walls is the operable mechanism for getting analyte species into the gas phase. Visual inspection indicated that the particles indeed were not hitting the cathode surface. Extension of the cathode height to affect this process resulted in unstable plasma operation.

In fact the same analyte response was seen with or without the particles hitting the cathode. The optimal temperature is found at 300 ℃, however, this is the preset maximum temperature of the present system, therefore 290 ℃ was used for the remainder of these studies.

Optimization of the operating conditions for the GD plasma is important when trying to obtain proper mass fragmentation patterns and efficient ionization.[7] There are two parameters that can be controlled with this GD source; the amount of argon gas entering the source (*i.e.*, discharge pressure) and the amount of voltage applied to the cathode (affecting the resultant current).[4] For GD sources, there is an optimal balance of pressure and current parameters.[27] Whether the primary ionization mechanism is Penning ionization (where argon metastables are created through electron collisions) or electron ionization, increases in discharge current should yield greater numbers of ions. In principle, the discharge can be operated at argon flow rates of 3.5–7.0 mL min^{-1}, equating to pressures of 6–10 × 10^{-4} Torr as measured in the mass analyzer chamber, though there is instability at both pressure extremes. The response of caffeine ($M^{+\cdot}$ @*m*/*z* = 194) was monitored over a current range of 0.5–2.5 mA, and argon flow rates of 4.15–6.0 mL min^{-1}. As seen with previous work of Gibeau and Marcus, the optimal signals were found at 2.0 mA, with charring of the cathode seen at currents above 2.0 mA.[7] Although not shown here, there is also an increase in variability seen for the higher current responses. These observations suggest some amount of pyrolysis at the cathode surface as it heats due to the sputtering process. Very importantly, the fragmentation patterns for caffeine test

molecule remained constant over all of the currents, implying that the energetics of the plasma (*i.e.*, ionization processes) remained constant. Based on these results, the optimal current to operate the plasma is 2.0 mA.

As described above, the role of discharge pressure on plasma ionization processes is more complicated than for current. Pressure (in concert with current) also effects the geometric distribution of the plasma within the ion volume. In practice, the maximum ion density is located on the negative glow side of this interface,[28, 29] and so this is where optimum analyte ion sampling occurs. While not shown for the sake of brevity, the interplay between pressure and current and the analyte signal responses were observed with the present system. This same relationship was seen by Krishna and Marcus for a variety of cathode material, discharge parameters, and analyte identities.[20] Based on these results, the plasma conditions remained fixed at a current of 2.0 mA and an Ar flow rate of 4.5 mL min^{-1} for the remainder of the studies.

Analytical characteristics

In order to set a preliminary benchmark of the capabilities of this instrument, comparisons were carried out first using the original EI source of the MSD instrument and the new GD source using the same PB interface. Caffeine response functions were determined for both sources. The GD source conditions found to be optimal in the previous sections were used. The EI source was operated at 70 eV using an established method provided by CSS Analytical to ensure that there was no bias. Table 3.1 presents the results from the two

sources; with the GD and the EI sources yielding very comparable performance. The quantification data were determined by analyzing the response over a range of 0.001–150 μg mL^{-1} of caffeine using the peak areas (background subtracted) in the extracted single ion monitoring (SIM) mode for *m*/*z* = 194 Da. The determined limits of detection (LODs) of 34 and 15 ng mL^{-1} caffeine for the EI and GD sources, respectively, are in good agreement with those previously found in this laboratory.[7, 20] The obtained LODs equate to single nanogram, absolute mass detection for 100 μL injections, which is on par with other LC-PB/MS results.[20] One key aspect of the calibration functions is the very large detector background that must be subtracted in the case of the GD source (reflected in the negative *y*-intercept). This background is due to the relatively high pressure in the analyzer region of the instrument upon introduction of the discharge gas. This problem will be eliminated with the use of either a larger turbomolecular pump or a smaller ion exit orifice. The reported variability (%RSD) values are cumulative over the entire calibration range, and so it is seen that the system is quite stable. Fig. 3.4a and b show the mass spectra of caffeine obtained from the EI and GD sources. A noticeable difference is that the EI spectrum has more fragmentation than the GD source, which is expected since the GD plasma is considered a softer ionization source than EI. Both spectra are consistent with the caffeine spectrum published in the National Institute of Standards and Technology (NIST) WebBook in terms of the fragment ion species and parent mass ion peak.[30]

Table 3.1 Comparison of response functions for the EI and GD sources. 100 µL injection loop. LOD = (3 * σ_{blank})/m

	Response Function	Correlation (R^2)	LOD (ng mL^{-1})	Absolute Mass (ng)	% RSD
EI	y = 2E+06x + 1E+08	0.9933	34	3.4	5.4
GD	y = 263284x - 2E+07	0.9910	15	1.5	8.6

(a)

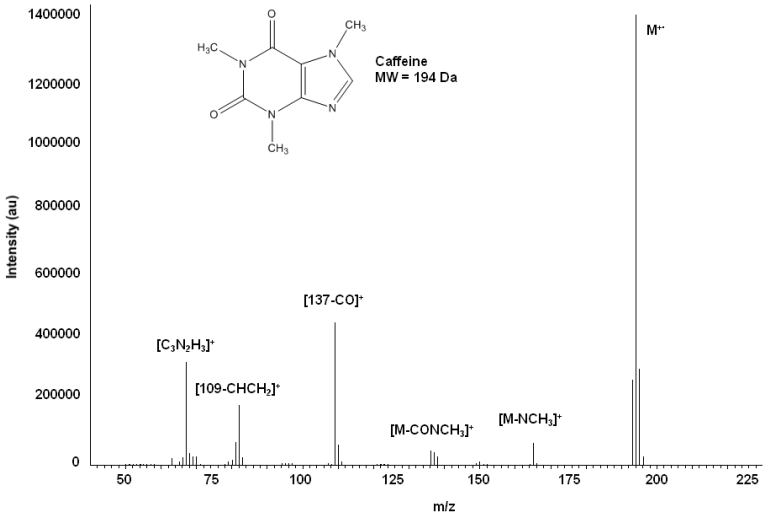

(b)

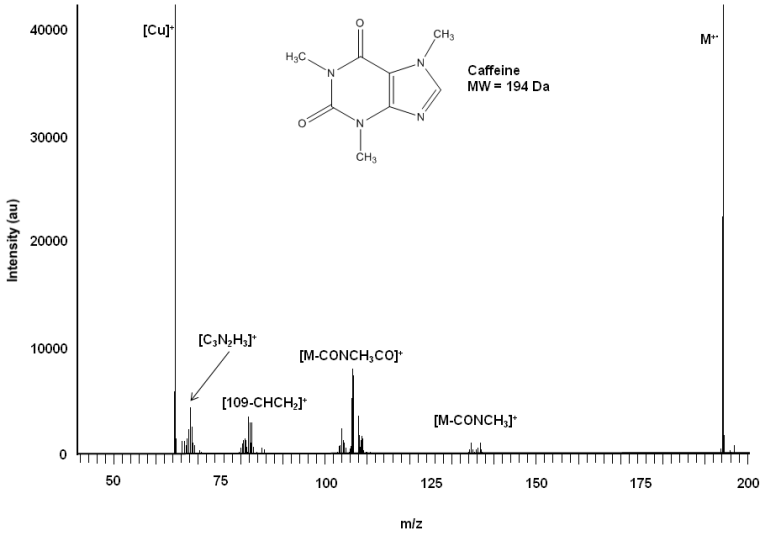

Figure 3.4 **a)** EI mass spectrum of 100 µL injection of 250 µg mL^{-1} caffeine. Conditions based on CCS Analytical Particle Beam method, nebulizer helium flow rate = 1.5 L min^{-1} (helium tank pressure = 30 psi), liquid flow rate = 0.3 mL min^{-1}, desolvation chamber temperature = 80 ℃, source temperature = 200 ℃. **b)** GD mass spectrum of 100 µL injection of 250 µg mL^{-1} caffeine. Solvent = 50:50 water:methanol, nebulizer helium flow rate = 3.5 L min^{-1} (70 psi), liquid flow rate = 0.7 mL min^{-1}, desolvation chamber temperature = 80 ℃, source temperature = 290 ℃, discharge current = 2.0 mA, argon flow = 4.5 mL min^{-1} (MS chamber pressure = 8.0 x 10^{-4} Torr Ar).

The overall goal of this project is to be able to use this instrument with LC separations as a detector for comprehensive speciation analysis, *i.e.* the capacity for determining both organic and inorganic species simultaneously. As a single example, Fig. 3.5 is a GD spectrum of 1000 µg mL^{-1} selenium-methyl-selenocysteine. As can be seen, the spectrum contains information-rich fragments, the Se isotope pattern, and a signal for the molecular ion (*m*/*z* = 182 Da). This is consistent across previous PB/GDMS studies from this laboratory, where fragmentation patterns very similar to those that would be expected from EI sources are obtained.[6, 7, 21] The mass spectra for creatinine and a tetrapeptide test compounds also showed predictable fragmentation patterns. Additionally, the GD mass spectra for metal salts are very simple, containing the isotopic pattern for the metal along with the argon discharge gas species, and a small contribution from the cathode material (Cu here). Table 3.2 represents the LODs for organic and inorganic compounds for this PB/GDMS instrument based on 100 µL injections over a range of 0.001–250 µg mL^{-1} for each of the analytes. The

LODs for the organic compounds are about an order of magnitude above what has been achieved on our laboratory-built instrument; which are typically on the sub-nanogram level.[15, 21] This may be due to the smaller quadrupoles that come equipped in the HP 5973 as well as the high backing pressures as described above. As for the elemental species, Cs and Pb, the detection limits are 2.4 and 250 ng mL^{-1} respectively. The cesium LOD is comparable with previous results in our laboratory,[7, 12, 20] but the Pb value is 2 orders of magnitude higher than those works where the characteristics for Cs and Pb were very similar. These LODs are indeed higher than those of ICP-MS and ESI-MS, but are low enough to detect the harmful concentrations of heavy metals that may be present in dietary

Table 3.2 Response functions for the LC-PB/GDMS. 100 μL injections. LOD = $(3 * \sigma_{blank})/m$

Compound	Response Function	Correlation (R^2)	LOD (ng mL^{-1})	Absolute Mass (ng)	% RSD
Caffeine	y = 263284x - 2E+07	0.9910	15	1.5	8.6
Creatinine	y = 8606x - 706589	0.9939	170	17	8.5
Peptide	y = 10052x - 1E+06	0.9993	310	31	4.7
Selenium-methyl-selenocysteine	y = 19852x - 4E+06	0.9985	160	16	7.1
CsCl	y = 659246x - 974974	0.9918	2.4	0.24	6.8
$PbNO_3$	y = 12745x - 8E+06	0.9927	250	25	9.2

supplements, and certainly what is required in profile actives and adulterants in those materials. Typically, carrier salts are used in PB/MS to increase the

sensitivity (carrier effect),[12, 31] but they were not used here to get a better picture of source performance. Future work with this instrument will investigate the role of carriers, usually LC buffer species, for increased sensitivity.

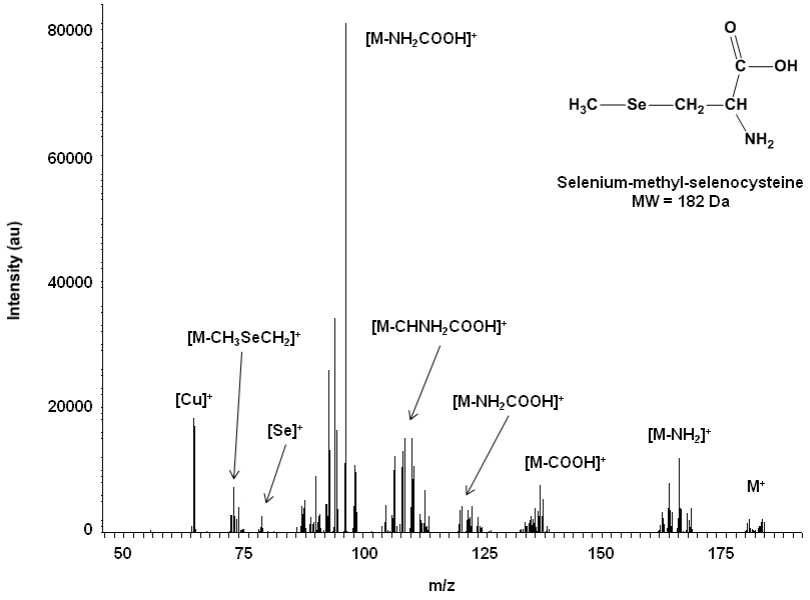

Figure 3.5 GD mass spectrum of 100 µL injection of 1000 µg mL^{-1} methyl-selenocysteine. Solvent = 50:50 water:methanol, nebulizer helium flow rate = 3.5 L min^{-1} (70 psi), liquid flow rate = 0.7 mL min^{-1}, desolvation chamber temperature = 80 ℃, source temperature = 290 ℃, discharge current = 2.0 mA, argon flow = 4.5 mL min^{-1} (MS chamber pressure = 8.0 x 10^{-4} Torr Ar).

CONCLUSIONS

The conversion of an HP 5973 MSD from a GC-MS equipped with an EI source to a LC-PB/GDMS has been demonstrated. In doing so, the scope of applicability of the instrument is dramatically increased with minimal capital investment. Most specifically, this instrument has been assembled for applications involving comprehensive speciation analysis. Previous works in this laboratory have also demonstrated the utility of LC-PB/GDMS for the profiling of active ingredients in botanical extracts. First-level evaluation of the particle beam and glow discharge source operation parameters reflect trends that are consistent with previous works. One primary difference is the realization that particle vaporization from the cell walls is very effective in terms of sample volatilization. The primary differences in performance with previous reports appear to rest with the transmission capabilities of the modest-sized (19 mm diameter) quadrupole rods of the commercial system as well as high background signal levels. Improvements in the overall (vacuum) pumping capacity of the instrument are needed as well. There is also a need to further optimize the design of the discharge cell and cathode geometry. In general, it is believed that this approach to converting an existing GC-MS into an LC-MS using a commercially available interface offers a wealth of attractive features that can be affected in a straightforward fashion opening the field of speciation and LC-MS to new users.

REFERENCES

1. R. Lobinski, D. Schaumloffel and J. Szpunar, *Mass Spectrom. Rev.*, 2006, **25**, 255-289.

2. W. W. Harrison, K. R. Hess, R. K. Marcus and F. L. King, *Anal. Chem.*, 1986, **58**, 341A-356A.

3. W. W. Harrison, C. Yang and E. Oxley, *Glow Discharge Plasmas in Analytical Spectroscopy*, 2003, 71-96.

4. D. Fang and R. K. Marcus, *Glow Discharge Spectrosc.*, 1993, 17-66.

5. M. A. Belkin, L. K. Olson and J. A. Caruso, *J. Anal. At. Spectrom.*, 1997, **12**, 1255-1261.

6. W. C. Davis, J. L. Venzie, B. Willis, R. L. Coffee, Jr., D. P. Arya and R. K. Marcus, *Rapid Comm. Mass Spectrom.*, 2003, **17**, 1749-1758.

7. T. E. Gibeau and R. K. Marcus, *Anal. Chem.*, 2000, **72**, 3833-3840.

8. J. P. Guzowski and G. M. Hieftje, *Anal. Chem.*, 2000, **72**, 3812-3820.

9. A. Sola-Vazquez, A. Martin, J. M. Costa-Fernandez, R. Pereiro and A. Sanz-Medel, *Anal. Chem.*, 2009, **81**, 2591-2599.

10. S. K. Ohorodnik, S. Degendt, S. L. Tong and W. W. Harrison, *J. Anal. At. Spectrom.*, 1993, **8**, 859-865.

11. P. H. Ratliff and W. W. Harrison, *Spectrochim. Acta, Part B*, 1994, **49**, 1747-1757.

12. T. M. Brewer, J. Castro and R. K. Marcus, *Spectrochim. Acta, Part B: Atomic Spectroscopy*, 2006, **61B**, 134-149.

13. R. C. Willoughby and R. F. Browner, *Anal. Chem.*, 1984, **56**, 2626-2631.

14. M. V. Krishna, J. Castro, T. M. Brewer and R. K. Marcus, *J. Anal. At. Spectrom.*, 2009, **24**, 199-208.

15. J. L. Venzie, J. Castro, M. V. B. Krishna, D. M. Nelson and R. K. Marcus, *Anal. Bioanal. Chem.*, 2007, **387**, 321-333.

16. C. F. Harrington, R. Clough, H. R. Hansen, S. J. Hill, S. A. Pergantis and J. F. Tyson, *J. Anal. At. Spectrom.*, 2009, **24**, 999-1025.

17. M. Weber, C. Knoy, K. Kindscher, R. C. D. Brown, S. Niemann and J. Chapman, *Am. Biotech. lab.*, 2007, **25**, 10-11.

18. W. C. Davis, D. Strand and R. K. Marcus, *Am. Lab.*, 2003, **35**, 28-29.

19. T. E. Gibeau and R. K. Marcus, *J. Chrom. A*, 2001, **915**, 117-128.

20. B. Krishna and R. K. Marcus, *Spectrochem. Acta Part B*, 2008, **63**, 673-684.

21. J. Castro, M. V. Krishna, J. Choinere and R. K. Marcus, *Anal. Bioanal. Chem.*, 2010, **397**, 1259-1271.

22. J. Castro, M. V. B. Krishna and R. K. Marcus, *Am. Lab.*, 2008, **40**, 8-10.

23. R. K. Marcus and J. A. C. Broekaert, *Glow Discharge Plasmas in Analytical Spectroscopy*, 2003.

24. J. L. Venzie, W. C. Davis and R. K. Marcus, *J. Anal. At. Spectrom.*, 2004, **19**, 1309-1314.

25. J. You, P. A. Depalma, Jr. and R. K. Marcus, *J. Anal. At. Spectrom.*, 1996, **11**, 483-490.

26. R. K. Marcus, *Glow discharge spectroscopies*, Plenum Press Publishing Corporation, New York, 1993.

27. D. Fang and R. K. Marcus, *Spectrochim. Acta, Part B: At. Spectr.*, 1990, **45B**, 1053-1074.

28. D. C. Duckworth and R. K. Marcus, *J. Anal. At. Spectrom.*, 1992, **7**, 711-715.

29. D. Fang and R. K. Marcus, *Spectrochim. Acta, Part B: At. Spectr.*, 1991, **46B**, 983-1000.

30. *NIST Chemistry WebBook*, National Institute of Standards and Technology, Gaithersburg, MD, 2003.

31. T. A. Bellar, T. D. Behymer and W. L. Budde, *J. Am. Soc. Mass Spectrom.*, 1990, **1**.

CHAPTER FOUR

SIMULTANEOUS MULTIPLE ELEMENT DETECTION BY PARTICLE BEAM/HOLLOW CATHODE-OPTICAL EMISSION SPECTROSCOPY AS A TOOL FOR METALLOMIC STUDIES: DETERMINATIONS OF METAL BINDING WITH APO-TRANSFERRIN

INTRODUCTION

The determination of how metals interact with proteins within the human body will help to form a better understanding of their roles in drugs (i.e. titanium cancer drugs),[1] diseases (i.e. iron deficiency anemia),[1-4] and essential cellular activities. Human serum transferrin (Tf) is the iron transport protein in serum, having a concentration of ~ 35 µM.[1] It is responsible for delivering iron to the cell, where it is used for oxygen transport, electron transfer, and DNA synthesis.[3] Transferrin consists of approximately 700 amino acids with a molecular weight of ~ 80 kDa and has two metal-binding lobes (referred to as *N*- and *C*-terminal lobes), both having similar pockets that bind one Fe^{3+} each. Figure 4.1 represents the binding pocket of apo-transferrin (i.e., the metal free form) which coordinates iron in a distorted octahedral geometry and consists of one histidine, one aspartic acid, and two tyrosine residues, as well as a synergistic anion (usually carbonate) that acts as a bidentate ligand to complete the octahedral coordination sphere.[5]

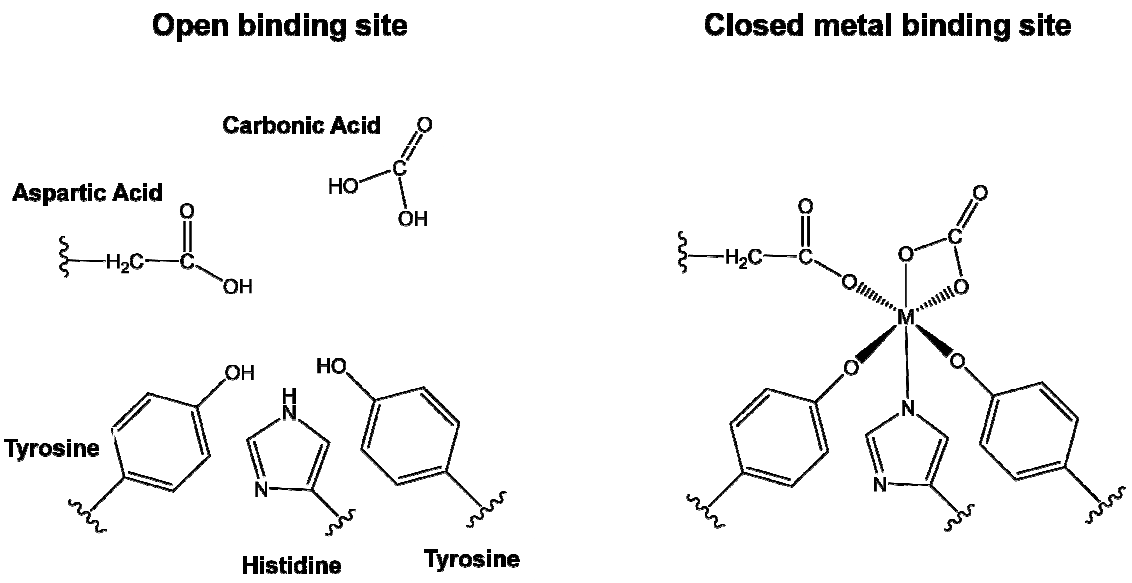

Figure 4.1 Structure of the open and closed metal binding sites found in the *N*-and *C*-lobes of transferrin (Tf).

Upon Fe^{3+} binding, each lobe of the Tf protein undergoes a change from an open conformation to a closed conformation (aka the Venus fly trap).[1] Transferrin receptor proteins on the cell surface only bind the completely closed (diferric) form of Tf, where it is taken into the cell by the process of receptor-mediated endocytosis.[1, 3] It has been determined that Tf is only 39% Fe^{3+}-saturated in serum, meaning that the empty lobes that are available for binding may potentially bind other metals.[6] The binding strengths of metal ions other than Fe^{3+} to Tf follows a trend similar to the stability constants for hydroxide binding to metal ions, meaning that the more acidic the metal, the stronger it binds to Tf.[1, 7, 8] The size of the metal ion also affects binding to Tf as well. In addition, NMR studies have shown that other metal ions that bind to Tf display similar spectral shifts to those corresponding to the open-to-closed conformation

change that occurs upon Fe^{3+} binding.[9, 10] Because of the selectivity of the Tf receptor for only the closed form of Tf, metal ions other than iron may be taken up into the cell if they bind in the empty lobes of Tf.

Tf is known to bind other metals such as Al^{3+}, Ni^{2+}, Cu^{2+}, and Zn^{2+}.[1] Of these metal ions, nickel forms the weakest Tf complex. This is counterbalanced by the fact that nickel exposure is prevalent (electroplating, alloy production and welding)[11] and can be considered hazardous. Research has confirmed that nickel interferes with cellular uptake of iron (presumably through binding to Tf) and ultimately decreases ferritin production within the cell.[11, 12] By the same token, zinc-rich diets elevate Zn^{2+} concentrations in plasma and compete with Fe^{3+} for binding by Tf.[13, 14] Copper and zinc ions have been reported to block Tf binding to the Tf receptor at the cell surface and thus prevent receptor-mediated endocytosis.[15] These examples point to the importance of knowing binding characteristics of various metals with Tf and how they will compete with Fe^{3+} binding.

Detection and quantification of Fe^{3+} bound to Tf is typically accomplished using UV-VIS absorbance by monitoring the change in the molecular band at ca. 470 nm, which is due to ligand-to-metal charge transfer (LMCT) of tyrosine to Fe^{3+}.[1] For the binding of other metal ions to Tf, the bands at ~255 and ~295 nm, characteristic of metal coordination to the tyrosine groups in the binding pocket of Tf, are monitored.[4] The concentration of the bound metal is related to the measured absorbance, and so is intimately tied to the efficiency of chromatographic protein recovery commonly used to purify proteins following the

binding experiments. These changes in absorbance are not metal ion specific in the way that atomic (optical) emission spectra are. In addition, the binding of multiple (different) metal ions contributes predominately to the overall strength of the bands, with very little spectral specificity. Thus, it is very difficult to detect multiple metal ions bound to Tf using UV-VIS absorbance measurements. In addition, many metal ion-amino acid complexes are spectroscopically inactive, and so their binding cannot be detected via absorbance. Overall, quantification of metal ion uptake in Tf is performed based on the respective peak absorbance values, which must be differentiated from the general molecular background absorbance that is always present.

In order to obtain unequivocal metal ion identification and quantification, atomic spectroscopy methods are required. Inductively coupled plasma-optical emission spectrometry (ICP-OES) and mass spectrometry (ICP-MS) are capable of quantifying and identifying specific metal ions bound to proteins such as Tf.[16-18] Using this technique, however, it is not possible to determine if the metal is specifically bound to Tf and not just present as free ions in solution. In principle, free and bound metal ions can be separated chromatographically, but this measurement only identifies the metals present in specific fractions, not the identity of those species. One common method for determining metal ion concentrations is ICP. However, the basic nature of the ICP source is such that all species in solution are broken down to elemental form, as are remnants of solvent species and buffer components. Therefore, there are no means of assessing the presence of protein as there is a continuous background of

carbon, hydrogen, and other elements in the solvent/buffer system. Electrospray ionization mass spectrometry (ESI-MS) also can be used to provide direct information that a metal is associated with a specific protein, but quantification of the metal ions is generally poor with this technique.[19-21] In order to obtain a complete, quantitative picture of the metal-protein interaction, ICP and ESI approaches must accompany each other in a complementary fashion.

An ideal spectroscopic tool for assessing metal ion binding to proteins would provide very high elemental specificity, precise quantification with micromolar sensitivities, and some method of confirming the association of the metal(s) with the protein. Other favorable qualities would include the ability to work with small sample quantities, perform simultaneous multielement determinations, and be readily interfaced with liquid chromatography separations employing various solvent systems. In this paper we present the application of the particle beam/hollow cathode-optical emission spectroscopy (PB/HC-OES) method as a means of performing metal-protein binding studies, specifically the metals Fe, Ni, Zn, and Ag with Tf. This instrument operates using a particle beam that interfaces a liquid delivery system (e.g. a liquid chromatography pump) to a hollow cathode glow discharge source operating in an inert atmosphere.[22] This approach effectively delivers dry analyte particles to the plasma, where thermal energy induces vaporization and dissociation of proteins and plasma excitation permits detection of metals and nonmetal atoms simultaneously. Atomic emission detection provides high specificity and sensitivity for metals analysis, while the operation in an inert plasma permits

protein determinations based on the constituent nonmetal (e.g., C, H, O, S, N) responses. This latter attribute makes the PB/HC-OES unique and different from ICP as association with a protein can be directly deduced. More specifically, the ability to obtain emission response ratios of metal to nonmetals (e.g., M^+/C or M^+/S) allows for direct stoichiometric determinations[23] and makes this technique protein-concentration independent.

In this study, the binding of Fe^{3+}, Ni^{2+}, Zn^{2+} and Ag^+ with the iron transport protein transferrin (Tf), both individually and competitively are described. Iron binding determinations were comparable to that of the standard UV-VIS absorbance method and thus confirmed the ability of the PB/HC-OES to determine metal binding within Tf. The loading of transition metals Ni^{2+} and Zn^{2+} was performed to assess the technique for metals that are spectroscopically difficult to discern by the absorbance method. Silver was chosen as a surrogate for Pt, a common therapeutic metal species that is thought to enter the cell via Tf, though bound to the transport protein in a different manner than the other transitions metals. It is believed that the characteristics demonstrated here can be used effectively across a broad range of metal-protein interaction studies. Chapter 4 was published in *Metallomics* (C. D. Quarles Jr., J. L. Brumaghim, R. K. Marcus, 2010, vol. 2, pp 154-161).

EXPERIMENTAL

Sample Preparation and Introduction

High-purity (18.2 MΩ-cm) Barnstead Nanopure (Dubuque, IA) water and methanol (EMD Chemicals, Cincinnati, OH) were used as the mobile phase solution. Stock solutions of human apo-transferrin (60 µM, Sigma-Aldrich, St. Louis, MO) were prepared in Tris Buffer (20 mM, TEKnova, Hollister, CA) at pH 7.4 and sodium carbonate (20 mM, Sigma-Aldrich). Iron solutions were prepared by adding iron nitrate (45 µM, Sigma-Aldrich) and nitriloacetic acid (90 µM, Sigma-Aldrich) in a 1:2 ratio respectively to hydrochloric acid (0.1 M, J. T. Baker, Phillipsburg, NJ) and adjusting the pH to 4.0.[2] Nickel solutions were prepared by adding nickel nitrate (1000 µM, Sigma-Aldrich) to nanopure water, silver solution prepared by adding silver nitrate (1000 µM, Sigma-Aldrich) to nanopure water, and zinc solutions were prepared by adding zinc acetate (1000 µM, Sigma-Aldrich) to nanopure water.[2, 4, 24] Addition of 0 – 4 molar equivalents of Fe^{3+},[2] and 0 – 10 molar equivalents of Ni^{2+}, Zn^{2+}, and Ag^{+} based on preliminary work were added to the apo-transferrin solution, followed by incubation at 37 ℃ of the samples for 24 hrs. The samples were then desalted using a Sephadex™ G-25 M PD-10 column (GE Healthcare, Buckinghamshire, UK) to remove any unbound metal ions from the protein prior to introduction to the PB/HC-OES system or analysis by UV-VIS absorbance, ensuring that only the metal ions bound to Tf are analyzed. A Waters (Milford, MA) model 510 high-performance liquid chromatography pump with a six-port Rheodyne 7125 (Rohnert Park, CA)

injection valve and a Rheodyne 200 µL injection loop was used for sample delivery of the protein solutions to the PB interface.

Particle Beam Interface

A Thermabeam (Extrel Corporation, Pittsburgh, PA) particle beam (PB) interface was used to introduce the sample into the hollow cathode glow discharge source. The interface consists of a thermoconcentric nebulizer, a desolvation chamber, and a two-stage momentum separator. Liquid flow from the HPLC enters the nebulizer through a fused-silica capillary (100 µm i.d.) positioned inside of a metal tube that has a DC potential (~ 1 V) applied across its length. This potential creates thermal energy (operated at 105 °C) that, when coupled with a coaxial flow of He gas, creates an aerosol spray from the capillary tip. The aerosol spray enters the heated (~ 150 ℃) desolvation chamber to further dry the aerosol particles. The particles are then introduced into a two-stage momentum separator that removes low mass molecules (solvent and He gas) leaving only the dry analyte particles ($\leq$ 10 µm size) to reach the HC source volume. [25, 26]

Hollow Cathode Glow Discharge Source

The copper hollow cathode (HC) is machined to have a cylindrical inner diameter of 3.5 mm and 26.5 mm in length with a particle entry hole of 3.5 mm in diameter in the side of the cathode. The hollow cathode is mounted in the center of a “thermoblock” made of stainless steel. Cartridge heaters (Model SC 2515,

Scientific Instruments, Ringoes, NJ) are located at the bottom of the block, yielding uniform heating of the HC, which is required to provide sufficient energy to vaporize and atomize the sample. The block temperature (~ 210 ℃) is monitored with a W-Re thermocouple and the gas pressure monitored with a Pirani-type vacuum gauge (VRC Model 912011, Pittsburgh, PA). Power (1.0 kV) is provided to the HC by a Bertan power supply (Model 915-1N, Hicksville, NY) that is operated in constant current (60.0 mA) mode. Helium (ultra high purity) is used as the discharge gas (2.0 Torr He).

Optical Emission Spectrometer and Data Acquisition

A JY RF-5000 (Jobin-Yvon, Division of Instruments, Edison, NJ) was used as the detector for the PB/HC system. The JY RF-5000 polychromator includes a 0.5-m Paschen-Runge polychromator with an ion-etched holographic grating with 2400 grooves/mm, with a practical resolution of ~0.01 nm. Photomultiplier tubes for each of the 26 optical channels sample data at a rate of 2 kHz. The optical path is nitrogen-purged to enable optical emission detection across the range of 110-620 nm. Spectrometer control and data acquisition were obtained using JY Quantum 2000 version 1.1 software on a Hewlett-Packard Vectra VE computer. Data files were then exported and processed as Microsoft Excel (Seattle, WA) files. Reported analyte responses (peak area) are the average of triplicate determinations (i.e. injections) taken using Quantum 2000 software.

pH Measurements

All solutions were pH measured with a Accumet Research AR 10 pH meter (Fisher Scientific) and an Accumet double junction Ag/AgCl pH probe (Fisher Scientific). Adjustments to pH were done with hydrochloric acid (6.0 M, Sigma-Aldrich) and sodium hydroxide (2.0 M, Sigma-Aldrich).

UV-VIS Absorbance

All absorbance measurements were performed with a Genesys 10-S UV-VIS spectrometer (Thermo Electron Corporation). The concentration of Tf was determined by measuring the absorbance at 280 nm and using an extinction coefficient of 87,200 M^{-1} cm^{-1}. Concentration of Fe^{3+} loaded into the Tf was determined by measuring the absorbance at 470 nm and using an extinction coefficient of 4,860 M^{-1} cm^{-1}.[2]

Optical Emission Analytical Responses

Calibration curves were prepared from aqueous standards of 0.1 – 500 µM Fe^{3+}, Ni^{2+}, Zn^{2+}, and Ag^{+}. An obvious question exists in whether or not response functions for (essentially) free ions are valid for what should be protein-bound metals. Studies by Brewer and Marcus in fact showed that the slopes (and resultant limits of detection) for functions derived for iron in the form of $FeCl_2$, myoglobin, and holotransferrin differed by less than 10%.[27] Typical response functions (derived from triplicate 200 µL injections at each concentration), linearity, and limits of detection for the transition metals and the

Tf carbon and sulfur constituents for the present study are presented in Table 4.1. In practice, the instrument was calibrated prior to each set of analyses for highest accuracy. The computed detection limits for the metals are “neat”, whereas those given for C and S refer to the molar concentration of protein that can be determined.

Table 4.1 Typical PB/HC-OES quantification data for metals and non-metals in present binding studies.

Element	Response Function	Accuracy (R^2)	LODs
Fe (I)	y = 0.0016x - 0.0018	0.9912	0.17 µM
Ni (I)	y = 0.0311x - 0.269	0.9789	0.08 µM
Zn (I)	y = 0.0518x - 0.5682	0.9874	0.51 µM
Ag (I)	y = 0.0185x - 0.7485	0.9833	0.03 µM
C (I)	y = 0.0047x - 0.9694	0.9694	0.20 µM
S (I)	y = 0.0006x + 0.0016	0.9858	1.86 µM

RESULTS AND DISCUSSION

Method Validation for Iron Loading into Tf

A comparison of UV-VIS absorbance and the PB/HC-OES method was carried out to demonstrate the ability of the system to detect the level of Fe^{3+} loading of Tf. As in other works, the percentage loading is based on the assumption that two molar equivalents of iron can be added to each one of transferrin (i.e., 100% loading would be a 2:1 Fe:Tf molar ratio). Figure 4.2, shows the response curves for iron loaded into Tf determined by the UV-VIS absorbance and PB/HC-OES methods. Given the fact that the data are obtained

using totally different methods, the agreement is quite good. To be clear, the UV-VIS data reflects changes in optical density of an optical band, regardless of what species contribute to that absorbance. On the other hand, the Fe (I) optical emission response simply reflects the amount of iron that is contained in the sample, regardless of its chemical identity. Neither approach can be said to be certain in terms of obtaining the desired information. Figure 4.2 implies that as the amount of Fe^{3+} increases, so does the amount of iron that is taken up by Tf. The UV-VIS data suggests that beyond the addition of 3 molar equivalents the loading reaches a maximum, consistent with similar studies. The PB/HC-OES response is more linear with the amount of Fe^{3+} added. The Fe loading (4 equivalents added) was determined to be 67.5 ± 2.5 % by the UV-VIS absorbance method and 71.2 ± 4.7 % for the PB/HC-OES method; essentially the same value. This demonstrates that the PB/HC-OES method is capable of determining iron loading and provides comparable results to that of UV-VIS. Furthermore, the complementary use of UV-VIS with the PB/HC-OES method further suggests that iron is incorporated within Tf and not just free in solution.

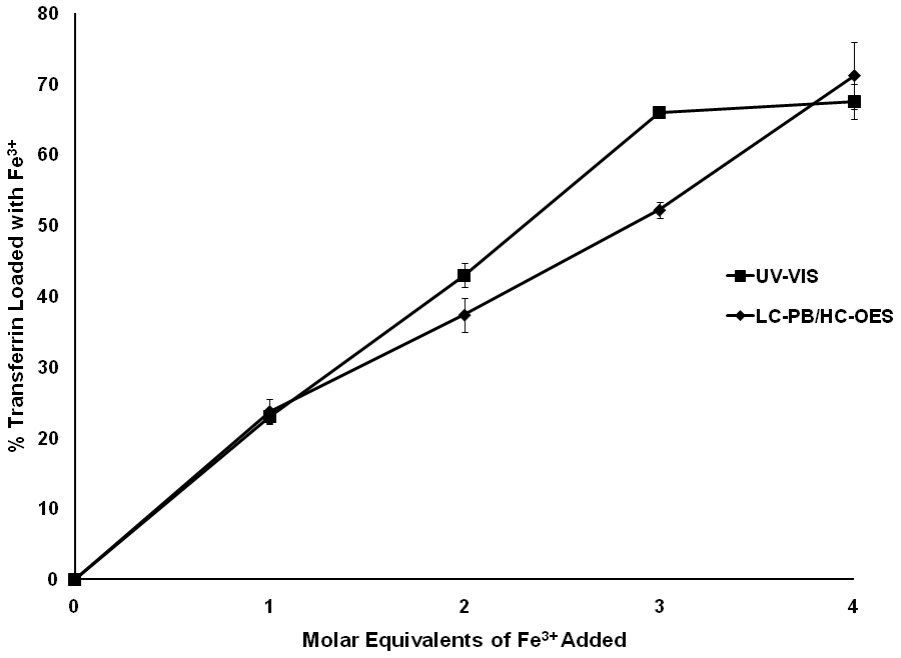

Figure 4.2 Comparison of the results found by UV-VIS absorbance and PB/HC-OES methods for determining Fe^{3+} loading in Tf. UV-VIS absorbance of Fe^{3+} loading monitored by change in absorbance at 470 nm. PB/HC-OES operating parameters: Mobile phase = 50:50 water:methanol, nebulizer gas flow rate = ~1400 mL min^{-1} He, nebulizer tip temperature = 105 ℃, HPLC flow rate = 1.0 mL min^{-1}, 200 µL injection loop, desolvation chamber temperature = 150 ℃, hollow cathode block temperature = 210 ℃, discharg e current = 60 mA, discharge pressure = 2 Torr He.

Ultimately, the desired information in metal loading studies is the molar stoichiometry reflecting the number of incorporated metal ions per molecule of protein. The data presented in Fig. 4.2, simply reflects species' concentrations. Previous studies in this laboratory have demonstrated the ability to determine empirical formulae based on the optical emission intensities of constituent elements in amino acids, metallo-organic compounds, and proteins.[23, 28-32]

Having the ability to detect carbon, sulfur, and iron simultaneously allows for the determination of the stoichiometry of the metal-protein complex. A subtle, yet very important, point is the fact that the loading results based on ratios are concentration independent; the process recovery can change, but the ratio will stay the same). Figure 4.3 shows the element emission ratios determined for Fe (I)/S (I) and Fe (I)/C (I) for each of the equivalent additions of Fe^{3+} to apo-transferrin. As would be anticipated, the ratios increase proportionately with the amount of Fe incorporated in the protein. The fact that the carbon- and sulfur-referenced responses track each other implies that either can be used as the internal standard to compute the empirical formula. This concept is illustrated in Fig. 4.4, wherein the measured Fe (I)/C (I) and Fe (I)/S (I) ratios are plotted as a function of the previously determined percentage of Fe^{3+} incorporated into Tf (Fig. 4.2). The degree of correlation between the emission ratios and the percentage loading is excellent (R^2 = 0.9958 and 0.9884). There is nonlinearity seen in the RSD values that result from the error in the sulfur response seen in Fig. 4.3, however this is not seen for the carbon response. Having generated these sorts of plots, they can be used in many situations, with the added advantage that they are independent of the actual metal/protein concentrations. The results of all the binding studies performed here are summarized in Table 4.2.

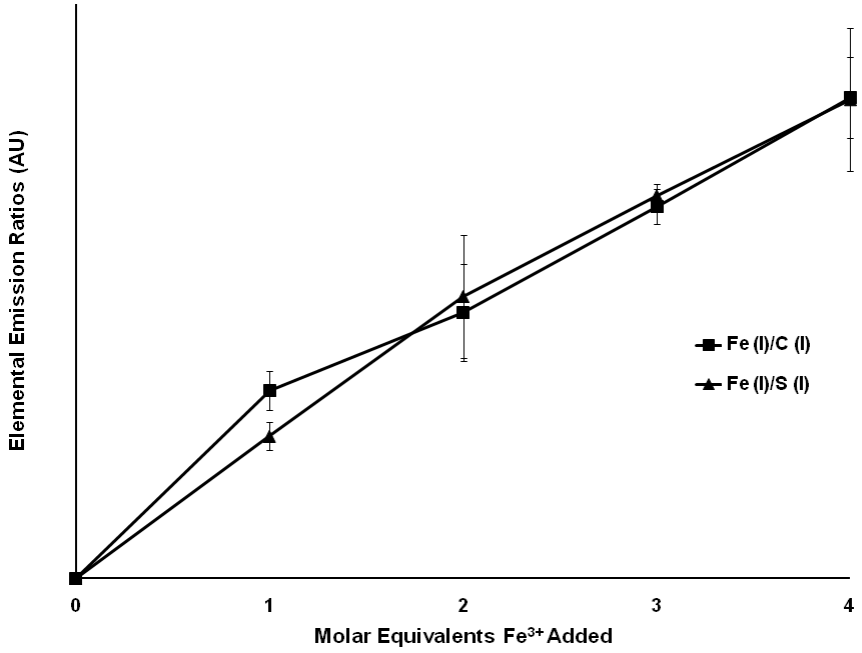

Figure 4.3 Element emission ratios of Fe (I)/C (I) and Fe (I)/S (I) normalized to show that the curve characteristics are the same for both elements. PB/HC-OES operating parameters are the same as Fig. 4.2

(a)

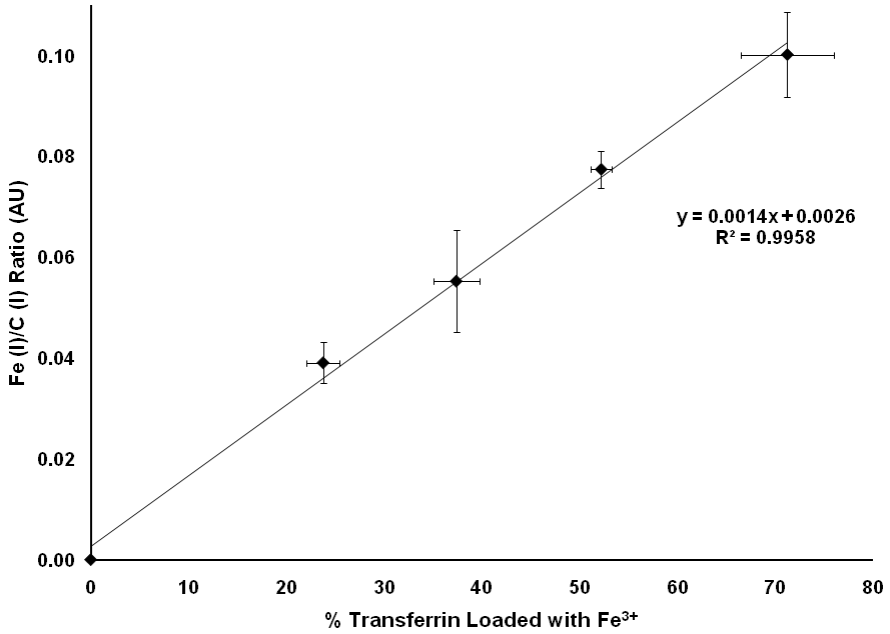

(b)

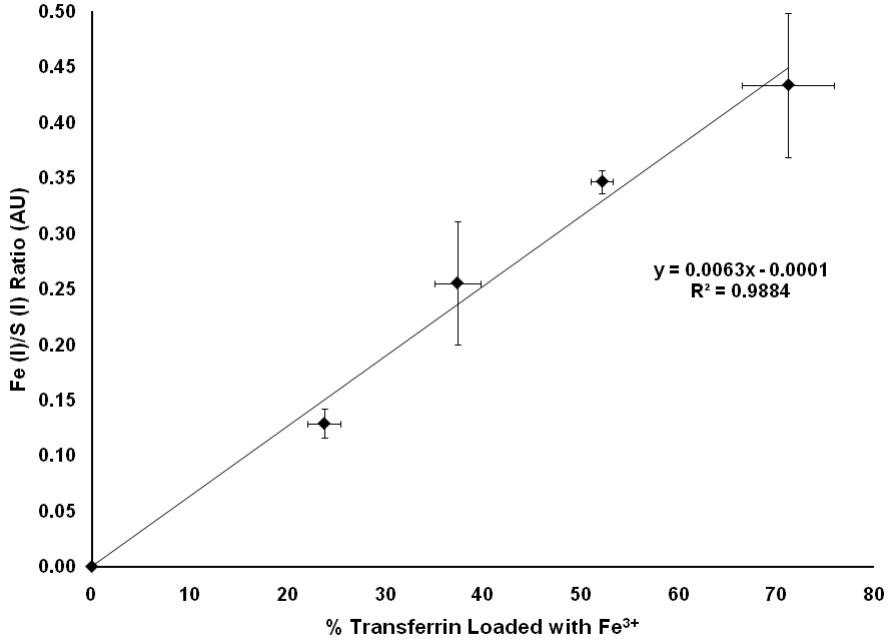

Figure 4.4 Comparison of experimentally obtained a) Fe (I)/C (I) and b) Fe (I)/S (I) emission intensity ratios to the actual loading percents of Fe^{3+} into Tf. PB/HC-OES operating parameters are the same as Fig. 4.2

Nickel Loading

Previous work determining binding constants of Ni^{2+}-Tf complexes using UV-VIS absorbance determinations reported that only about 1 molar equivalent may bind to Tf.[4] Ni^{2+} is a d^8 transition metal that often prefers square planar geometry In the formation of a Ni^{2+}-Tf complex, Ni^{2+} would have to adopt a distorted octahedral geometry, which would result in a loss of crystal field stabilization energy (CFSE) compared to square planar geometry, and therefore result in a less favorable interaction than that of the Fe^{3+}-Tf complex.[4] Ultimately, studies by Harris indicated that less than one equivalent of Ni^{2+} was incorporated per Tf molecule. Figure 4.5 represents the percentage of Tf loaded with Ni^{2+}, reaching a maximum value of ~ 19.5 % loading (based on two potential sites) at a 10-fold molar excess of Ni^{2+}. Harris suggested that a large excess (7×) was needed to drive Ni-Tf complex formation,[4] but the seeming bi-modal addition depicted in Fig. 4.5 was not mentioned in that work. In fact, a larger excess was employed here, and the second increase in uptake is beyond the excess range used by Harris. The shape of this response might suggest the sequential filling of the two different sites (*N*- and *C*-lobes). Also shown in Fig. 4.5, the shapes of the Ni (I)/C (I) and Ni (I)/S (I) responses mirror those of the loading curve, providing supporting evidence that the addition of Ni^{2+} to the Tf-containing solution does lead to the assumed metal-protein complex, but only to the extent that the molar ratio is ~0.4:1 (Ni:Tf).

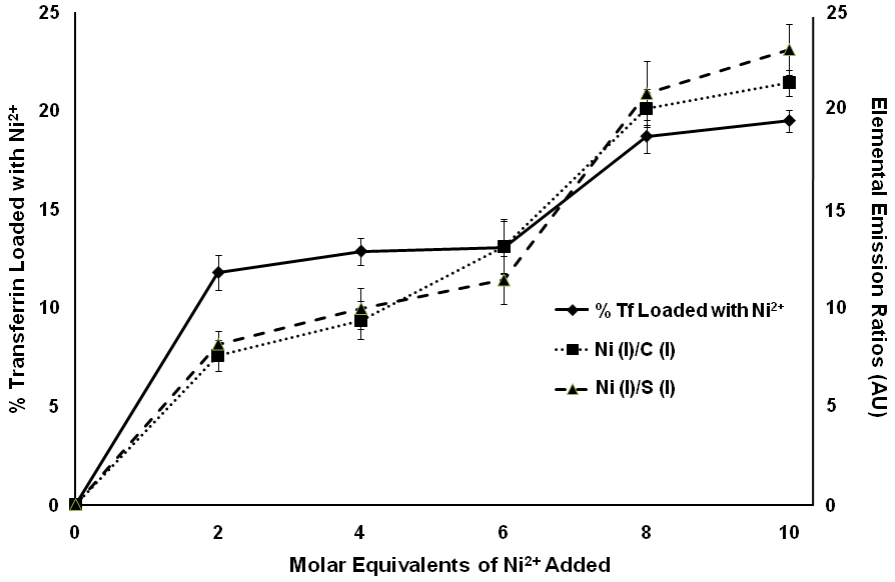

Figure 4.5 Percentage of Tf loaded with Ni^{2+} and relative Ni (I)/C (I) and Ni (I)/S (I) emission intensity ratios as a function of molar excess addition. PB/HC-OES operating parameters are the same as Fig. 4.2

Zinc Loading

The Zn^{2+} ion is similar in size to Ni^{2+} and has very similar hard soft acid base (HSAB) properties, suggesting that they would have similar binding abilities to Tf. According to Harris, the binding constant of Zn^{2+} to Tf is greater than that of Ni^{2+}, but less than Fe^{3+}.[4, 33] Figure 4.6 presents the loading response for Zn^{2+} in Tf, which appears to reach a plateau equivalent to a loading of ~ 41.0 % at an excess of 10 molar equivalents. On a molar basis, this is equivalent to a ratio of ~0.8:1 (Zn:Tf). Zn^{2+} is a d^{10} transition metal that upon complexation with Tf has no change in CFSE, making the Zn^{2+}-Tf complex more stable than that of Ni^{2+}.[4]

The element emission ratios of Zn (I)/C (I) and Zn (I)/S (I) show the same general responses as seen with the loading curve.

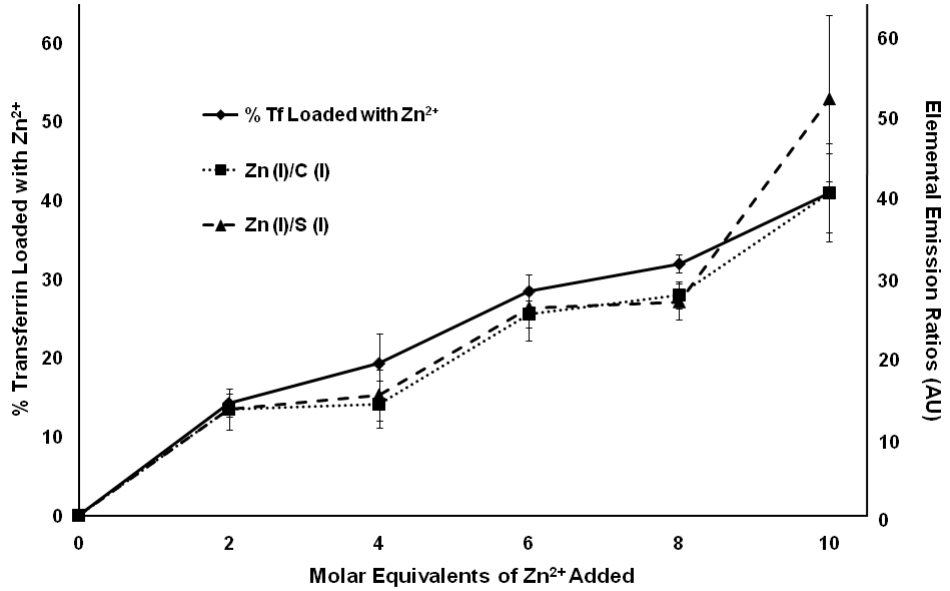

Figure 4.6 Percentage of Tf loaded with Zn^{2+} and relative Zn (I)/C (I) and Zn (I)/S (I) emission intensity ratios as a function of molar excess addition. PB/HC-OES operating parameters are the same as Fig. 4.2

Silver Loading

Platinum-based drugs are well known in cancer therapies, and so there is question on the possible role that Tf may play in their transport. Platinum-Tf complexes have been studied by Sadler and co-workers who suggested that there are 3 potential metal binding locations on Tf, all involving methionine (Met) residues; two of which are on the protein surface and one that is accessible within the N-lobe.[34] NMR studies ruled out binding in *N*- and *C*-lobe sites

depicted in Fig. 4.1. Unfortunately, the preset spectrometer configuration does not permit Pt (I) emission monitoring, but there is an Ag (I) channel. The interaction of silver and sulfur is a favorable interaction due to soft character of both elements (HSAB). To date, there have been no literature reports of Ag^{+}-Tf binding and this is the first report to our knowledge. It was hoped that the chemical similarities between Pt^{2+} and Ag^{+} would yield loading responses that might be relevant. The loading curve for silver seen in Fig. 4.7 shows some interesting characteristics; far different from the other transition metals presented previously. A steady increase in loading is seen up to molar excesses of 10:1 (Ag:Tf), with a maximum loading value of ~141.2 % based on the two-lobe model. In practice, the data reflects a stoichiometry of ~2.8 Ag:Tf. This is far greater loading than seen for the other metal ions. The Ag^{+} data here seems to strongly support the Pt^{2+} work of Sadler,[34] implying that there are two easily-accessible sites, and one of perhaps more hindered access. This latter supposition will be addressed in the discussion of competitive binding.

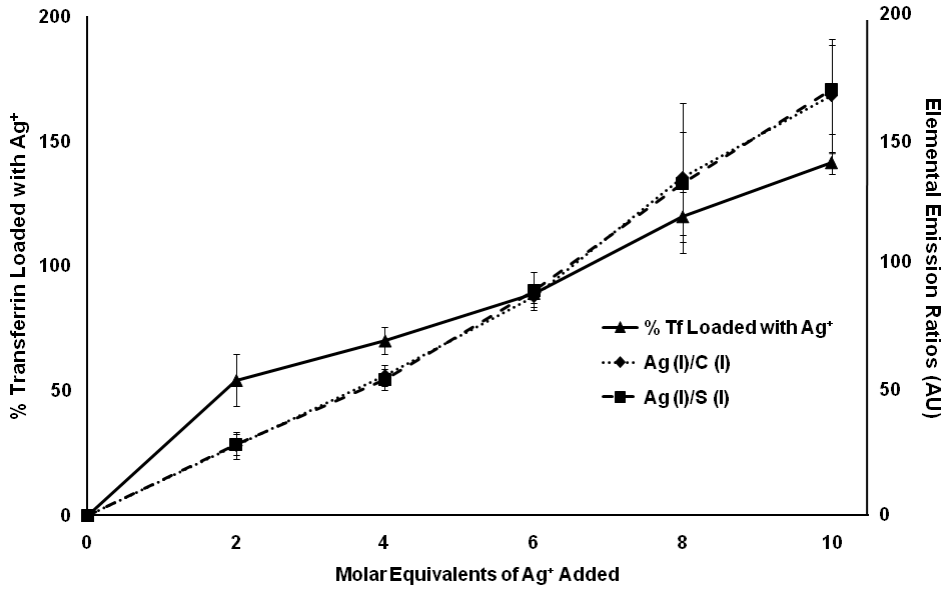

Figure 4.7 Percentage of Tf loaded with Ag^+ and relative Ag (I)/C (I) and Ag (I)/S (I) emission intensity ratios as a function of molar excess addition. PB/HC-OES operating parameters are the same as Fig. 4.2

Competitive Metal Binding with Tf

Other than the case of Fe^{3+} which produces a somewhat unique response ca. 470 nm when complexed with Tf, the responses seen in the 255 and 295 nm regions upon metal binding within the Tf lobe structure are completely non-specific. The uniqueness of the PB/HC-OES method is that the response of multiple elements can be detected simultaneously. This allows for competition studies to be carried out, with the OES signals being reflective of the amounts of incorporated metal ions. A mixture containing 10 molar equivalent excesses of Fe^{3+}, Ni^{2+}, and Zn^{2+} (each) was added to the apo-Tf solution and the mixture

allowed to incubate at 37 ºC for 24 hours (pH = 7.4) to ensure an equilibrium situation was attained (as was the case in the previous loading experiments). Figure 4.8 represents the loading values for each metal ion as well as the total loading. Harris has reported that Ni^{2+} binding prefers the *N* lobe of Tf, and that Fe^{3+} and Zn^{2+} prefer to bind the *C* lobe.[4] As indicated in the figure, the Fe^{3+} and Zn^{2+} loading values are reduced by ~50% in comparison to those of the single metal ion loading studies, suggesting that Fe^{3+} and Zn^{2+} are competing over the *C* lobe binding sites available. Ni^{2+} loading values were only lowered by 4 % in the competitive binding case versus the Ni^{2+}-only study, suggesting that there may not be any competition with Ni^{2+} for the *N*-lobe binding site. Therefore, the general picture taken from this study is the Ni^{2+} fills the *N*-lobe, to the exclusion of Fe^{3+} and Zn^{2+}, whose total loading is limited by not having access to that region of Tf. The 50% suppression of Fe^{3+} binding is consistent to the amounts observed previously. [11, 12] The cumulative loading of the transferrin is only ~72% (based on two—lobe binding), meaning that the protein loading is still not stoichiometric.

Table 4.2 Summary of metal loading of human serum apo-transferrin.

Metal	Loading Percentage
Fe^{3+}	71.2 ± 4.7 %
Ni^{2+}	19.5 ± 0.4 %
Zn^{2+}	41.0 ± 4.4 %
Ag^{+}	141.2 ± 4.3 %
1st Competition Study	
Fe^{3+}	33.4 ± 6.1 %
Ni^{2+}	14.0 ± 1.3 %
Zn^{2+}	24.9 ± 0.8 %
Total M^{n+}	72.3 ± 6.3%
2nd Competition Study	
Fe^{3+}	24.2 ± 4.8 %
Ni^{2+}	15.3 ± 1.0 %
Zn^{2+}	19.6 ± 5.2 %
Ag^{+}	101.0 ± 12.3 %
Total M^{n+}	160.1 ± 14.2 %

A second competitive metal loading experiment was performed to provide better understanding of the Ag^{+} binding mechanism to Tf. In this case, a 10-fold excess of Ag^{+} was added to the mixed transition metal solution prior to incubation with apo-Tf as described above. The relative binding depicted in Fig. 4.8 is quite striking. First, the loading percentages of the transition metals are statistically the same as the first study. Second, the relative loadings of Fe^{3+}, Ni^{2+}, and Zn^{2+} are also not affected by the presence of Ag^{+}. Finally, the extent of Ag^{+} incorporation is equivalent to 2 atoms per molecule of Tf (100 % based on the two-site model), instead of the ~2.8 atoms in the Ag^{+}-only binding study. These data fully support the findings of Sadler as the Ag^{+} occupies the two surface-Met sites, and does not fill the site located within the region of the N-lobe. This is not

surprising as the closing of the *N*-lobe upon filling with the other transition metals makes the third site (which was not completely occupied in the Ag-only case) inaccessible. Keeping in mind that only closed-lobe transferrin is recognized and passed in to the cell by the Tf receptor, these data imply that Pt^{2+} is transported passively with closed-lobe Tf, and does not compete to the exclusion of Fe^{3+} entering the cell.

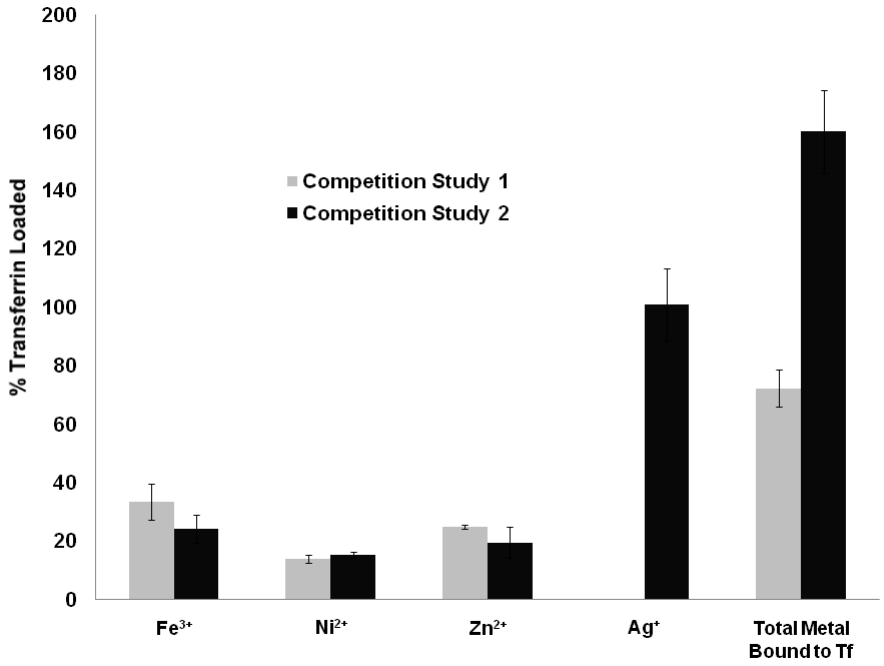

Figure 4.8 Results of competitive metal binding study of Fe^{3+}, Ni^{2+}, and Zn^{2+} simultaneously added to Tf (incubation for 24 hrs. at 37 ℃) and r esults of competitive metal binding study of Fe^{3+}, Ni^{2+}, Zn^{2+}, and Ag^{+} simultaneously added to Tf (incubation for 24 hrs. at 37 ℃). PB/HC -OES operating parameters are the same as Fig. 4.2

CONCLUSION

The PB/HC-OES method has been shown to be a useful tool for metallomics studies, specifically metal binding to proteins. The ability to

unambiguously determine the identity and concentration of incorporated metals (including as mixed metal systems) provides far greater information than can be obtained via UV-VIS absorbance spectrophotometry. The basic method was validated by comparing the PB/HC-OES results with those of UV-VIS experiments, with the two methods yielding values of 71.2 and 67.5 %, respectively. The ability to monitor the optical emission of protein constituent elements (C and S here) provides a means better assuring that the metals are indeed bound to the protein, as well as provide direct stoichiometric evidence of incorporation. Ultimately, the ratio method makes the empirical formulae determinations independent of the actual protein concentrations. Detection limits in the low µM to nM range allow for detection of small sample quantities and the evaluation of metals that may have small binding constants with Tf. Ni^{2+}, Zn^{2+}, and Ag^{+} were loaded individually into Tf and determined to bind at 19.5 ± 0.4 %, 41.0 ± 4.4 %, and 141.2 ± 4.3 % relative to a two-site Tf model, respectively. Ag^{+} loading suggest that another mode of binding is taking place, presumably reflective of the three Met associations seen in the past for Pt^{2+} binding. Competitive metal binding studies with Tf have shown that Ni^{2+} inhibits the binding of Fe^{3+} and Zn^{2+} by ~50%, reflecting its occupancy of the *N*-lobe to exclude the access of the others. Near saturation of the two primary binding lobes has little effect on the Ag^{+} binding to surface Met groups, but hinders addition to the buried Met group. It is believed that the PB/HC-OES method provides a level of specificity and sensitivity not available in more typical methods, on a relatively simple instrumental platform.

REFERENCES

1. H. Sun, H. Li and P. J. Sadler, *Chem. Rev.*, 1999, **99**, 2817-2842.

2. E. E. Battin, A. Lawhon, D. H. Hamilton and J. L. Brumaghim, *J. Chem. Ed.*, 2009, **86**, 969-972.

3. A. C. G. Chua and R. M. Graham, *Critical Rev. Clin. Lab.*, 2007, **44**, 413-459.

4. W. R. Harris, *J. Inorg. Chem.*, 1986, **27**, 41-52.

5. S. J. Lippard and J. M. Berg, in *Principles of Bioinorganic Chemistry*, University Science Books, Mill Valley, CA, 1994, pp. 141-148.

6. J. Williams and K. Moreton, *Biochem. J.*, 1980, **185**, 483-488.

7. H. Li, P. J. Sadler and H. Sun, *Eur. J. Biochem.*, 1996, **242**, 387-393.

8. H. Sun, M. C. Cox, H. Li and P. J. Sadler, *Struct. Bond.*, 1997, **88**, 71-102.

9. G. Kubal, A. B. Mason, P. J. Sadler, A. Tucker and R. C. Woodworth, *Biochem. J.*, 1992, **285**, 711-714.

10. H. Sun, M. C. Cox, H. Li, A. B. Mason, R. C. Woodworth and P. J. Sadler, *FEBS lett.*, 1998, **422**, 315-320.

11. H. Chen, T. Davidson, S. Singleton, M. D. Garrick and M. Costa, *Tox. and Appl. Pharma.*, 2005, **206**, 275-287.

12. T. Davidson, H. Chen, M. D. Garrick, G. D'Angelo and M. Costa, *Mol. and Cell. Biochem.*, 2005, **279**, 157-162.

13. J. J. Fickel, J. H. Freeland-Graves and M. J. Roby, *Am. J. Clin. Nutr.*, 1986, **43**, 47-58.

14. T. L. Wright, P. Brissot, W.-L. Ma and R. A. Weisiger, *J. Biol. Chem.*, 1986, **261**, 10909-10914.

15. D. D. McAbee and X. Jiang, *J. Biol. Chem.*, 1999, **274**, 14750-14758.

16. R. Pereiro, N. G. Orellana-Velado and A. Sanz-Medel, *Glow Discharge Plasmas in Analytical Spectroscopy*, 2003, 381-400.

17. C. N. Ferrarello, M. R. Fernandez de la Campa and A. Sanz-Medel, *Anal. Bioanal. Chem.*, 2002, **373**, 412-421.

18. A. Sarmiento-Gonzalez, J. R. Encinar, A. M. Cantarero-Roldan, J. M. Marchante-Gayon and A. Sanz-Medel, *Anal. Chem.*, 2008, **80**, 8702-8711.

19. J. Szpunar and R. Lobinski, *Anal. Bioanal. Chem.*, 2002, **373**, 404-411.

20. J. Szpunar, R. Lobinski and A. Prange, *Appl. Spectr.*, 2003, **57**, 102A-112A.

21. J. Szpunar, *Analyst*, 2005, **130**, 442-465.

22. T. M. Brewer, J. Castro and R. K. Marcus, *Spectrochim. Acta, Part B: At. Spectr.*, 2006, **61B**, 134-149.

23. T. M. Brewer and R. K. Marcus, *Anal. Chem.*, 2007, **79**, 2402-2411.

24. T. Kiss, T. Jakusch, D. Hollender, E. A. Enyedy and L. Horvath, *J. Inorg. Chem.*, 2009, **103**, 527-535.

25. M. A. Dempster, W. C. Davis, R. K. Marcus and P. R. Cable-Dunlap, *J. Anal. At. Spectrom.*, 2001, **16**, 115-121.

26. J. You, M. A. Dempster and R. K. Marcus, *J. Anal. At. Spectrom.*, 1997, **12**, 807-815.

27. T. M. Brewer and R. K. Marcus, *J. Anal. At. Spectrom.*, 2007, **22**, 1067-1075.

28. T. M. Brewer, B. Fernandez and R. K. Marcus, *J. Anal. At. Spectrom.*, 2005, **20**, 924-931.

29. M. A. Dempster and R. K. Marcus, *J. Anal. At. Spectrom.*, 2000, **15**, 43-48.

30. F. Jin and R. K. Marcus, *J. Anal. At. Spectrom.,* 2003, **18**, 589-595.

31. F. Jin, K. Lenghaus, J. Hickman and R. K. Marcus, *Anal. Chem.*, 2003, **75**, 4801-4810.

32. J. You, M. A. Dempster and R. K. Marcus, *Anal. Chem.*, 1997, **69**, 3419-3426.

33. W. R. Harris, *Biochem.*, 1983, **22**, 3920-3926.

34. M. C. Cox, K. J. Barnham, T. A. Frenkiel, J. D. Hoeschele, A. B. Mason, Q.-Y. He, R. C. Woodworth and P. J. Sadler, *J. Biol. Inorg. Chem.*, 1999, **4**, 621-631.

CHAPTER FIVE

INSTRUMENTAL COMPARISON OF THE DETERMINATION OF Cr^{3+} UPTAKE BY HUMAN TRANSFERRIN

INTRODUCTION

Metallomics is the field of research that involves understanding how metal species interact and function within biological systems.[1] Metal containing proteins, known as metalloproteins, make up approximately one-third of all known proteins and the understanding of how these metals are trafficked in the body is the ultimate goal.[2-4] The transport proteins albumin and transferrin are found in human serum and are responsible for much of the metal trafficking and uptake of essential metals required by the body. Transferrin (Tf), an iron transport protein, is found at a concentration of ~ 35 μM in human serum.[5] Transferrin consists of two almost identical lobes known as the *N*- and *C*-terminal lobes that can each bind a single Fe^{3+} ion. Upon iron binding to apo-transferrin (the metal free form), the metal coordinates in a distorted octahedral geometry bound to four amino acids (histidine, aspartic acid, and two tyrosines) and a synergistic anion, most commonly carbonate, acting as a bidentate ligand.[6, 7] It has been found that iron only binds to approximately 30% of the transferrin circulating in the serum of the human body. As such, the ~ 70% of the remaining transferrin (i.e., apo- or mono- forms) is available to potentially bind other metal ions found in human serum.[8] These metals may be introduced into the body by

diet, supplementation, implants, or contaminants from the environment. Al^{3+}, Cr^{3+}, Cu^{2+}, Ga^{3+}, Ni^{2+}, Ti^{4+}, and Zn^{2+} are all known to bind to transferrin, with the stability constants for these metal-protein complexes generally following the same trend as the stability constants for metal-hydroxide binding.[5, 9, 10]

Understanding the role of Cr^{3+} on human health has been a topic of much debate over recent years.[11-17] Chromium(III) is considered an essential nutrient for carbohydrate metabolism and is thought to enhance insulin binding and activity.[11] Transferrin is believed to be the major transporter for delivering Cr^{3+} from serum to the cell.[17] It has been determined that Cr^{3+} binds to apo-transferrin with binding constants of $K_1 = 1.42 \times 10^{10}\ M^{-1}$ and $K_2 = 2.06 \times 10^{5}\ M^{-1}$.[18] It has been proposed that chromium-loaded transferrin will bind to the transferrin receptors on the cell membrane and through receptor mediated endocytosis the metal ion will be released into the cell, where it is believed that chromodulin sequesters the Cr^{3+} ion.[12] Reports have shown that increases in serum insulin result in an increased amount of transferrin receptor on the cell surface, which could lead to excess uptake of transferrin-bound metal ions.[17] Vincent posed the question as to whether increased loading of transferrin with iron prevents adequate chromium binding and transfer by transferrin, resulting in insulin resistance and diabetes.[17] Along those same lines, it has been proposed that excessive amounts of Cr^{3+} ions in the body from corrosion of metal prosthetic implants may impede the necessary iron binding and/or uptake for cell survival.[19]

In order to study the effects of Cr^{3+} binding to transferrin under various conditions, proper chemical instrumentation is required. Most transferrin studies involving a single-metal utilize UV-VIS absorbance techniques to determine protein concentration and the ligand-to-metal charge transfer (LMCT) bands (tyrosine to metal) to characterize the complex.[5, 10, 20, 21] Although a very simple and useful technique, UV-VIS does not provide species-specific (ion-complex) signatures, therefore it must be coupled with some form of atomic spectroscopy in order to distinguish between multiple metal ions that may be bound. Inductively coupled plasma-optical emission spectroscopy or mass spectrometry (ICP-OES or -MS) can provide the ability to detect the multiple metals bound to transferrin with very good precision and sensitivity. The primary drawback is that most ICP sources are operated at atmospheric pressure and are unable to detect H, C, N, or O responses which reflect the composition and concentration of proteins. The stoichiometry of metal to protein composition is what ultimately is needed to determine loading percentages for metal loaded protein studies. The Sanz-Medel group recently reported the interactions of cisplatin with serum proteins using S responses (reflective of protein concentration) via ICP-MS to identify protein-metal complexes.[22] Sulfur and phosphorous signals are widely interfered with by polyatomic ions and not sensitive due to high ionization potentials, making their determinations difficult with conventional ICP-MS instrumentation.[23] Thus in order to determine protein concentrations and loading abilities in most studies, both ICP and UV-VIS are used jointly.

As an alternative, electrospray ionization-mass spectrometry/mass spectrometry (ESI-MS/MS) can be used as a qualitative method to determine whether or not metal is bound within the protein, but ESI-MS offers poor quantification capabilities.[24] Recently ESI-MS was used to determine reactivity and selectivity of anticancer metallodrugs with transferrin, allowing for the determination of the specific site to which the metallodrug binds.[25] Analyzing metal-protein complexes in physiological conditions requires the sample to be in a buffered solution. Buffer solutions are typically high in salt content and suppress ionization of the desired product,[26] so to analyze the sample it must be in an ESI-compatible solution, such as acetonitrile. This will change the pH and ionic strength of the sample media, both of which may cause the metals to be released from complexes. Ideally, a technique that allows analysis of the metal-protein complexes without changing the sample media and allows for detection of non-metals and metals simultaneously would provide a more comprehensive technique for determining metal-protein interactions.

The particle beam/hollow cathode-optical emission spectrometer (PB/HC-OES), operates at inert atmosphere, utilizing glow discharge phenomena which allows detection of metals (i.e. Fe, Cr, Ni, or Ag) and non-metals (i.e. H, C, N, S, and O) simultaneously.[7] The use of the particle beam allows for metal-protein complexes to be introduced from the original sample media by removing all solvent vapors and leaving only the dry analyte particle of interest to enter the hollow cathode source. Once particles enter the heated hollow cathode source (consisting of the glow discharge plasma) they are vaporized, atomized, and

excited. The excited analyte atoms emit photons that are detected using a high resolution, vacuum polychromator, allowing for the determination of non-metal and metal species' emission responses simultaneously. Recently, this laboratory has demonstrated the use of this instrument for determinations of loading percentages of Fe^{3+}, Ni^{2+}, Zn^{2+}, and Ag^{+} bound to transferrin individually and as a competition study using M^{n+} (I)/C (I) ratios to determine empirical formulas that represent the loading percentages of each metal bound to transferrin.[7] In addition, detection limits are in the low nM to µM range which allows for the analysis of metals that may have weak binding constants to transferrin with good precision and accuracy. Presented in this study is a comparison of UV-VIS absorbance, ICP-OES, and PB/HC-OES methods for investigating the interactions of Cr^{3+} with human transferrin to determine loading characteristics. Evaluation of the aforementioned methods will be conducted by studying chromium upload at equilibrium conditions, kinetic aspects, varying companion anions, and under competition with iron for upload into apo- and holo-transferrin. Chapter 5 was published in *Metallomics* (C. D. Quarles Jr., J. L. Brumaghim, R. K. Marcus, 2010, vol. 2, pp. 792-799).

EXPERIMENTAL

Sample Preparation

High-purity (18.2 MΩ-cm) Barnstead Nanopure (Dubuque, IA) water and methanol (EMD Chemicals, Cincinnati, OH) were used as the primary solvents.

Samples were prepared in 15 mL centrifuge tubes that had been washed with 1M HCl, thoroughly rinsed, and dried to remove residual metals. Stock solutions of human holo- and apo-transferrin (50 μM, Sigma-Aldrich, St. Louis, MO) were prepared separately in Tris buffer (20 mM, TEKnova, Hollister, CA) at pH 7.4. Sodium carbonate (20 mM, Sigma-Aldrich) was added to all Tf solutions unless otherwise noted. Iron solutions were prepared by adding iron nitrate (45 μM, Sigma-Aldrich) and nitriloacetic acid (NTA, 90 μM, Sigma-Aldrich) in a 1:2 ratio respectively to hydrochloric acid (0.1 M, J. T. Baker, Phillipsburg, NJ) and adjusting the pH to 4.0.[27] Sodium citrate (1000 μM, Sigma-Aldrich) solutions were prepared in nanopure water. Chromium solutions were prepared by adding chromium nitrate or chromium chloride (1000 μM, Sigma-Aldrich) to nanopure water. Transferrin was loaded with chromium by adding 0 – 10 molar equivalents of $Cr(NO_3)_3$ to the apo-transferrin solution, followed by incubation of the samples at 37 ℃ for 24 h.[7] Following the incubation period the unbound metal was separated from the metal-loaded transferrin using a desalting Sephadex™ G-25 M PD-10 column (GE Healthcare, Buckinghamshire, UK).[7] Since the chromium bound transferrin is colorless the desalting separation was done in a methodical way and repeated for all samples to ensure that all unbound chromium was separated prior to analysis. The procedure previously employed for the loading of the iron in transferrin,[7] was shown to be quite robust and was incorporated here. In that method, the sample (2 mL of M^{n+}-Tf) was added to the desalting column, followed by 1 mL of tris buffer, and then an additional 2 mL of tris buffer was added and the 2 mL fraction was collected. After obtaining the sample

fraction, re-equilibration of the column was done with 3 mL of tris buffer prior to the next usage.

pH Measurements

All solutions were pH measured with an Accumet Research AR 10 pH meter (Fisher Scientific, Pittsburgh, PA) with an Accumet double junction Ag/AgCl pH probe (Fisher Scientific). Adjustments to pH were made with hydrochloric acid (6.0 M, Sigma-Aldrich) and sodium hydroxide (2.0 M, Sigma-Aldrich).

Kinetic study

10 molar equivalents of $Cr(NO_3)_3$ were added to a stock solution of apo-transferrin, followed by incubation at 37 ℃, 2 mL a liquots were removed at 1, 3, 7, and 10 d (desalting took place immediately following incubation period prior to analysis).

Anion and Ligand Study

10 molar equivalents of $Cr(NO_3)_3$ and $CrCl_3$ with and without excess sodium carbonate (excess = 20 mM) and sodium citrate (1 mM) were added to the apo-transferrin solution, followed by incubation at 37 ℃ of the samples for 24 h (desalting took place immediately following incubation period prior to analysis).

Fe^{3+} vs. Cr^{3+} Apo-transferrin Competition Study

0 – 10 molar equivalent ratios of $Fe(NTA)_2$ to $Cr(NO_3)_3$ were added to the apo-transferrin solution, followed by incubation at 37 ℃ of the samples for 24 h (desalting took place immediately following incubation period prior to analysis).

Displacement Study

0 – 10 molar equivalents of $Cr(NO_3)_3$ were added to the holo-transferrin solution, followed by incubation at 37 ℃ of the samples for 24 h (desalting took place immediately following incubation period prior to analysis).

All of the samples from each study above were then analyzed by ICP-OES, PB/HC-OES, and UV-VIS absorbance. All samples were kept in buffered solutions (pH 7.4) throughout the experiment so that no species-interconversion should have occurred during the metal loading process.[7]

UV-VIS Absorbance

All absorbance measurements were performed with a Genesys 10-S UV-VIS spectrometer (Thermo Electron Corporation, Waltham, MA). The concentration of Tf was determined by measuring the absorbance at 280 nm and using an extinction coefficient of 87,200 M^{-1} cm^{-1}.[27] The concentration of Fe^{3+} loaded into the Tf was determined by measuring the absorbance at 470 nm and using an extinction coefficient of 4,860 M^{-1} cm^{-1}.[27] Metal-protein spectra were measured using an apo-transferrin solution (no loaded metal ion) as the blank.

ICP-OES

A Jobin-Yvon Ultima 2 (JY Horiba, Longjumeau, France) was used to determine metal concentrations for each Tf solution and the loading percentage values were calculated using the Tf concentration determined by UV-VIS absorbance. All sample solutions were delivered from the AS-500 auto-sampler and introduced into the cyclonic spray chamber by way of a Meinhard concentric glass nebulizer. The Ultima 2 optical emission spectrometer consists of a 1.0 m Czerny-Turner monochromator equipped with a holographic grating (2400 grooves mm^{-1}) and a single photomultiplier tube as the detector. Data acquisition and instrument control were obtained by the JY Analyst v5.2 software. Operating parameters: power = 1000 W, Ar gas flow rate = 12.0 L min^{-1}, nebulizer = 0.02 L min^{-1} at 1.0 bar, sheath gas flow rate = 0.20 L min^{-1}, peristaltic pump speed = 20.0 rpm, Fe (I) 259.94 nm, Cr (I) 283.56 nm.

PB/HC-OES

A particle beam/hollow cathode-optical emission spectrometer was used to determine metal and non-metal concentrations of the metal-loaded Tf solutions simultaneously as previously described.[7] The PB/HC-OES instrument is a home-built system that has been through 15 years of improvements and optimization.[7, 28-43] The particle beam consists of a thermoconcentric nebulizer, desolvation chamber, and a two stage momentum separator. The nebulizer creates a aerosol spray that enters the desolvation chamber where the particles are further desolvated before passing through a two stage momentum separator that

removes all low mass particles (e.g. solvent and nebulizer gas). After passing through the momentum separator, dry analyte particles enter into the copper hollow cathode glow discharge source where the particles are vaporized, atomized, and excited. A 0.5-m Paschen-Runge polychromator (JY RF-5000) consists of an ion-etched holographic grating (2400 grooves mm^{-1}) with a practical resolution of ~0.01 mm utilizing 26 photomultiplier tubes to detect the emission signals. The optical path was nitrogen-purged to allow for detection across the spectral range of 110-620 nm. The operating parameters: mobile phase = 50:50 water:methanol, nebulizer gas flow rate = ~1400 mL min^{-1} He, nebulizer tip temperature = 105 ℃, HPLC flow rate = 1.0 mL min^{-1}, 200 μL injection loop, desolvation chamber temperature = 150 ℃, hollow cathode block temperature = 210 ℃, discharge current = 60 mA, discharge pressure = 2 Torr He, C (I) 156.14 nm, Cr (I) 425.43 nm, Fe (I) 371.99 nm.

Analytical Responses

ICP-OES calibration curves of 0.1 – 100 μM were prepared from stock standard solutions of Fe^{3+} and Cr^{3+} (High Purity Standards, Charleston, SC). PB/HC-OES calibration curves were prepared from aqueous standards of 0.1 – 500 μM Fe^{3+} and Cr^{3+}, it has been previously determined that responses for metal ions are the same regardless of the sample matrix, allowing for quantitative analysis of the metal in both organic and inorganic forms.[7, 30] Typical response functions (derived from triplicate measurements from continuous sample introduction) for the ICP-OES system and response functions (derived from

triplicate 200 µL injections at each concentration) for the PB/HC-OES system are presented in Table 5.1. Calibration prior to each set of analyses was performed to provide the highest accuracy for the sample results.

Loading Percentages

All loading percentages are calculated based on the assumption that 2 molar equivalents of metal ions can be loaded into transferrin, meaning a 2 Fe:1 Tf molar ratio would equate to 100% loading.

Table 5.1 Typical elemental quantification data for PB/HC-OES and ICP-OES methods.

	Element	Response Function	Accuracy (R^2)	LODs (µM)
PB/HC-OES	Fe (I)	y = 0.0016x - 0.0018	0.9912	0.17
	Cr (I)	y = 0.0397x - 0.1470	0.9899	0.07
	C (I)	y = 0.0047x - 0.0082	0.9694	0.2
ICP-OES	Fe (I)	y = 7819.7x + 1421.9	0.9997	0.05
	Cr (I)	y = 0.0397x - 0.1470	0.9999	0.003

RESULTS AND DISCUSSION

Concentration Effects on Chromium Loading

Previous work determining Cr^{3+}-Tf complexes using UV-VIS absorbance reported spectral bands at 293, 440, and 615 nm.[44] Figure 5.1a displays the spectral response of increased amounts of chromium loaded into apo-transferrin over a range of 225 – 650 nm. The spectra show spectral bands at 254, 298, 428 nm that correspond to LMCT of tyrosine to the metal ion (chromium in this

case), each showing increased absorbance values with increasing Cr^{3+} exposure. The weak band at 428 nm is specific to the chromium ion, while the two bands at 254 and 298 nm are the strongest, but are non-specific and represent the LMCT of any bound metal ion. For iron, spectral bands are found at 254, 298, and 470 nm that represent iron being loaded into the binding lobes of transferrin.[21] These bands all show an increase that is proportional to the increasing amount of chromium available to bind to apo-transferrin. Figure 5.1b represents the corresponding loading percentages of Cr^{3+} bound to apo-transferrin determined by both the ICP-OES and PB/HC-OES methods. The loading percentages in Table 5.2, found by both methods are in good agreement and are not significantly different at any value based on p values (< 0.05). The loading percentages for the ICP method were determined with the use of the UV-VIS spectrophotometer (i.e. Cr concentration via ICP and Tf concentration via UV-VIS). The loading percentages for the PB/HC-OES method are reflective of the directly-measured ratio of Cr (I)/C (I).[7] The maximum loading at a 10 molar equivalent excess was determined to be 26.8 ± 3.5 % and 25.3 ± 2.2 % for the ICP-OES and PB/HC-OES methods, respectively. This loading percentage was below expectations and should be much higher based on the stability constants of Cr^{3+} (K_1 = 17, estimated) and Fe^{3+} (K_1 = 21, measured).[10] Previously, Fe^{3+} was found to load into transferrin at 71.2 ± 4.7% using this same method.[7] Based on the aforementioned iron loading percentage and stability constant, it was expected that chromium would load into approximately 50% of the available apo-transferrin. A reasonable explanation to the lower than expected loading

values is the fact that Cr^{3+} is an inert metal ion while Fe^{3+} is labile, so longer incubation times (than the 24 hours used here) may be needed to fully load Cr^{3+} into transferrin.

(a)

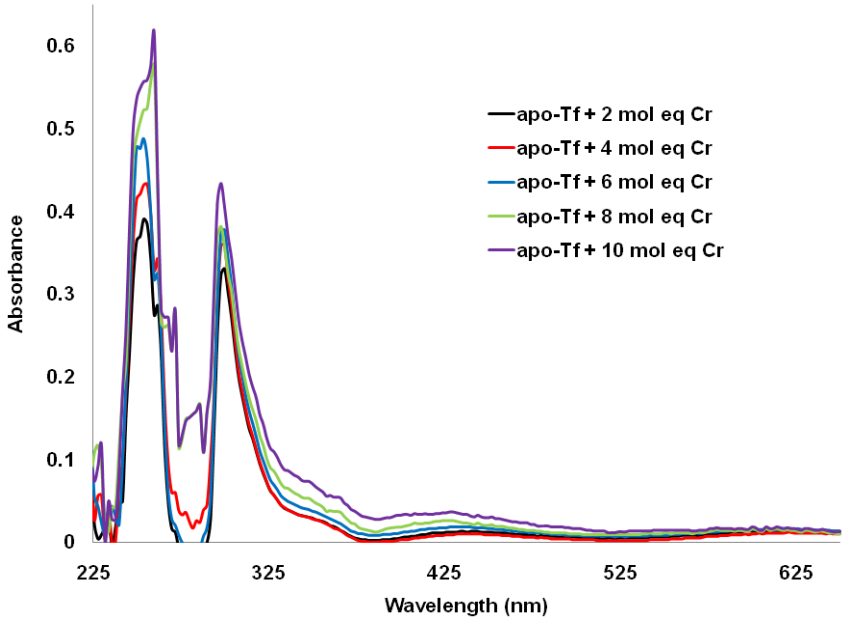

(b)

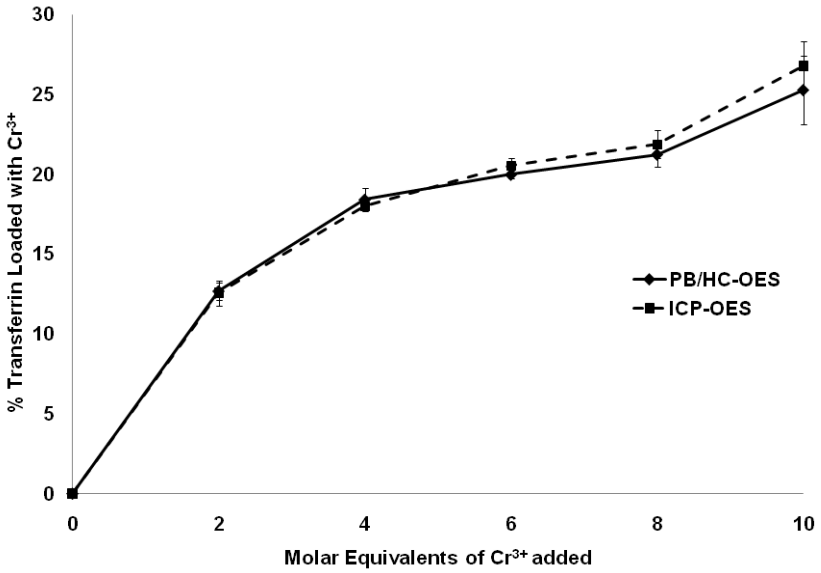

Figure 5.1 Additions of 0 -10 molar equivalents of Cr^{3+} loaded into apo-transferrin. **a)** UV-VIS spectrum and **b)** loading percentages determined by PB/HC-OES method from Cr^{3+}/C ratios and ICP-OES method with UV-VIS absorbance jointly to determine metal and protein concentrations for loading percentages.

Table 5.2 Cr^{3+} Loading into apo-Tf, incubated @ 37 ℃ for 24 h.

	ICP-OES	PB/HC-OES	
Molar Equivalent Additions of Cr^{3+}	**% Tf Loaded with Cr^{3+}**	**Cr^{3+}/C Ratio**	**% Tf Loaded with Cr^{3+}**
0	0	0	0
2	12.6 ± 1.8	0.220	12.7 ± 0.5
4	18.0 ± 2.1	0.242	18.4 ± 0.7
6	20.5 ± 2.8	0.248	20.0 ± 0.2
8	21.9 ± 2.4	0.253	21.2 ± 0.8
10	26.8 ± 3.5	0.268	25.3 ± 2.2

Kinetic Aspects of Chromium Loading

In order to determine if kinetics are limiting the exchange of Cr^{3+} from the solution environment to transferrin, excess sodium carbonate and a 10 molar equivalent excess of Cr^{3+} was added to a stock solution of apo-transferrin and allowed to incubate for 10 days. Figure 5.2 represents the UV-VIS spectra ranging from 225 – 650 nm for aliquots removed from the stock solution ranging from day 1 to day 10. As can be seen from the spectra, the absorbance bands observed at 254 and 298 nm increase as the sample undergoes longer incubation times. The background increases with each sample over the range of 300-650 nm, making it impossible to quantify the amount of Cr^{3+} loaded into apo-transferrin using the 428 nm spectral band. Analysis of these chromium-

transferrin complexes by the atomic spectroscopy methods confirms that changes in the absorbance spectra at 428 nm do not coincide with the actual amount of Cr^{3+} loaded into apo-transferrin. The data obtained from both instruments were in good agreement for all but the day 1 sample (p value < 0.05). Table 5.3 shows after 10 days of incubation the loading percentages increased to 49.7 ± 4.5 % and 55.7 ± 3.2 % transferrin loaded with Cr^{3+} as determined by the ICP-OES and PB/HC-OES methods, respectively. A loading value of ~ 55 % transferrin loaded with Cr^{3+} is closer to expectations based on the estimated stability constant for a Cr^{3+}-Tf complex.[10] Based on these results, it is necessary for Cr^{3+} to be in the presence of transferrin for an extended period of time (up to 10 days) to get maximum loading.

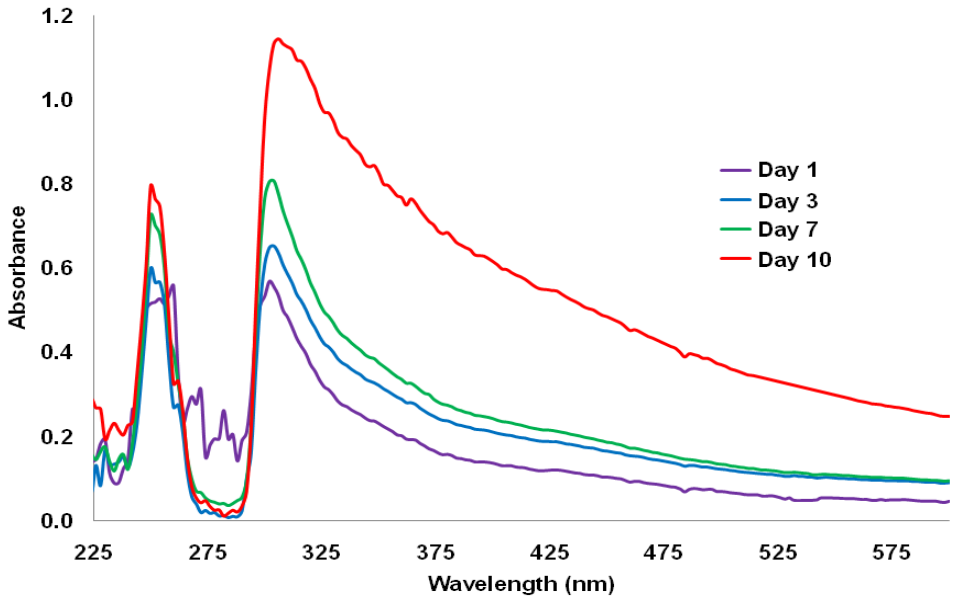

Figure 5.2 Cr^{3+} loading study over a 10 day period examined by UV-VIS absorbance.

Table 5.3 Kinetic study of Cr^{3+} loading into apo-Tf.

10 Molar Equivalents of Cr^{3+} Incubated for	ICP-OES % Tf Loaded with Cr^{3+}	PB/HC-OES Cr^{3+}/C Ratio	PB/HC-OES % Tf Loaded with Cr^{3+}
1 Day	35.5 ± 3.5	0.280	28.5 ± 2.9
3 Days	37.7 ± 3.9	0.308	35.9 ± 2.4
7 Days	47.8 ± 3.3	0.345	45.6 ± 3.4
10 Days	49.7 ± 4.5	0.383	55.7 ± 3.2

Anion Ligand Effects on Chromium Loading

Carbonate is a synergistic anion that is important for the binding of metal ions into the *N*- and *C*-terminus lobes of transferrin; without carbonate, metal-transferrin binding is weak.[5] Citrate is a chelating agent that is commonly used to load Cr^{3+} (i.e. chromium-citrate) into apo-transferrin in vitro, with pK_a (2.9, 4.3, and 5.6) all well below the physiological pH 7.4.[45] The presence of citrate and carbonate in solution with Cr^{3+} plays a role in the loading of chromium into apo-transferrin. Table 5.4 represents the loading percentages of transferrin bound with Cr^{3+} under various loading conditions with and without excess citrate and carbonate. The UV-VIS spectra (not presented here) of chromium nitrate and chromium chloride do not reflect the actual amount of Cr^{3+} that has been loaded into apo-transferrin. As presented above, the higher amounts of Cr^{3+} loaded into apo-transferrin result in an increased background that interferes with the 428 nm band so the study was monitored using the ICP-OES and PB/HC-OES methods.

Table 5.4 Anion and ligand effects on Cr^{3+} loading into apo-Tf, incubated @ 37 ℃ for 24 h.

	ICP-OES	PB/HC-OES	
10 Molar Equivalent Additions	**% Tf Loaded with Cr^{3+}**	**Cr^{3+}/C Ratio**	**% Tf Loaded with Cr^{3+}**
$Cr(NO_3)_3$	71.0 ± 3.1	0.437	69.1 ± 1.7
$Cr(NO_3)_3$ + citrate	57.2 ± 2.5	0.391	57.7 ± 0.8
$Cr(NO_3)_3$ + citrate + CO_3^-	31.0 ± 3.7	0.293	32.0 ± 0.2
$Cr(NO_3)_3$ + CO_3^-	28.8 ± 4.1	0.275	27.1 ± 1.3
$CrCl_3$	60.7 ± 2.1	0.411	63.0 ± 0.7
$CrCl_3$ + citrate	52.6 ± 3.3	0.373	53.2 ± 1.9
$CrCl_3$ + citrate + CO_3^-	35.5 ± 2.1	0.315	37.8 ± 1.7
$CrCl_3$ + CO_3^-	34.7 ± 3.9	0.304	34.8 ± 1.4

As demonstrated by the data presented in Table 5.4, the addition of anions limits the uptake of Cr^{3+} into transferrin as a larger amount of chromium was loaded into apo-transferrin when there was no citrate present. The loading percentages suggest that citrate is competing with transferrin for Cr^{3+} binding during the 24 hour incubation time. When comparing the nitrate versus chloride Cr^{3+} species, it would seem that the larger loading percentages observed for nitrate are due to it acting as a better synergistic anion than chloride when there is no excess carbonate present. Another possibility is the fact that chloride plays an important part in the release of iron from transferrin,[46] so the excess chloride may promote some loss of Cr^{3+} from the transferrin binding pocket. Once carbonate is introduced into the loading environment, the loading percentages are cut almost in half as a competition between carbonate and transferrin for chromium may be occurring in solution. Under these experimental conditions, the inertness of Cr^{3+} combined with the presence of carbonate results in lower

binding percentages of Cr^{3+} into apo-transferrin (i.e., with preference to carbonate). Bertini and co-workers studied the effects of chloride and carbonate on copper-transferrin complexes, presenting results showing that increased amounts of chloride will cause copper to be released from transferrin and that increased amounts of carbonate could cause the reloading of copper into transferrin.[47]

The results of the above experiments show that chromium binds into apo-transferrin more efficiently when citrate and carbonate are not present in excess. Under physiological conditions carbonate will always be present at 20 mM, thus this concentration of carbonate was used for the remainder of the studies. It was also revealed that it takes > 24 hours to get maximum loading amounts of Cr^{3+} into apo-transferrin. The kidneys remove most substances in approximately 24 hours, however the half life for chromium varies from 4 to 35 hours.[48] Therefore, the remainder of the studies presented here were kept at 24 hours to allow for closer approximations to equilibrium conditions and comparisons to other loading experiments. It was also deemed unnecessary to use citrate for the loading procedure, since there was suppression in loading observed with citrate. Additionally, serum concentrations of citrate would be 10x lower *in vivo* (~ 100 μM).[49]

Competitive Binding of Cr^{3+} and Fe^{3+} into Apo-Transferrin

To understand the effects of Cr^{3+} and Fe^{3+} binding into apo-transferrin under both low metal and excess metal conditions, various iron to chromium

ratios were introduced into the test media. Figure 5.3 represents the UV-VIS absorbance spectra of the competition between iron and chromium loading into apo-transferrin. Bands at 254 and 298 nm, which are non-specific to the identity of the metal loaded into transferrin, increase representing increased total metal ions bound to the tyrosine residues in the binding lobes. More importantly for these studies, there is an overlap of the bands at 428 and 470 nm for Cr^{3+} and Fe^{3+}, respectively, that makes determining the amount of each individual metal very difficult. Figures 5.4a and 5.4b graphically display the results of the competitive binding experiments for the two metal ions (Fe^{3+} and Cr^{3+}, respectively) as determined by ICP-OES (in conjunction with UV-VIS absorbance), PB/HC-OES, and UV-VIS absorbance. Fig. 5.4a displays the amount of Fe^{3+} loaded into apo-transferrin determined by all three methods. A noticeable difference in the amount of Fe^{3+} bound to transferrin can be seen for the situations where excess metal was used for the loading study. These discrepancies are most likely attributed to the spectral interferences and overlap of the two absorption bands for iron and chromium. Therefore, UV-VIS cannot be used by itself for determining the amount of iron bound when multiple metals are available for loading into apo-transferrin.

Figure 5.4b represents the amount of Cr^{3+} that was loaded into apo-transferrin under the competitive conditions. Note first that UV-VIS in and of itself is not applicable for Cr^{3+} loading determinations. Looking at the loading trends from the ICP-OES and PB/HC-OES methods, displayed Figs. 5.4a and 5.4b, there is no competition between Cr^{3+} and Fe^{3+} when added at a 2:2 molar

equivalent ratio (compared to the values of each metal ion separately). However, when the molar equivalent ratio of iron is 5 x that of chromium (10:2 ratio), the iron loading is 5.75 times that of chromium. In order to get equal amounts of Fe^{3+} to Cr^{3+} loaded into apo-transferrin, 5 times the amount of chromium to iron is required. When both metals are introduced to the apo-transferrin at excess (10:10 ratio), iron loads into apo-transferrin at a ratio 2.58 times greater than chromium. There are many reports suggesting that the presence of iron reduces the amount of chromium loading into transferrin and report a 1 Fe:1 Cr loading ratio,[44, 50-53] but these reports lack quantitative data to support this.

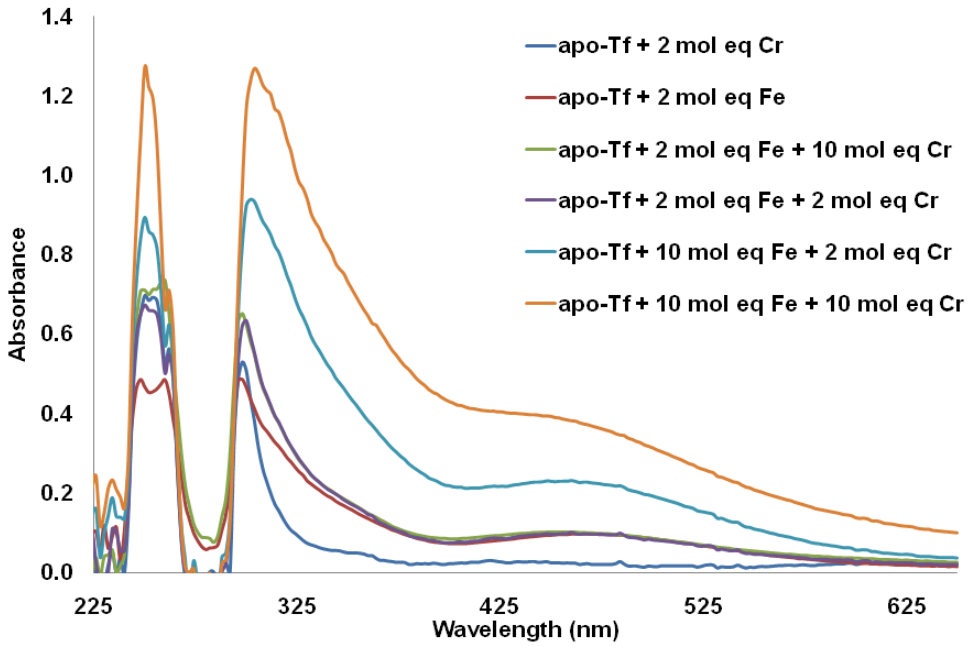

Figure 5.3 UV-VIS absorbance spectrum displaying the visual changes in LMCT bands caused by molar equivalent ratios of Fe^{3+} and Cr^{3+} competitions for loading into apo-transferrin.

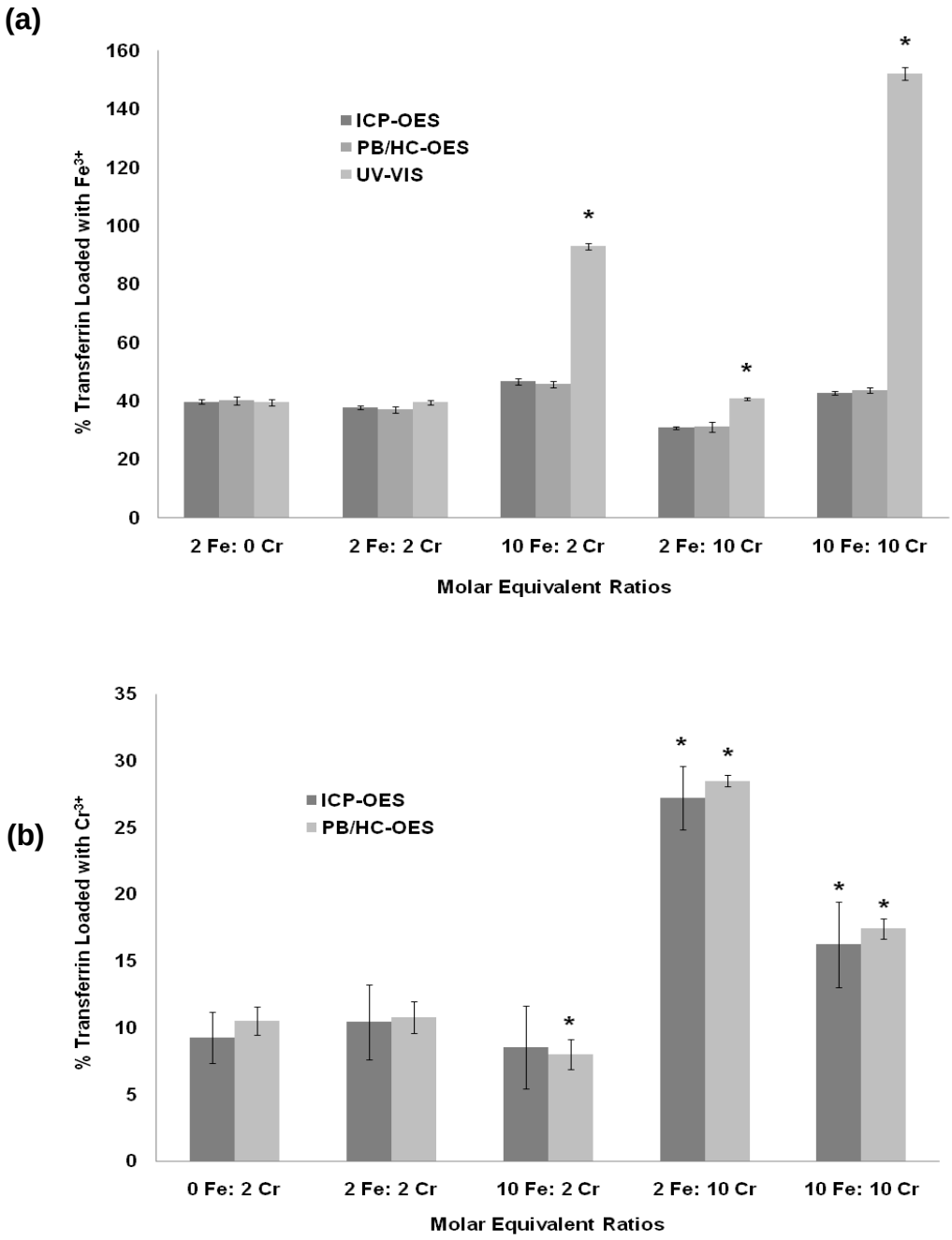

Figure 5.4 **a)** Displays a comparison of the Fe^{3+} loading percentages by UV-VIS, ICP-OES, and PB/HC-OES methods. * denotes a significant difference between the ICP-OES percentage and the UV-VIS absorbance percentage determined by p value < 0.05. **b)** Displays a comparison of the Cr^{3+} loading percentages by ICP-OES and PB/HC-OES methods. * denotes a significant difference from the first data points (0 Fe: 2 Cr) determined by p value < 0.05.

In summary the data suggests that in the case of excess Cr^{3+} (as might occur in cases of chromium toxicity), apo-transferrin binds up to 30% iron meaning that cells should still uptake close to the normal amount of iron.[5] According to Vincent, there may be a direct link between diabetes and hemachromatosis.[17] The data presented here reveals that chromium loading decreases under excess iron conditions (hemochromatosis patients), suggesting that hemochromatosis leads to lower chromium levels in the body. It is clear from the data that regardless of the amount of Cr exposure (up to 10X stoichiometry), the iron loading percentages always remain at or above the physiological values found in the body.

Competition of Cr^{3+} with Bound Iron in Holo-Transferrin

To further understand how Cr^{3+} affects Fe^{3+} loading into transferrin, molar equivalent additions of Cr^{3+} were added to holo-transferrin (~90% iron loaded, 1.8 Fe:1 Tf). The pH was monitored and maintained at 7.4 throughout the studies to assure that a change to more acidic conditions was not the cause of iron release. Although not shown here, the UV-VIS spectrum for molar additions of Cr^{3+} added to holo-transferrin reveals a decrease in Fe^{3+} loading due to the decrease in absorbance seen at 470 nm. As seen for the previous data, it is impossible to determine whether or not Cr^{3+} was loaded into the transferrin binding pockets after the iron was displaced using the UV-VIS absorbance spectrum alone. In order to determine the loading percentages for both metal ions, ICP-OES and PB/HC-OES methods were used. The data presented in

Figure 5.5 reflect a scenario wherein Cr^{3+} displaces the iron and is then loaded into the now empty binding pocket of transferrin. This is consistent with reports in the literature of decreased iron loading due to Cr^{3+} presence in the loading environment.[44, 50-53]

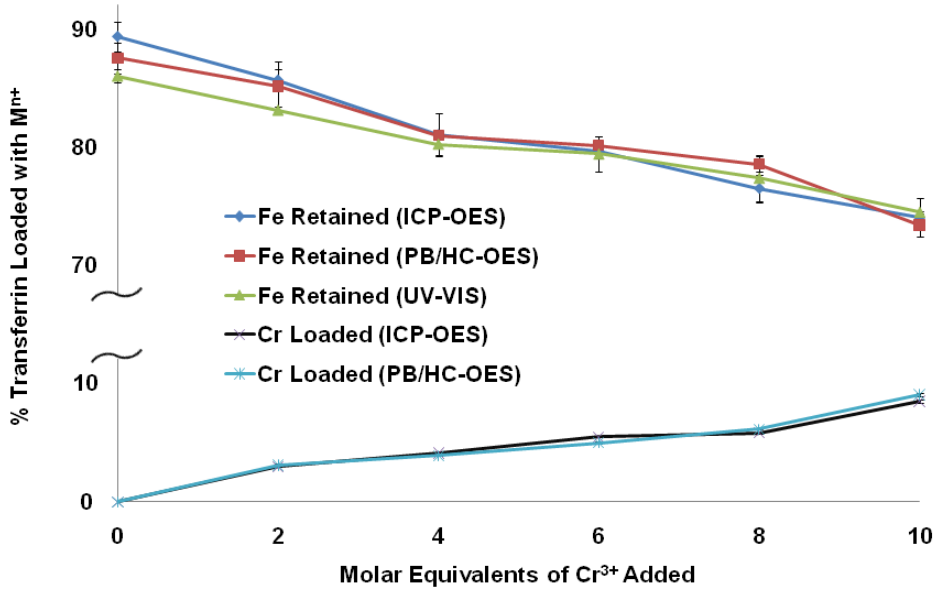

Figure 5.5 Displays the loading percentages of Fe^{3+} and Cr^{3+} as monitored by UV-VIS, ICP-OES, and PB/HC-OES methods for 0 – 10 molar equivalent additions of Cr^{3+} to holo-transferrin.

CONCLUSION

The data acquired from the PB/HC-OES method matches the data obtained from the ICP-OES method in combination with the UV-VIS spectrophotometer. This further supports the use of the PB/HC-OES method as a potential metallomics tool for studying metal binding proteins. The uniqueness

of this method allows acquisition of metal/protein ratios that are not affected by recovery losses and are a direct representation of the metal-protein complex. Spectral interference issues and overlapping LMCT absorbance bands with the UV-VIS spectra have been displayed for scenarios involving Cr^{3+}-transferrin complexes and multiple metals loaded into apo-transferrin. It must be made clear that UV-VIS absorbance is still a very useful technique and must be used jointly with the ICP-OES method. It has also been demonstrated that the PB/HC-OES method provides information that is normally collected from multiple instruments on a single platform.

Results of these studies provide new insight into Cr^{3+}/Fe^{3+}-transferrin chemistry. Due to the inert nature, loading of Cr^{3+} into apo-transferrin is much slower than for Fe^{3+} and requires up to 10 days to achieve 50 % loading. In order to get loading values similar to that of Fe^{3+} (~ 72% Fe loading reported previously with this same PB/HC-OES method[7]) non-physiological conditions were required. Although the presence of Cr^{3+} caused some inhibition of the ability for Fe^{3+} to be loaded into transferrin, 5 times the amount of chromium to iron was required to get an equal loading scenario (30% Fe: 30% Cr). This potentially means that even at ratios of 1 Fe: 0.8 Cr as might be seen with chromium toxicity, iron is still delivered into the cell. For the case where iron is in excess of up to 5 times that of Cr^{3+} there is a slight inhibition in the ability for Cr^{3+} to be loaded into apo-transferrin. In addition, holo-transferrin was observed to release Fe^{3+} in the presence of increasing amounts of Cr^{3+}.

REFERENCES

1. D. W. Koppenaal and G. M. Hieftje, *J. Anal. At. Spectrom.*, 2007, **22**, 855.

2. C. G. Fraga, *Mol. Asp. Medi.*, 2005, **26**, 235-244.

3. S. Mounicou, J. Szpunar and R. Lobinski, *Chem. Soc. Rev.*, 2009, **38**, 1119-1138.

4. J. A. Tainer, V. A. Roberts and E. D. Getzoff, *Cur. Opin. Biotech.*, 1991, **2**, 582-591.

5. H. Sun, H. Li and P. J. Sadler, *Chem. Rev.*, 1999, **99**, 2817-2842.

6. S. J. Lippard and J. M. Berg, in *Principles of Bioinorganic Chemistry*, University Science Books, Mill Valley, CA, 1994, pp. 141-148.

7. C. D. Quarles Jr, J. L. Brumaghim and R. K. Marcus, *Metallomics*, 2010, **2**, 154-161.

8. J. Williams and K. Moreton, *Biochem. J.*, 1980, **185**, 483-488.

9. H. Li, P. J. Sadler and H. Sun, *Eur. J. Biochem.*, 1996, **242**, 387-393.

10. H. Sun, M. C. Cox, H. Li and P. J. Sadler, *Struct. Bond.*, 1997, **88**, 71-102.

11. W. T. Cefalu and F. B. Hu, *Diabetes Care*, 2004, **27**, 2741-2751.

12. B. J. Clodfelder, J. Emamaullee, D. D. D. Hepburn, N. E. Chakov, H. S. Nettles and J. B. Vincent, *J. Biol. Inorg. Chem.,* 2001, **6**, 608-617.

13. B. J. Clodfelder, R. G. Upchurch and J. B. Vincent, *J. Inorg. Biochem.*, 2004, **98**, 522-533.

14. B. J. Clodfelder and J. B. Vincent, *J. Biol. Inorg. Chem.*, 2005, **10**, 383-393.

15. Y. N. Ordonez, M. Montes-Bayon, E. Blanco-Gonzalez, J. Paz-Jimenez, J. M. Tejerina-Lobo, J. M. Pena-Lopez and A. Sanz-Medal, *J. Anal. At. Spectrom.*, 2009, **24**, 1037-1043.

16. A. Pechova and L. Pavlata, *Veterin. Medic.*, 2007, **52**, 1-18.

17. J. B. Vincent, *J. Nutr.*, 2000, **130**, 715-718.

18. Y. Sun, J. Ramirez, S. A. Woski and J. B. Vincent, *J. Biol. Inorg. Chem.*, 2000, **5**, 129-136.

19. M. Silva, C. Heisel and T. P. Schmalzried, *Cur. Orthop. Pract.*, 2005, **430**, 53-61.

20. W. R. Harris, *Biochem.*, 1983, **22**, 3920-3926.

21. W. R. Harris, *J. Inorg. Chem.*, 1986, **27**, 41-52.

22. D. Esteban-Fernandez, M. Montes-Bayon, E. B. Gonzalez, M. M. Gomez Gomez, M. A. Palacios and A. Sanz-Medal, *J. Anal. At. Spectrom.*, 2008, 378-384.

23. J. Bettmer, M. M. Bayon, J. R. Encinar, M. L. Fernandez Sanchez, M. d. R. Fernandez de la Campa and A. Sanz-Medal, *J. Proteom.*, 2009, **72**, 989-1005.

24. J. S. Becker and N. Jakubowski, *Chem. Soc. Rev.*, 2009, **38**, 1969-1983.

25. M. Groessl, M. Terenghi, A. Casini, L. Elviri, R. Lobinski and P. J. Dyson, *J. Anal. At. Spectrom.*, 2010, **25**, 305-313.

26. S. Canarelli, I. Fisch and R. Freitag, *J. Chrom. A*, 2002, **948**, 139-149.

27. E. E. Battin, A. Lawhon, D. H. Hamilton and J. L. Brumaghim, *J. Chem. Educ.*, 2009, **86**, 969-972.

28. T. M. Brewer, J. Castro and R. K. Marcus, *Spectrochim. Acta, Part B: At. Spectr.*, 2006, **61B**, 134-149.

29. T. M. Brewer, B. Fernandez and R. K. Marcus, *J. Anal. At. Spectr.*, 2005, **20**, 924-931.

30. T. M. Brewer and R. K. Marcus, *J. Anal. At. Spectrom.*, 2007, **22**, 1067-1075.

31. T. M. Brewer and R. K. Marcus, *Anal. Chem.*, 2007, **79**, 2402-2411.

32. W. C. Davis, F. Jin, M. A. Dempster, J. L. Robichaud and R. K. Marcus, *J. Anal. At. Spectrom.*, 2002, **17**, 99-103.

33. M. A. Dempster, W. C. Davis, R. K. Marcus and P. R. Cable-Dunlap, *J. Anal. At. Spectrom.*, 2001, **16**, 115-121.

34. M. A. Dempster and R. K. Marcus, *J. Anal. At. Spectrom.*, 2000, **15**, 43-48.

35. F. Jin, J. J. Hickman, K. Lenghaus and R. K. Marcus, *Anal. Bioanal. Chem.*, 2004, **380**, 204-211.

36. F. Jin, J. J. Hickman, K. Lenghaus and R. K. Marcus, *J. Anal. At. Spectrom.*, 2004, **19**, 1199-1205.

37. F. Jin, K. Lenghaus, J. Hickman and R. K. Marcus, *Anal. Chem.*, 2003, **75**, 4801-4810.

38. F. Jin and R. K. Marcus, *J. Anal. At. Spectrom.*, 2003, **18**, 589-595.

39. C. D. Quarles Jr. and R. K. Marcus, *Spectrochim. Acta Part B: At.Spectr.*, 2009, **64**, 1185-1193.

40. J. You, M. A. Dempster and R. K. Marcus, *J. Anal. At. Spectrom.*, 1997, **12**, 807-815.

41. J. You, M. A. Dempster and R. K. Marcus, *Anal. Chem.*, 1997, **69**, 3419-3426.

42. J. You, P. A. Depalma, Jr. and R. K. Marcus, *J. Anal. At. Spectrom.*, 1996, **11**, 483-490.

43. J. You, J. C. Fanning and R. K. Marcus, *Anal. Chem.*, 1994, **66**, 3916-3924.

44. P. Aisen, R. Aasa and A. G. Redfield, *J. Biol. Chem.*, 1969, **244**, 4628-4633.

45. M. Barac-Nieto, *Am. J. Physiol. Renal. Physiol.*, 1984, **247**, 282-290.

46. D. H. Hamilton, I. Turcot, A. Stintzi and K. N. Raymond, *J. Biol. Inorg. Chem.*, 2004, **9**, 936-944.

47. I. Bertini, J. Hirose, H. Kozlowski, C. Luchinat and L. Messori, *Inorg. Chem.*, 1988, **27**, 1081-1086.

48. R. Petersen, J. F. Thomsen and N. K. Jorgensen, *Occup. Environ. Med.*, 2000, **57**, 140-142.

49. D. Tompkins and J. Toffaletti, *Clin. Chem.*, 1982, **28**, 192-195.

50. E. W. Ainscough, A. M. Brodie, J. E. Plowman, S. J. Bloor, J. S. Loehr and T. M. Loehr, *Biochem.*, 1980, **19**, 4072-4079.

51. M. Ani and A. A. Moshtaghie, *Biol. Trace El. Res.*, 1992, **32**, 57-64.

52. D. Harris, *Biochem.*, 1977, **16**, 560-564.

53. A. A. Moshtaghie, M. Ani and M. R. Bazrafshan, *Biol. Trace El. Res.*, 1992, **32**, 39-46.

CHAPTER SIX

COMPETITIVE BINDING OF Fe^{3+}, Cr^{3+}, AND Ni^{2+} TO TRANSFERRIN

INTRODUCTION

Iron is essential for cellular survival and is necessary in proteins for oxygen transport and electron transfer processes.[1] Human serum transferrin (Tf) is the iron transport protein responsible for delivering iron and a variety of other metals to cells.[2] It is an approximately 80 kDa protein consisting of two almost identical lobes, referred to as the *C*- and *N*-lobes, that can bind one metal ion each.[3] The binding pockets of Tf (Fig. 6.1) consist of aspartic acid, histidine, and two tyrosine residues, along with a carbonate ion that acts as a bidentate synergistic ion to complete the Fe^{3+} octahedral binding geometry. The binding constants for Fe^{3+} loading in transferrin *in vitro* are $K_{C\text{-lobe}} = 4.7 \times 10^{20}\ M^{-1}$ and $K_{N\text{-lobe}} = 2.4 \times 10^{19}\ M^{-1}$ for the *C*- lobe and *N*-lobe, respectively, indicating that Fe^{3+} binding to the *C*-lobe is approximately 20 times stronger than binding to the *N*-lobe.[4] Unsurprisingly, Fe^{3+} typically binds to the *C*-lobe first, followed by loading in the *N*-lobe.[3] Upon metal coordination to either binding pocket, the occupied lobe undergoes a conformational change from an open to a closed conformation.[5] Tf with both lobes in the closed conformation has the highest affinity for binding to the transferrin receptor protein (TfR) on cell surfaces. After receptor binding, the Tf-iron complex is taken into the cell by receptor mediated endocytosis.[6, 7] Normal iron saturation of Tf is typically around 30 %, but can vary among individuals. In serum it has been found that Tf is typically 27 %

diferric, 23 % monoferric *N*-lobe, 11 % monoferric *C*-lobe, and 40 % apo-transferrin.[8, 9] *In vitro*, Fe^{3+} release from the *C*-lobe and *N*-lobes occurs at somewhat different pH values.[7]

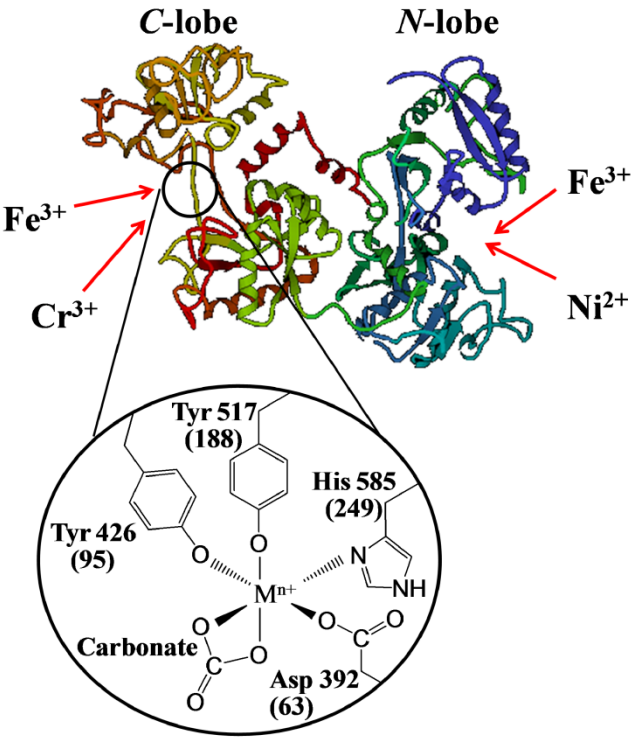

Figure 6.1 Representation of the transferrin protein (adapted from RCSB Protein Data Bank, 1AOV).[10] Arrows show the potential competition between Fe^{3+} and Cr^{3+} or Fe^{3+} and Ni^{2+} for Tf binding. The lower structure is a representation of the metal binding pocket consisting of histidine, aspartic acid, two tyrosines, and carbonate with sequence assignment for the *C*-terminal lobe (*N*-terminal lobe assignments in parentheses).

To regulate cellular iron uptake, transferrin receptor protein production decreases as Fe^{3+} levels within the cell increase; conversely, low cellular Fe^{3+} levels result in increased transferrin receptor protein production.[2] Normal iron

concentrations in human serum are approximately 18 μM, whereas Tf concentrations range from 25 – 50 μM.[3, 11] Iron deficiency can arise from an iron deficient diet, chronic disease, or inflammation.[12-14] Iron deficiency resulting from the aforementioned causes refers to conditions where Fe^{3+} is in the 4.0 – 9.0 μM range, and these low iron levels are usually associated with less than approximately 18 % of iron-loaded Tf.[12-14] In contrast, iron overload (greater than 36 μM Fe^{3+}) is defined as an iron saturation of Tf that exceeds approximately 45 %.[12] The most common cause of iron overload is hemochromatosis, a hereditary disease that causes increased iron absorption and eventually can cause organ damage, type 1 diabetes, cardiomyopathy, and arthritis.[12, 15]

As previously mentioned, under normal conditions only approximately 30 % of the potential Fe^{3+} binding sites in Tf are occupied, leaving unoccupied binding sites either in the *C*-lobe, *N*-lobe, or both, to potentially bind other metal ions.[7] Al^{3+} , Cr^{3+} , Cu^{2+}, Ga^{3+}, Ni^{2+}, Ti^{4+}, and Zn^{2+} are known to bind to Tf,[7, 16] and these metal ions could either compete with Fe^{3+} for Tf coordination or bind to the unoccupied lobes of Tf. Soft metal ions such as Pt^{2+} and Ag^{+} may also bind to sulfur-containing Met residues on the surface of Tf and be potentially carried into the cell during endocytosis.[17, 18] Other serum proteins, such as human serum albumin are also known to bind and transport metal ions,[19] so metal ion binding and transport in the blood is potentially a complex competition between available metal ions and proteins.[20]

Sadler, et al. reported that Cr^{3+} preferentially binds to the *C*-lobe of Tf,[3] suggesting that it has potential to compete with Fe^{3+} for that binding pocket. Experimental binding constants for Cr^{3+} are $K_{C\text{-lobe}} = 1.41 \times 10^{10}\ M^{-1}$ and $K_{N\text{-lobe}} = 2.04 \times 10^{5}\ M^{-1}$, suggesting that there would be limited or no competition with Fe^{3+} for Tf binding.[3, 7, 21] Sun, et al. reported an overall effective binding constant of $2.92 \times 10^{15}\ M^{-2}$ for Cr^{3+} binding to apo-Tf, a value weaker than that for Fe^{3+}, but suggesting that competition between Cr^{3+} and Fe^{3+} for Tf binding may occur at physiological pH. In contrast to Fe^{3+}, Cr^{3+} is a kinetically inert metal ion that requires up to 5 – 10 days to achieve maximum loading into apo-Tf,[22] likely leading to the discrepancies between the estimated and experimentally determined binding constants. Alternatively, Ni^{2+} is known to preferentially bind to the *N*-lobe of Tf.[3] The binding constants for Ni^{2+} are $K_{C\text{-lobe}} = 1.70 \times 10^{3}\ M^{-1}$ and $K_{N\text{-lobe}} = 1.26 \times 10^{4}\ M^{-1}$, much lower than for Fe^{3+}, suggesting that nickel may bind only to empty lobes instead of competing for Tf binding with Fe^{3+}.[23]

Cr^{3+} is a required metal ion proposed to play an important part in glucose metabolism.[24, 25] The recommended dietary intake for chromium is 50 – 200 µg per day, although only about 0.5 – 2.0 % of chromium is absorbed.[21, 26] Typical human serum Cr^{3+} concentrations are in the range of 6.0 nM to 0.5 µM, with toxic levels reported to be as low as 0.9 µM and as high as 19.0 µM.[27-29] Transferrin has been identified as a likely transporter of serum Cr^{3+}, suggesting that Tf-mediated Cr^{3+} uptake may be a prominent mechanism for chromium delivery into the cell. Once Cr^{3+} enters the cell, it binds to the chromium-binding peptide chromodulin, which in turn, activates insulin receptor kinase to lower insulin

concentration in the blood.[21, 25, 30] Vincent and co-workers have proposed that iron overload (hemochromatosis) may prevent chromium uptake by Tf, thus leading to insulin resistance and diabetes.[25] It is also possible that, under excess serum chromium conditions, Cr^{3+} binding to Tf interferes with normal iron uptake, thus affecting iron metabolism.[24]

Little is understood about the effects of nickel deficiency in humans, but nickel deficiency in rats can cause retarded growth, skeletal malformations, anemia, and glucose metabolism disorders.[26, 31] Additionally, nickel deficiency interferes with iron uptake from rat intestines, disrupting iron metabolism.[31] Typical serum Ni^{2+} concentrations are in the range of 4 nM to 0.8 µM, with toxic levels reported as low as 4.8 µM and as high as 10.3 µM.[28, 31-35] Insoluble nickel compounds exposed to cells gain entry via phagocytosis and are considered carcinogenic.[36, 37] Soluble nickel compounds are considered less carcinogenic, but can still disturb metal homeostasis within the cell.[38] Soluble Ni^{2+} ions enter cells by binding to Tf or competing with Mg^{2+} and/or Ca^{2+} transport via ion-channels.[26, 36] The literature available on Ni-Tf complexation is very sparse[23, 39] and, to our knowledge, competitive binding of nickel and iron to Tf has not been investigated.

The ability to detect simultaneous binding of multiple metals in transferrin is a difficult task. Semi-quantitative measurements can be made using UV-VIS absorbance spectroscopy, but the overlap of LMCT bands of multiple Tf-bound metal ions makes this difficult.[22] Atomic spectroscopy (e.g. inductively coupled plasma-optical emission spectroscopy) offers the best method for obtaining

multiple metal determinations for quantitative analysis. The major drawback for this method is the inability to detect the metal and protein concentrations simultaneously; an additional method is required to determine protein concentration. Both the Tf and metal concentrations are needed to determine the percentages of metal loading into Tf and thus ICP-OES and UV-VIS absorbance must be undertaken in parallel. The problem with this method is that two separate instruments must be used, requiring two different types of sample preparation and increasing the chances for measurement error. This problem of simultaneously measuring metal ions and protein can be overcome using the particle beam/hollow cathode-optical emission spectroscopy (PB/HC-OES) method. The PB/HC-OES plasma source operates under inert atmosphere conditions and allows simultaneous detection of metals and non-metals (by measuring, in this case, Fe (I), Ni (I), Cr (I), and C (I) emission signals).[18, 22, 40-42] Tf loading percentages are then calculated based on the emission ratio of metal to carbon, as the carbon emission intensity is reflective of the Tf concentration. This PB/HC-OES method compared favorably to UV-VIS absorbance and ICP-OES methods for determination of Fe^{3+} and Cr^{3+} loading into Tf.[18, 22]

In this work, the loading percentages for metal ions into human transferrin were monitored under a variety of physiologically relevant iron conditions (iron deficiency, chronic disease, inflammation, normal, and iron overload), providing insight as to how Cr^{3+} and Ni^{2+} Tf loading and perhaps transport are affected by iron deficient and excess scenarios. Additionally, kinetic studies of loading for Fe^{3+}, Cr^{3+}, and Ni^{2+} into Tf were performed to evaluate whether these metal ions

(at normal or excess amounts) change the uptake of iron under normal serum iron concentrations. Up to this point, instrumentation has been limited in the ability to investigate multiple metals for binding to Tf simultaneously. The method used here allows analysis of multiple metal ions in simultaneous competition for Tf binding, providing metal loading percentages for a variety of metal ions into Tf. Chapter 6 has been submitted to the *Journal of Biological Inorganic Chemistry.*

MATERIALS AND METHODS

Sample Preparation

All samples were prepared in 15 or 50 mL centrifuge tubes that were rinsed with 1M HCl prior to sample preparation to ensure that any contaminants (residual metals) were removed. High-purity (18.2 MΩ-cm) Barnstead Nanopure (Dubuque, IA) water was used to prepare solutions. Stock solutions of human apo-transferrin (50 µM, Sigma-Aldrich, St. Louis, MO) were prepared in Tris buffer (20 mM, TEKnova, Hollister, CA) at pH 7.4. Apo-Tf solutions contained no iron as measured by UV-VIS absorbance and PB/HC-OES methods. Sodium carbonate (20 mM, Sigma-Aldrich) was added to the transferrin stock solutions to maintain physiologically relevant conditions. Iron solutions were prepared by adding iron nitrate (45 µM, Sigma-Aldrich) and nitriloacetic acid (NTA, 90 µM, Sigma-Aldrich) in a 1:2 ratio, respectively, to hydrochloric acid (0.1 M, J. T. Baker, Phillipsburg, NJ) and adjusting the pH to 4.0.[43] Addition of $Fe(NTA)_2$ allows for selective loading of Fe^{3+} into the *C*-lobe of Tf.[4, 44] Chromium solutions were prepared by adding $Cr(NO_3)_3 \cdot 9H_2O$ (1000 µM, Sigma-Aldrich) to nanopure water. Nickel solutions were prepared by adding $Ni(NO_3)_2 \cdot 6H_2O$ (1000 µM,

Sigma-Aldrich) to nanopure water. Transferrin was loaded by adding the appropriate Cr^{3+}, Fe^{3+}, or Ni^{2+} concentrations (molar equivalents) to the apo-transferrin, followed by incubation at 37 ℃ for up to 24 h.[18] After the desired incubation time, the unbound metal ions, excess sodium carbonate, and excess NTA were separated from the metal-loaded transferrin using a desalting column (Sephadex™ G-25 M PD-10 column, GE Healthcare, Buckinghamshire, UK).[18] The sample (2 mL of M^{n+}-Tf, 50 μM) was added to the desalting column, and after initial 2 mL of Tf solution had completely entered the stationary phase an addition of 1 mL of Tris buffer was added to the column. After this 1 mL of buffer had completely moved into the column an additional 2 mL of Tris buffer was added to move the 2 mL fraction containing the M^{n+}-Tf complex out of the column for collection.[18] Control experiments were performed using a 2 mL Tris buffer solution containing iron, chromium, or nickel (500 μM) without addition of Tf. Using the same separation procedure, less than 3.5 μM of iron, chromium, or nickel was present in the fraction where the Tf complex would elute. Since this value for free metal ion concentration is less than the error reported in the loading percentages throughout these studies, unbound metal ions do not affect reported loading percentages. All solutions were measured for pH with an Accumet Research AR 10 pH meter (Fisher Scientific, Pittsburgh, PA) with an Accumet double junction Ag/AgCl pH probe (Fisher Scientific). Adjustments to pH were made with hydrochloric acid (6.0 M, Sigma-Aldrich) and sodium hydroxide (2.0 M, Sigma-Aldrich) to ensure all solutions for metal loading into transferrin were at pH 7.4.

Instrumentation

A particle beam/hollow cathode-optical emission spectrometer (PB/HC-OES) was used to analyze the metal-loaded transferrin samples.[18, 22, 41, 42, 45-50] Instrument parameters and method validation for Tf loading have been previously described.[18] Transferrin samples (200 µL) were injected into a liquid flow via a high performance liquid chromatography pump (1.0 mL min^{-1}) and introduced into a particle beam interface that consisted of a thermoconcentric nebulizer (creating an aerosol spray), desolvation chamber (desolvating particles), and a two-stage momentum separator (removing the solvent and nebulizer gases) leaving dry analyte particles to enter the HC glow discharge source. Once particles enter the source they are atomized, vaporized, and excited for subsequent photon detection using a 0.5-m Paschen-Runge polychromator (JY RF-5000) equipped with 26 photomultiplier tubes. This method allows the detection of both non-metals (C (I) 156.14 nm) and metals (Fe (I) 371.99 nm, Cr (I) 425.43 nm, and Ni (I) 341.47 nm) simultaneously. The Fe, Cr, and Ni emission responses for the metal-loaded transferrin complexes reflect how much metal is bound to Tf, and the carbon emission response (20 mM Tris buffer was used as the blank and was subtracted from total carbon emission response) is reflective of the Tf concentration. The percentage of carbonate bound to Tf in these loading studies is very small compared to the total carbon content of Tf (metal-bound carbonate contributes to 0.03 – 0.06 % of the carbon response and is therefore negligible). The metal and carbon emission responses yield an emission ratio that allows a loading percentage to be calculated that is independent of absolute

concentration.[18, 22] Reported loading percentages are the averages of triplicate determinations of separately prepared samples with calculated standard deviations.

RESULTS AND DISCUSSION

Studies Under Equilibrium Conditions

Transferrin is known as the iron transport protein, but empty lobes permit other metal ions to bind Tf. Cr^{3+} and Ni^{2+} transport by Tf has been suggested as a factor in the toxicity of these metal ions, since Tf binding may lead to increased cellular uptake.[7, 25] Therefore, the main goal of this study is to determine how Cr^{3+} and Ni^{2+} at normal and toxic levels affect iron loading into Tf under physiologically relevant conditions. Tf loading percentages are determined by the ratio of metal ion emission signal to carbon emission signal (reflects Tf concentration) for each sample as discussed in the experimental section.[18, 22]

Iron and Tf concentrations can vary depending on the individual.[2, 8, 9, 11] Table 6.1 lists the average measured amounts of Fe^{3+} and Tf found in the literature for serum under normal, iron deficient, chronic disease, inflammatory response, and iron overload conditions.[3, 7, 13-15] For conditions involving iron overload or iron deficiency, variations in the average amounts of Tf have been found compared to normal iron conditions. The molar ratio of Fe^{3+}/Tf was determined from the values in Table 6.1 to find the benchmark ratios for Fe-Tf loading used for comparison in this study. To provide a uniform baseline for these experiments, Tf concentrations were held constant (50 µM Tf in 20 mM Tris

buffer, 20 mM carbonate, and pH 7.4) to obtain the greatest signal to noise, and the Fe-Tf loading ratios were varied to mimic iron deficient and iron overload conditions. Theoretical loading values are based on loading of 2 metal ions to 1 Tf, meaning that a 2:1 ratio would equal 100% Tf loading.

Table 6.1 Reported iron and transferrin concentrations under different physiological conditions.

	Fe^{3+} (μM)	Tf (μM)	Ratio Fe^{3+}/Tf	Fe Loaded (Theoretical)
Normal[3,11]	18.0	35.0	0.510	25.5 %
Chronic Disease[12-14]	9.0	25.0	0.360	18.0 %
Inflammation[12-14]	6.0	34.0	0.176	8.8 %
Iron Deficient[12-14]	4.0	46.0	.0869	4.0 %
Iron Overload[12, 14]	36.0	25.0	1.44	72.0 %

Table 6.2 Reported concentrations of chromium and nickel in serum.

	Tf (μM)	Cr^{3+} (μM)	Ni^{2+} (μM)	Cr Loaded (Theoretical)	Ni Loaded (Theoretical)
Normal[26] Cr^{3+}	50.0	0.5	---	0.5 %	---
Elevated[28] Cr^{3+}	50.0	15.0	---	15.0 %	---
Normal[26] Ni^{2+}	50.0	---	0.8	---	0.8 %
Elevated[28, 51] Ni^{2+}	50.0	---	10.3	---	10.3 %

Table 6.2 lists the normal and elevated concentrations of chromium and nickel used for the metal binding studies.[26, 28, 51] The limits of quantification for chromium (0.3 μM) and nickel (0.8 μM) using the PB/HC-OES method[18, 22] dictated that the normal concentrations used were on the higher end of the normal ranges. Unless otherwise stated, iron and chromium or nickel was added to apo-transferrin (50 μM in Tris buffer at pH 7.4 with 20 mM carbonate) simultaneously to allow for competition of the metal ions for Tf binding.

Samples were then incubated for 24 hours at 37 ℃, de salted to remove any unbound metal and other ions, and then analyzed by the PB/HC-OES method to determine metal ion:Tf ratios that were used to calculate loading percentages.

Table 6.3 Measured loading of iron and chromium into transferrin under simulated physiological conditions. Values are averages of sample measurements performed in triplicate with calculated standard deviations.

	Fe (I)/C (I) Emission Ratio	**% Fe Loaded**	**Cr (I)/C (I) Emission Ratio**	**% Cr Loaded**
Normal (25.5 µM Fe^{3+}, 0.51 Fe:Tf)	0.0114	23.5 ± 2.0	---	---
+ 0.5 µM Cr^{3+}	0.0127	26.7 ± 1.1	0.00218	0.2 ± 1.3
+ 15.0 µM Cr^{3+}	0.0120	24.9 ± 2.6	0.291	11.8 ± 2.0
Chronic Disease (18.0 µM Fe^{3+}, 0.36 Fe:Tf)	0.00906	17.6 ± 2.5	---	---
+ 0.5 µM Cr^{3+}	0.00968	19.2 ± 2.2	0.00277	0.2 ± 1.6
+ 15.0 µM Cr^{3+}	0.00907	17.7 ± 3.1	0.331	13.4 ± 1.3
Inflammation (9.0 µM Fe^{3+}, 0.18 Fe:Tf)	0.00542	8.6 ± 1.2	---	---
+ 0.5 µM Cr^{3+}	0.00577	9.4 ± 0.9	0.0290	1.6 ± 0.8
+ 15.0 µM Cr^{3+}	0.00618	10.4 ± 1.9	0.331	13.4 ± 2.1
Iron Deficient (4.5 µM Fe^{3+}, 0.09 Fe:Tf)	0.00384	4.6 ± 1.9	---	---
+ 0.5 µM Cr^{3+}	0.00397	4.9 ± 1.4	0.0323	1.7 ± 1.2
+ 15.0 µM Cr^{3+}	0.00379	4.5 ± 2.3	0.355	14.4 ± 1.7
Iron Overload (72.0 µM Fe^{3+}, 1.44 Fe:Tf)	0.0300	69.9 ± 3.5	---	---
+ 0.5 µM Cr^{3+}	0.0298	69.5 ± 2.1	0	0
+ 15.0 µM Cr^{3+}	0.0272	63.1 ± 2.9	0.134	5.5 ± 1.5

The data presented in Tables 6.3 and 6.4 were obtained at a 24 h equilibrium state and indicate that under normal iron conditions (25.5 μM Fe^{3+}, 0.51 Fe:Tf), 23.5 ± 2.0 % of Tf was loaded with Fe^{3+}. As the ratio of Fe:Tf is decreased from the normal ratio, the percentages of Tf loaded with Fe also decrease. For chronic disease (18.0 μM Fe^{3+}, 0.36 Fe:Tf), inflammation (9.0 μM Fe^{3+}, 0.18 Fe:Tf), and iron deficient (4.5 μM Fe^{3+}, 0.09 Fe:Tf) simulated serum conditions, the percentage of Tf loaded with Fe^{3+} was found to be 17.6 ± 2.5 %, 8.6 ± 1.2 %, and 4.6 ± 1.9 % respectively. Under iron overload conditions (72.0 μM Fe^{3+}, 1.44 Fe:Tf), the amount of Tf loaded with iron was 69.9 ± 3.5 %.

Table 6.3 lists the iron and chromium loading observed at different iron and chromium concentrations. Under normal Cr^{3+} concentrations (0.5 μM, 0.01 Cr:Tf), the loading of Cr^{3+} into Tf is very low, but the data in Table 6.3 indicate that the average loading percentages of Cr^{3+} under inflammation and iron-deficient conditions are roughly 8 times greater than Cr^{3+} loaded under normal and chronic disease states. With elevated Cr^{3+} concentrations (15.0 μM, 0.30 Cr:Tf) typically found to be toxic, Cr^{3+} binding to Tf shows statistically the same loading values for the normal, iron deficient, chronic disease, and inflammation simulated conditions. In contrast, at iron overload concentrations, the chromium loading is half of what was found under normal iron conditions. Also, the iron loading percentage has decreased by approximately 6 % in the presence of elevated Cr^{3+}, suggesting Cr^{3+} competes with Fe^{3+} for Tf binding. Since it is known that the *C*-lobe of Tf is preferentially loaded using $Fe(NTA)_2$ as the iron source,[4, 44] and Cr^{3+} also preferentially loads into the *C*-lobe,[3] competition

between iron and chromium when *C*-lobe binding is at maximum capacity (more metal ions available than *C*-lobe sites) is likely.

Table 6.4 Measured loading of iron and nickel into transferrin under simulated physiological conditions. Values are averages of sample measurements performed in triplicate with calculated standard deviations.

	Fe (I)/C (I) Emission Ratio	**% Fe Loaded**	**Ni (I)/C (I) Emission Ratio**	**% Ni Loaded**
Normal (25.5 µM Fe^{3+}, 0.51 Fe:Tf)		23.5 ± 2.0	---	---
+ 0.8 µM Ni^{2+}	0.0261	23.9 ± 1.1	0.0124	0.5 ± 0.5
+ 10.3 µM Ni^{2+}	0.0238	21.1 ± 2.0	0.0407	10.0 ± 2.3
Chronic Disease (18.0 µM Fe^{3+}, 0.36 Fe:Tf)		17.6 ± 2.5	---	---
+ 0.8 µM Ni^{2+}	0.0205	16.9 ± 2.8	0.0178	2.3 ± 1.7
+ 10.3 µM Ni^{2+}	0.0202	16.5 ± 3.0	0.0376	8.9 ± 2.2
Inflammation (9.0 µM Fe^{3+}, 0.18 Fe:Tf)		8.6 ± 1.2	---	---
+ 0.8 µM Ni^{2+}	0.0155	10.5 ± 1.6	0.0133	0.8 ± 0.5
+ 10.3 µM Ni^{2+}	0.0153	10.3 ± 1.1	0.0284	5.8 ± 1.6
Iron Deficient (4.5 µM Fe^{3+}, 0.09 Fe:Tf)		4.6 ± 1.9	---	---
+ 0.8 µM Ni^{2+}	0.0117	5.7 ± 0.9	0.0119	0.3 ± 0.1
+ 10.3 µM Ni^{2+}	0.00795	4.0 ± 1.4	0.0248	4.6 ± 1.4
Iron Overload (72.0 µM Fe^{3+}, 1.44 Fe:Tf)		69.9 ± 3.5	---	---
+ 0.8 µM Ni^{2+}	0.0586	70.0 ± 3.6	0.0154	1.5 ± 0.7
+ 10.3 µM Ni^{2+}	0.0568	62.7 ± 1.6	0.0408	10.0 ± 2.5

Table 6.4 reports the measured iron and nickel Tf loading values under the different iron conditions. As observed for the chromium experiments, normal nickel concentrations (0.8 µM, 0.016 Ni:Tf) give very low loading values that are statistically indistinguishable from zero. At toxic nickel concentration (10.3 µM, 0.21 Ni:Tf), Ni^{2+} loading of Tf shows a trend that follows that of iron loading. As iron-Tf loading decreases, nickel-Tf loading also decreases, so that at iron deficiency and inflammation concentrations, nickel loading is roughly half of what was found at normal iron concentrations. As the iron loading increases, the nickel loading increases as well. $Fe(NTA)_2$ binding to the *C*-lobe of Tf causes a conformational change that closes this lobe,[7] and this conformational change may act as a trigger to help close the binding pocket of the *N*-lobe where Ni^{2+} is loosely bound (i.e., there is a synergistic effect). This idea is supported by the fact that Ni^{2+} preferentially binds the *N*-lobe of Tf, but with a much lower binding constant compared to Fe^{3+}.[23] Recent work by Groessl and co-workers reports increased binding of metallodrugs (cisplatin and Ru^{2+} complexes) to the empty binding pockets of Tf as the amount of iron-bound Tf increased.[52] Interestingly, iron loading into Tf under iron overload conditions (enough Fe^{3+} to fill the *C*-lobe and result in Fe^{3+} loading of the *N*-lobe) was reduced by high nickel concentrations. Since nickel binding occurs first in the *N*-lobe,[23] high concentrations of Ni^{2+} may inhibit iron from binding in the *N*-lobe, causing a slight decrease in Tf iron loading.

In summary, excess nickel and chromium only affect the iron loading in Tf under iron overload conditions. Chromium loading is lower when there is an

excess of Fe^{3+} available to load into Tf. In contrast, nickel loading is lower when iron levels are low, suggesting the need to have the *C*-lobe closed (i.e., bound with iron) to bind nickel efficiently in the *N*-lobe.

Kinetic Studies of Metal Binding

Transferrin in serum has a half life of approximately 1.35 h [53], whereas the half life of Tf-bound iron in serum is 50 min [2]. Therefore, understanding the loading of iron and chromium (or nickel) into apo-Tf as a function of incubation time may be useful to complete the picture of how metals compete with iron for binding to Tf. In the following studies, apo-Tf solutions with additions of iron and chromium (or nickel) ions were incubated, and samples were removed at time intervals up to 24 h before desalting for analysis by the PB/HC-OES method. Figure 6.2 displays the determined Fe^{3+} loading into Tf for iron alone (25.5 µM Fe^{3+}), iron and nickel (25.5 µM Fe^{3+} + 0.8 µM Ni^{2+}), and iron and chromium (25.5 µM Fe^{3+} + 0.5 µM Cr^{3+}) as a function of incubation time (Tables 6.5, 6.6, and 6.8). A small amount of Fe^{3+} loading into apo-Tf is instantaneous upon addition of $Fe(NTA)_{2,}$ [43] verified by the orange color change upon adding Fe^{3+} to the Tf solution. For iron only conditions, the data show an increase in iron loading starting at 8.23 ± 0.25 % at 1 h and ending at 24.17 ± 0.91 % after 24 h ($p = 0.0006$).

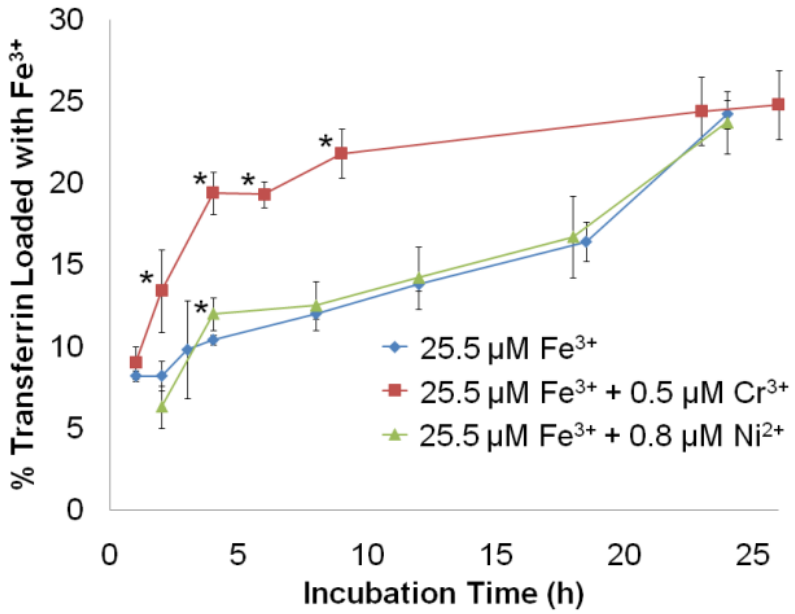

Figure 6.2 Comparison of iron loading percentages over a 24 h time period. Iron loading alone is compared with iron loading in the presence of normal Cr^{3+} and Ni^{2+} concentrations; asterisks denote *p* values < 0.05 in comparison to the Fe^{3+} only Tf loading. Error bars represent standard deviations of triplicate measurements.

Table 6.5 Effect of incubation time on iron loading into transferrin under "normal iron" concentration conditions (0.51 Fe:Tf). Values are averages of sample measurements performed in triplicate with calculated standard deviations.

Incubation Time (h)	Fe (I)/C (I) Emission Ratio	% Fe Loaded
1	0.00986	8.2 ± 0.3
2	0.00975	8.2 ± 0.9
3	0.0175	9.8 ± 3.0
4	0.0207	10.4 ± 0.3
8	0.0289	12.0 ± 0.3
12	0.0376	13.8 ± 0.4
18.5	0.0509	16.4 ± 1.2
24	0.0896	24.2 ± 0.9

Table 6.6 Role of incubation time on iron and chromium (0.5 µM, 0.01 Cr:Tf) loading into apo-transferrin under "normal iron" concentration conditions (0.51 Fe:Tf). Values are averages of sample measurements performed in triplicate with calculated standard deviations.

Incubation Time (h)	Fe (I)/C (I) Emission Ratio	% Fe Loaded	Cr (I)/C (I) Emission Ratio	% Cr Loaded
1	0.00939	9.0 ± 1.0	0.0124	0.3 ± 1.0
2	0.0132	13.4 ± 2.5	0.0137	0.3 ± 0.8
4	0.0180	19.4 ± 1.3	0.0180	0.4 ± 1.5
6	0.0179	19.3 ± 0.8	0.0178	0.4 ± 1.0
9	0.0199	21.8 ± 1.5	0.0179	0.4 ± 1.1
23	0.0225	24.4 ± 2.1	0.0482	1.1 ± 2.3
26	0.0215	24.8 ± 2.1	0.0482	1.1 ± 1.1

Table 6.7 Role of incubation time on iron and elevated chromium (15.0 µM, 0.30 Cr:Tf) loading into apo-transferrin under "normal iron" concentration conditions (0.51 Fe:Tf). Values are averages of sample measurements performed in triplicate with calculated standard deviations.

Incubation Time (h)	Fe (I)/C (I) Emission Ratio	% Fe Loaded	Cr (I)/C (I) Emission Ratio	% Cr Loaded
1	0.0914	8.2 ± 0.5	0.667	1.9 ± 0.4
2	0.106	10.3 ± 1.1	0.670	2.0 ± 0.3
3	0.135	14.4 ± 0.5	0.632	1.1 ± 1.6
4	0.146	15.9 ± 0.6	0.715	3.0 ± 1.2
8	0.191	22.3 ± 2.3	0.884	7.0 ± 2.2
12	0.190	22.2 ± 3.6	1.00	9.8 ± 1.6
18.5	0.195	22.9 ± 1.0	1.01	10.2 ± 2.9
24	0.208	24.7 ± 1.6	1.21	12.6 ± 1.6

Table 6.8 Role of incubation time on iron and nickel loading (0.8 µM, 0.016 Ni:Tf) into apo-transferrin under "normal iron" concentration conditions (0.51 Fe:Tf). Values are averages of sample measurements performed in triplicate with calculated standard deviations.

Incubation Time (h)	Fe (I)/C (I) Emission Ratio	% Fe Loaded	Ni (I)/C (I) Emission Ratio	% Ni Loaded
2	0.00431	6.3 ± 1.3	ND	ND
4	0.00817	12.0 ± 1.0	0.0291	0.2 ± 0.5
8	0.00854	12.5 ± 1.5	0.0435	0.5 ± 0.7
12	0.00971	14.2 ± 1.9	0.0643	0.8 ± 0.8
18	0.0114	16.7 ± 2.5	0.0717	1.0 ± 0.8
24	0.0162	23.7 ± 1.9	0.0728	1.0 ± 0.6

Table 6.9 Role of incubation time on iron and elevated nickel (10.3 µM, 0.21 Ni:Tf) loading into apo-transferrin under "normal iron" concentration conditions (0.51 Fe:Tf). Values are averages of sample measurements performed in triplicate with calculated standard deviations.

Incubation Time (h)	Fe (I)/C (I) Emission Ratio	% Fe Loaded	Ni (I)/C (I) Emission Ratio	% Ni Loaded
1	0.00515	6.3 ± 0.3	ND	ND
2	0.0159	10.0 ± 0.5	ND	ND
3	0.0216	11.9 ± 1.1	0.0505	2.7 ± 0.5
4	0.0257	13.4 ± 1.2	0.0668	5.0 ± 0.8
8	0.0272	13.9 ± 1.8	0.0813	7.1 ± 1.5
12	0.0358	16.8 ± 4.2	0.0910	8.4 ± 2.2
18.5	0.0361	16.9 ± 1.6	0.0991	9.6 ± 0.4
24	0.0532	22.8 ± 5.9	0.114	11.7 ± 2.0

The effect of the addition of 0.5 μM Cr^{3+} (0.01 Cr:Tf) on iron uptake by Tf is presented in Fig. 6.2. Cr^{3+} is kinetically very inert compared to Fe^{3+}, and maximal loading of Cr^{3+} into Tf may take up to 5 -10 days;[22] however, the short half-life of Tf in the serum would not allow full Cr^{3+} binding under physiological conditions. In the presence of Cr^{3+} and Fe^{3+}, Fe^{3+} binding to Tf increases in comparison to the addition of Fe^{3+} alone. Figure 6.3 displays the determined Fe^{3+} loading into Tf for iron alone (25.5 μM Fe^{3+}), iron and nickel (25.5 μM Fe^{3+} + 10.3 μM Ni^{2+}), and iron and chromium (25.5 μM Fe^{3+} + 15.0 μM Cr^{3+}) as a function of incubation time (Tables 6.5, 6.6, and 6.8). The data in Fig. 6.3 indicate that the presence of excess Cr^{3+} (15.0 μM, 0.30 Cr:Tf) increases Fe^{3+} binding to Tf when compared to Fe^{3+} alone and slightly more than Fe^{3+} plus 0.5 μM Cr^{3+} (0.01 Cr:Tf). Under these loading conditions, the concentrations of Fe^{3+} and Cr^{3+} are less than the concentration required to potentially fill 50 % of the binding sites in Tf. Therefore, it is likely that the *C*-lobe of Tf is the only lobe being filled based, on the larger formation constants of Fe^{3+} and Cr^{3+} for *C*-lobe binding. If competition were occurring between Cr^{3+} (15.0 μM, 0.30 Cr:Tf) and Fe^{3+} (0.51 Fe:Tf) for Tf loading, a decrease in the uptake of Fe^{3+} into Tf would be observed. Comparison of the loading percentages for iron into apo-Tf with Fe^{3+} alone (24.2 %, Fig. 6.3) and Fe^{3+} + Cr^{3+} (24.7 %, Fig. 6.3) reveals no change in Fe^{3+}-Tf binding percentage.

In contrast, the amount of Cr^{3+} loaded into apo-Tf (under high Cr^{3+} conditions) in the presence of normal Fe^{3+} concentrations increases from 1.9 ± 0.4 % at 1 h to 12.6 ± 1.6 % after 24 h (Fig. 6.4). In comparison, 0.5 μM Cr^{3+}

(0.01 Cr:Tf) addition resulted in a 1.1 ± 1.1 % loading value after 24 h, whereas 15.0 µM Cr^{3+} (0.30 Cr:Tf, 30 times the normal Cr^{3+} concentration) increased the loading value to 12.6 ± 1.6 %, approximately 12 times the amount of Cr^{3+} being loaded into apo-Tf under normal Cr^{3+} concentrations (Fig. 6.4).

As discussed previously, nickel binds more tightly to the *N*-lobe of Tf and therefore should have little effect on Fe^{3+} uptake into Tf when it is less than 50 % iron loaded. Figure 6.2 shows the loading percentages of 0.51 Fe:Tf (normal) and 0.016 Ni:Tf (0.8 µM Ni^{2+}, normal) over 24 h. At normal Ni^{2+} concentrations, the loading percentage of iron (23.7 %) is very similar to Tf loading with iron

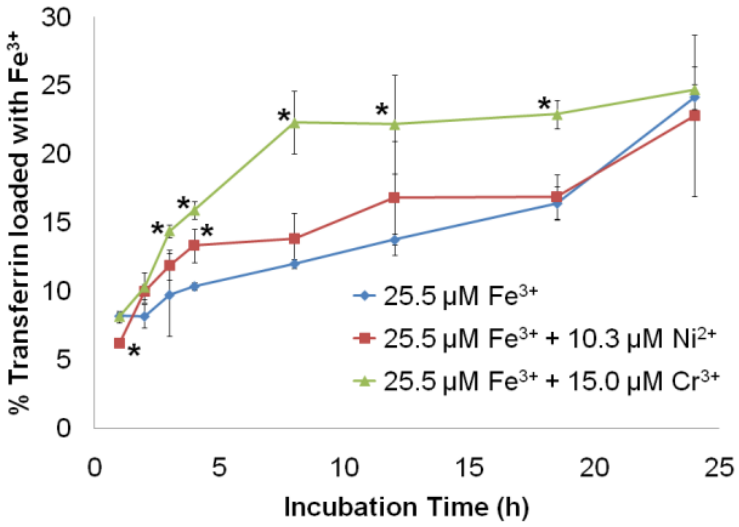

Figure 6.3 Comparison of iron loading percentages over a 24 h time period. Iron loading alone is compared with iron loading in the presence of toxic Cr^{3+} and Ni^{2+} concentrations; asterisks denote *p* values < 0.05 in comparison to the Fe^{3+} only Tf loading. Error bars represent standard deviations of triplicate measurements.

alone (24.2 %, Fig. 6.2). At toxic nickel concentrations (10.3 µM, 0.21 Ni:Tf), the iron loading is similar (22.8 %), but the iron loading after the first 4 h significantly increases in comparison to the iron loading found at normal Ni^{2+} concentrations (Fig. 6.3).

Overall, Fe^{3+} uptake into Tf is slower when Ni^{2+} is present than when Cr^{3+} is present, and significant Ni^{2+} loading did not occur until the 4 h time point (Fig. 6.4; Tables 6.6-6.9). The formation constants for Fe^{3+} and Ni^{2+} favor binding to Tf in the *C*-lobe and *N*-lobe, respectively, and as a result it is possible that Fe^{3+} binding to one lobe of Tf results in a conformational change that helps to close the binding pocket where Ni^{2+} may be loosely bound.

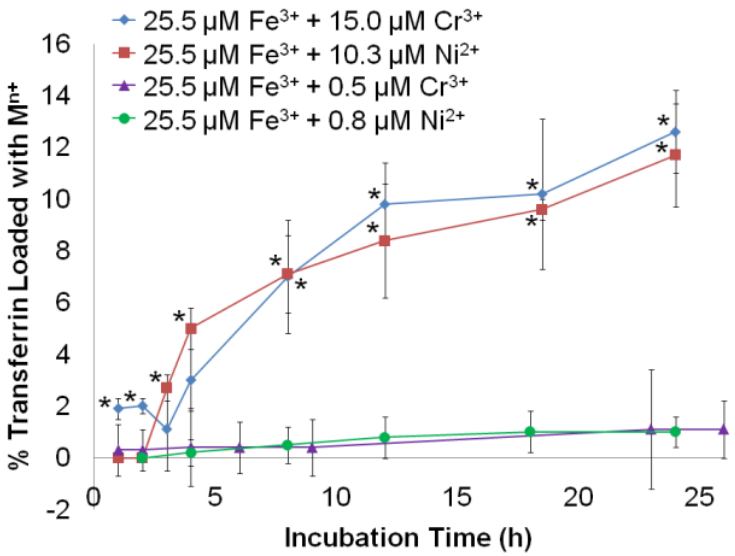

Figure 6.4 Comparison of Cr^{3+} and Ni^{2+} loading percentages in the presence of normal iron concentrations over 24 h. Loading of chromium and nickel at toxic concentrations is compared with the loading of Cr^{3+} and Ni^{2+} normal concentrations; asterisks denote *p* values < 0.05 in comparison to the normal Cr^{3+} or Ni^{2+} loading results. Error bars represent standard deviations of triplicate measurements.

The data in Figs. 6.2 and 6.3 indicate that the presence of Cr^{3+} and Ni^{2+} ions does not change the overall percentage of Fe^{3+} loaded into Tf after 24 h. The initial rate for Fe^{3+} loading alone was found to be 0.8 ± 0.2 μM^{-1} h^{-1}; this iron-Tf loading rate increases by approximately 3-fold in the presence of high chromium or nickel concentrations (2.7 ± 0.4 μM^{-1} h^{-1} ($p = 0.002$) and 2.3 ± 0.4 μM^{-1} h^{-1} ($p = 0.003$), respectively. Accurate initial rates for Cr^{3+} or Ni^{2+} loading could not be determined due to the low percentage loading for these metal ions. Although the initial iron uptake rate differs depending on the presence of metal ions in addition to iron, the overall metal loading percentages in all three cases are essentially the same after 24 h. These studies represent the first kinetic measurements of multiple metal ions binding simultaneously to Tf.

The final study to determine how these metal ions affect Tf loading was conducted by first loading Tf with 50 % Fe^{3+} so that, in theory, the *C*-lobe of Tf would be completely filled and the *N*-lobe would be vacant.[4, 44] The *C*-lobe of Tf is preferentially loaded using $Fe(NTA)_2$ as the iron source;[4, 44] therefore, enough iron was introduced to result in a 50 % Fe^{3+} loaded Tf complex in the *C*-lobe. After removal of unbound iron from the Fe^{3+}-Tf solution, Cr^{3+} (15.0 µM, 0.30 Cr:Tf) and/or Ni^{2+} (10.3 µM, 0.21 Ni:Tf) solutions were added to the pre-iron-loaded Tf samples and incubated for 24 h before removal of unbound metal ions.

Table 6.5 displays the loading results for additions of chromium and nickel to a 50 % pre-iron loaded Tf complex. Addition of Cr^{3+} (15.0 µM, 0.30 Cr:Tf) has a negative effect on Fe^{3+} loading, since approximately 13 % of Tf bound with Fe^{3+} was lost. In addition to the loss of iron, 7.6 ± 1.3 % of Tf was bound with Cr^{3+},

suggesting that displacement of iron from the Tf binding pocket occurs under excess chromium conditions and that Cr^{3+} may be binding to the *C*-lobe of Tf. Addition of Ni^{2+} (10.3 µM, 0.21 Ni:Tf) did not displace iron from Tf. In addition, it was also observed that 10.7 ± 1.5 % of Tf was loaded with Ni^{2+} under these conditions with no appreciable change in Fe^{3+} loading. This result suggests that Ni^{2+} may bind to the *N*-lobe and that there may be no direct competition with iron loading. When both Cr^{3+} (15.0 µM, 0.30 Cr:Tf) and Ni^{2+} (10.3 µM, 0.21 Ni:Tf) are introduced simultaneously to compete with the pre-loaded Fe^{3+}-Tf, displacement of Fe^{3+} from Tf is consistent with that from the Cr^{3+}-only samples (34.4 ± 1.3 % and 37.4 ± 4.2 %, respectively). The amount of Cr^{3+} and Ni^{2+} loaded into the pre-loaded Fe^{3+}-Tf, both simultaneously (6.9 ± 2.3 % Cr^{3+} and 9.3 ± 3.2 % Ni^{2+}) and separately (7.6 ± 1.3% Cr^{3+} and 10.7 ± 1.5 % Ni^{2+}), are statistically indistinguishable. Therefore, it is likely that Cr^{3+} competes for binding of the *C*-lobe with Fe^{3+}, whereas it is likely that Ni^{2+} is loaded only into the *N*-lobe and does not compete with Fe^{3+} binding in the *C*-lobe. Taken together, this work suggests that Tf maintains approximately 30 % Fe^{3+} loaded Tf even in the presence of other metal ions. The ability to directly measure metal ion competition for Tf binding using the novel PB-HC/OES method provides insight into how potentially toxic metals may be transported in the blood and how the presence of these metal ions affect normal iron uptake by Tf.

Table 6.10 Effects of high Cr^{3+} (15.0 µM, 0.30 Cr:Tf) and Ni^{2+} (10.3 µM, 0.21 Ni:Tf) concentrations on 50 % iron-loaded transferrin; *p* values obtained in comparison to 50.8 ± 1.9 % Tf bound with Fe^{3+}. Error bars represent standard deviations of triplicate measurements.

Transferrin	% Fe Loaded (p value)	% Cr Loaded	% Ni Loaded
50 % Iron Loaded	50.8 ± 1.9	---	---
+ 15.0 µM Cr^{3+}	37.4 ± 4.2 (0.015)	7.6 ± 1.3	---
+ 10.3 µM Ni^{2+}	48.1 ± 2.4 (0.208)	---	10.7 ± 1.5
+ 15.0 µM Cr^{3+} + 10.3 µM Ni^{2+}	34.4 ± 1.3 (< 0.001)	6.9 ± 2.3	9.3 ± 3.2

CONCLUSIONS

The use of the PB/HC-OES method allows monitoring of the direct competition of metal ions binding to Tf to be analyzed simultaneously, giving a comprehensive understanding of how each metal ion is interacting with Tf. Fe^{3+} loading to transferrin was not affected by introduction of other metal ions (i.e., Cr^{3+} and Ni^{2+}) at normal or excess (toxic) concentrations. Transferrin binding of Cr^{3+} is affected only when the amount of Fe^{3+} is in extreme excess (greater than 50 % Fe^{3+} loaded), as in the case with iron-overload serum conditions. For Ni^{2+}, Tf binding is only affected when iron concentrations are extremely low. In fact, Ni^{2+} loading into Tf increases when Fe^{3+} is bound in Tf, an effect that has not been previously noted. Addition of a competing metal ion (chromium or nickel) increases initial loading of Fe^{3+} into Tf; however, the same overall iron loading percentages (24.2 %, 24.7 %, and 22.8 %) are achieved after 24 h. When predicting binding behavior of metal ions with Tf, both binding affinity and lability

need to be considered. This method has provided insight into how metal ions compete with Fe^{3+} for Tf binding and suggests that the preferential lobe loading of the metal ion in Tf may be a critical factor in determining metal competition for Tf binding.

REFERENCES

1. S. J. Lippard and J. M. Berg, in *Principles of Bioinorganic Chemistry*, University Science Books, Mill Valley, CA, 1994, pp. 141-148.

2. A. C. G. Chua and R. M. Graham, *Crit. Rev. Clin. Lab. Sci.*, 2007, **44**, 413-459.

3. H. Sun, M. C. Cox, H. Li and P. J. Sadler, *Struct. Bond.*, 1997, **88**, 71-102.

4. P. Aisen, A. Leibman and J. Zweier, *Biol. Chem.*, 1978, **253**, 1930-1937.

5. J. G. Grossman, M. Neu, R. W. Evans, P. F. Lindley, H. Appel and S. S. Hasnain, *J. Mol. Biol.*, 1993, **229**, 585-590.

6. A. Dautry-Varsat, A. Ciechano and H. F. Lodish, *Proc. Natl. Acad. Sci.*, 1983, **80**, 2258-2262.

7. H. Sun, H. Li and P. J. Sadler, *Chem. Rev.*, 1999, **99**, 2817-2842.

8. H. Huebers, B. Josephson, E. Huebers, E. Csiba and C. Finch, *Proc. Natl. Acad. Sci. USA*, 1981, **78**, 2572-2576.

9. J. Williams and K. Moreton, *Biochem. J.*, 1980, **185**, 483-488.

10. A. Rawas, K. Moreton, H. Muirhead and J. Williams, *J Mol. Biol.*, 1989, **208**, 213-214.

11. S. L. Byrne and A. B. Mason, *J Biol Inorg Chem*, 2009, **14**, 771-781.

12. M. W. Hentze, M. U. Muckenthaler, B. Galy and C. Camaschella, *Cell*, 2010, **142**, 24-38.

13. K. Punnonen, K. Irjala and A. Rajamaki, *Clin. Chem.*, 1994, **40**, 774-776.

14. K. Punnonen, K. Irjala and A. Rajamaki, *Blood*, 1997, **89**, 1052-1057.

15. R. V. Anderson, A. Tybjaerg-Hansen, M. Appleyard, H. Birgens and B. G. Nordestgaard, *Blood*, 2004, **103**, 2914-2919.

16. A. D. Tinoco and A. M. Valentine, *J. Am. Chem. Soc.*, 2005, **127**, 11218-11219.

17. M. C. Cox, K. J. Barnham, T. A. Frenkiel, J. D. Hoeschele, A. B. Mason, Q.-Y. He, R. C. Woodworth and P. J. Sadler, *J. Biol. Inorg. Chem.*, 1999, **4**, 621-631.

18. C. D. Quarles Jr, J. L. Brumaghim and R. K. Marcus, *Metallomics*, 2010, **2**, 154-161.

19. J. Masuoka, J. Hegenauer, B. R. Van Dyke and P. Saltman, *J. Biol. Chem.*, 1993, **268**, 21533-21537

20. A. D. Tinoco, E. V. Eames and A. M. Valentine, *J. Am. Chem. Soc.*, 2008, **130**, 2262-2270.

21. B. J. Clodfelder, J. Emamaullee, D. D. D. Hepburn, N. E. Chakov, H. S. Nettles and J. B. Vincent, *J. Biol. Inorg. Chem.*, 2001, **6**, 608-617.

22. C. D. Quarles Jr, J. L. Brumaghim and R. K. Marcus, *Metallomics*, 2010, **2**, 792-799.

23. W. R. Harris, *J. Inorg. Chem.*, 1986, **27**, 41-52.

24. W. T. Cefalu and F. B. Hu, *Diabetes Care*, 2004, **27**, 2741-2751.

25. J. B. Vincent, *J. Nutr.*, 2000, **130**, 715-718.

26. R. K. Zalups and J. Koropatnick, *Molecular Biology and Toxicology of Metals*, Taylor and Francis Inc., New York, 2000.

27. K. N. Jeejeebhoy, *Nutr. Rev.*, 1999, **57**, 329-335.

28. N. Lavi and Z. B. Alfassi, *Analyst*, 1990, **115**, 817-822.

29. J. B. Vincent, *Acc. Chem. Res.* , 2000, **33**, 503-510.

30. B. J. Clodfelder, R. G. Upchurch and J. B. Vincent, *J. Inorg. Chem*, 2004, **98**, 522-533.

31. E. Denkhaus and K. Salnikow, *Crit. Rev. Oncology/Hematology*, 2002, **42**, 35-56.

32. J. M. H. Howard, *Clin Chem*, 1980, **26**, 1515.

33. E. L. Noveli, N. L. Rodrigues and B. O. Ribas, *Hum. Exp. Toxicol.*, 1995, **14**, 248-251.

34. F. W. Sunderman, B. Dingle, S. M. Hopfer and T. Swift, *Am. J. Ind. Med.*, 1988, **14**, 257-266.

35. D. M. Templeton, F. W. Sunderman Jr and R. F. M. Herber, *Sci. Tot. Environ.*, 1994, **148**, 243-251.

36. M. Costa, Z. Zhuang, X. Huang, S. Cosentino, C. B. Klein and K. Salnikow, *Sci. Total Environ.*, 1994, **148**, 191-199.

37. K. S. Kasprzak, P. Gabryel and K. Jarczewska, *Carcinogenesis*, 1983, **4**, 275-279.

38. H. Chen, T. Davidson, S. Singleton, M. D. Garrick and M. Costa, *Toxicol. Appl. Pharmacol.*, 2005, **206**, 275-287.

39. T. Davidson, H. Chen, M. D. Garrick, G. D'Angelo and M. Costa, *Mol. Cell. Biochem.*, 2005, **279**, 157-162.

40. T. M. Brewer and R. K. Marcus, *Anal. Chem.*, 2007, **79**, 2402-2411.

41. M. A. Dempster and R. K. Marcus, *J. Anal. At. Spectrom.*, 2000, **15**, 43-48.

42. F. Jin and R. K. Marcus, *J. Anal. At. Spectrom.*, 2003, **18**, 589-595.

43. E. E. Battin, A. Lawhon, D. H. Hamilton and J. L. Brumaghim, *J. Chem. Educ.*, 2009, **86**, 969-972.

44. R. W. Evans and J. Williams, *Biochem J.*, 1978, **173**, 543-552.

45. T. M. Brewer, J. Castro and R. K. Marcus, *Spectrochim. Acta, Part B: At. Spect.*, 2006, **61B**, 134-149.

46. T. M. Brewer, B. Fernandez and R. K. Marcus, *J. Anal. At. Spectrom.*, 2005, **20**, 924-931.

47. F. Jin, K. Lenghaus, J. Hickman and R. K. Marcus, *Anal. Chem.*, 2003, **75**, 4801-4810.

48. C. D. Quarles Jr. and R. K. Marcus, *Spectrochim. Acta, Part B: At. Spect.*, 2009, **64**, 1185-1193.

49. J. You, M. A. Dempster and R. K. Marcus, *Anal. Chem.*, 1997, **69**, 3419-3426.

50. J. You, J. C. Fanning and R. K. Marcus, *Anal. Chem.*, 1994, **66**, 3916-3924.

51. C. Minoia and A. Cavalleri, *Sci. Total Environ.*, 1988, **71**, 323-327.

52. M. Groessl, M. Terenghi, A. Casini, L. Elviri, R. Lobinski and P. J. Dyson, *J. Anal. At. Spectrom.*, 2010, **25**, 305-313.

53. S. Osaki, D. A. Johnson and E. Frieden, *J. Biol. Chem.*, 1966, **241**, 2746-2751.

CHAPTER SEVEN

SUMMARY

The research presented here displays the utility of the particle beam glow discharge source for both optical emission spectroscopy and mass spectrometry to analyze a wide range of samples obtaining both elemental and molecular species information simultaneously. The use of the PB/HC-OES has been demonstrated as a valuable tool for monitoring the competitive metal loading characteristics of Tf. Chapter 1 introduced the need for new instrumentation for the area of Metallomics based research and introduced glow discharge as a viable source for obtaining elemental and molecular species information simultaneously. Accordingly, the glow discharge kinetic processes, basic geometries, and operational modes are described in detail. Chapter 1 also describes the basis for the introduction of a liquid flow into a glow discharge source using the particle beam technology.

Chapter 2 provided a detailed evaluation of the operational parameters that were used for the PB/HC source once it was mounted onto the front of the existing JY RF-5000 polychromator. The instrument parameters determined in this study were used as the basis for the remainder of the work involving the PB/HC-OES system. Additionally, a mixture of metals (Ag, Ni, and Pb) was analyzed by the PB/HC-OES system to determine analytical responses. This chapter shows the potential of the PB/HC-OES system to determine interelement

and matrix effects and the ability to simultaneously monitor element emission responses for protein determinations.

Chapter 3 presented the conversion of a commercially available HP5973 GC-MS to a LC-PB/GDMS utilizing the Genesis II PB interface made available from CSS Analytical Inc. The conversion of an existing GC-MS into a LC-PB/GDMS allowed generation of molecular and elemental information simultaneously, within a single LC separation. The optimum sample introduction and glow discharge operating conditions were determined using caffeine as a test solution. These parameters were used to obtain the analytical responses for a variety of organic and inorganic samples using the LC-PB/GDMS system. This chapter outlined the conversion, operation, and potential use of this instrument as a tool for comprehensive speciation analysis.

Chapter 4 demonstrated how the PB/HC-OES system can be used in metallomics-based research. Validation of the method was performed by monitoring the loading of Fe^{3+} into apo-Tf by both the PB/HC-OES and UV-VIS absorbance methods (from the literature) and the agreement of both methods were found to be in good correlation, 71.2 ± 4.7 % and 67.5 ± 2.5 % respectively. In addition to Fe^{3+} loading into apo-Tf, Ni^{2+} and Zn^{2+} were loaded into apo-Tf and monitored using the PB/HC-OES method. Interestingly, Ag^{+} was found to bind to the surface of Tf, it is believed to bind to Tf in a similar fashion to Pt^{2+}, binding to the surface methionines.

Chapter 5 provided further validation of the PB/HC-OES method for monitoring Cr^{3+} loading into apo-Tf. Comparison of the loading percentages

obtained by the PB/HC-OES method to an ICP-OES/UV-VIS absorbance method showed good agreement in determining the amount of Cr^{3+} loaded into apo-Tf. It was determined that the loading of Cr^{3+} into apo-Tf, which is inert compared to Fe^{3+}, takes 5 – 10 days to reach maximum values. This chapter also presented some of the pitfalls to using UV-VIS absorbance for monitoring metal ions other than Fe^{3+} or in competition with Fe^{3+}. It was shown that an atomic spectroscopy method (ICP-OES or PB/HC-OES) was necessary to evaluate the competitive binding of Cr^{3+} and Fe^{3+} for apo-Tf because the signal obtained is specific to the identity of the metal ions present and not relying solely on the change in LMCT bands that are not metal ion specific.

Chapter 6 examined the competitive binding of Fe^{3+}, Cr^{3+}, and Ni^{2+} into transferrin under various physiological iron to transferrin concentration ratios using the PB/HC-OES method. This was the first known study to involve the direct investigation of competitive metal binding to transferrin under varying physiologically relevant iron concentrations. This chapter demonstrated the influence of low to high physiological iron concentrations on the Cr^{3+} and Ni^{2+} binding to Tf. It was determined that Cr^{3+} competes with Fe^{3+} for binding of Tf only when Cr^{3+} concentrations were elevated. Ni^{2+} was found to load into Tf best when Fe^{3+} was already bound in Tf.

The ability to monitor multiple elements simultaneously has opened the door for many potential applications. It would be desired to continue the current work, investigating the influence of other metal ions (i.e. Ti^{4+}, $Mn^{2+/3+}$, or Zn^{2+}) on Fe^{3+} loading into Tf under physiologically relevant concentrations. Future work in

this laboratory should utilize the PB/HC-OES system to investigate other metal binding proteins (i.e. human serum albumin or metallothionein). These proteins are known to be metal ion transporters that potentially can compete with Tf for the binding of metal ions. It would be of great importance to monitor these proteins for the binding of essential and toxic metal ions, which would provide an understanding of how these proteins maintain the metal homeostasis within the body. These types of metal binding studies will not be possible until proper chromatography methods are developed that will keep the proteins in their native state and not disrupt the metal ion complex within each protein. Initial studies (appendix A) suggest that ion exchange chromatography conditions may be the least disruptive to the metal-Tf complex. With the right type of chromatography in place it would be possible to move towards more complex matrices such as using simulated blood conditions for the metal-loading studies. The aforementioned studies have provided a reliable method to monitor competitive metal-binding studies that were not possible with a single instrument platform.

APPENDICES

APPENDIX A

CONSEQUENCES OF SOLVENT COMPOSITION USED FOR ANALYTICAL SAMPLE PREPARATION METHODS ON THE METAL RETENTION IN HUMAN TRANSFERRIN

INTRODUCTION

Metalloproteins make up approximately one-third of all known proteins[1] and are extensively studied to understand their roles in biological systems. Transferrin (Tf), human serum albumin (HSA), and metallothionein are metal binding transport proteins essential for trafficking metal ions in humans. Metal ions other than normal amounts of Fe^{3+} that are transported into cells by Tf can be potentially harmful, leading to diseases from long term exposure, or potentially interfere with normal dietary iron uptake. The most common approaches for determining metal content in metalloproteins involves some type of chromatography method coupled to an atomic or molecular species analyzer.[2] Many types of chromatographic separations (i.e., reversed-phase, ion exchange, and electrophoresis) involve solvents or conditions that can potentially alter a protein's native state, thereby changing its stability and metal-binding capabilities and potentially damaging the metal-protein complex. It is vital to keep the protein-metal complex intact and in its native state to fully understand its binding capabilities and role in biological systems. In addition, the solvent requirements for sample introduction in inductively coupled plasma-mass spectrometry or –optical emission spectroscopy (ICP-MS or –OES) as well as electrospray

ionization-mass spectrometry (ESI-MS) detection methods can disrupt the physiological conditions of the Tf complex potentially resulting in denaturing or loss of metal ion(s). In order to evaluate the metal-protein complex in its native state, careful consideration of solvent identity, pH, and salt content should be considered prior to analysis.

Reversed-phase chromatography conditions commonly involve use of organic solvents and ion pairing agents, both capable of denaturing or disturbing the integrity of the protein-metal complex. To keep biological samples in their proper physiological state, separations such as size exclusion chromatography can be used because this involves buffered solutions which are typically non-denaturing, but these separation methods are of limited utility when proteins are of similar molecular weight (e.g. Tf = ~ 80 kDa and HSA = ~ 66.5 kDa). Ion exchange chromatography is also an effective non-denaturing separation technique, but the large changes in ionic strength (0 – 1 M) required for elution can potentially have a negative effect on metal binding in metalloproteins (e.g. metal binding strengths or protein conformation). Gel chromatography/electrophoresis is typically used to determine structural aspects of a protein using either native gels or adding denaturants (e.g. guanidine HCl or urea), but there is always the risk of denaturing the protein using either technique.[3-5] The addition of guanidinium to a protein will disrupt ionic interactions and cleave disulfide bonds that hold the protein in its native state, whereas addition of urea affects the hydrophobicity of the protein complex in solution. In general, a better understanding of how the breadth of sample

manipulations effect metal-retention in proteins will help in the development of combined chromatography-spectroscopic methods to evaluate metal-binding proteins.

To demonstrate the potential effects of sample manipulation, transferrin will be used as the example metal-binding protein. Transferrin has a high binding constant for Fe^{3+} ($K = 4.7 \times 10^{20}$ M^{-1} and 2.4×10^{19} M^{-1}) and does not consist of a metal co-factor (e.g. hemoglobin, where iron is part of the structure) making it a good test protein for investigating metal retention.[6] Transferrin is the iron transport protein, responsible for delivery of Fe^{3+} to the cells, found at concentrations of ~ 35 μM in serum.[6] Transferrin contains two almost-identical lobes, referred to as the *N*- and *C*-lobes, each capable of binding one Fe^{3+} ion. Upon Fe^{3+} binding, a distorted octahedral geometry is achieved with four amino acids (aspartic acid, histidine, and two tyrosines) and a bidentate ligand (most commonly carbonate) acting as a synergistic anion (Fig. 1).[6] Iron binding causes a change in lobe conformation from an open to a closed state.[6] Both lobes must be in the closed conformation for optimal Tf binding to the Tf receptor protein on cell surfaces.[7] In humans, only 30 % of transferrin is in the holo- form (both lobes bound with Fe^{3+}) with the remaining 70 % in either the apo- or mono-Tf forms circulating throughout the body.[8] Therefore, other metal ions that are introduced into the body can potentially bind to empty Tf binding sites.[6] Metal-binding has been extensively studied since beyond normal dietary uptake, these metal ions can be introduced into the body in various ways including ingestion of dietary supplements (e.g. Cr^{3+}, Mn^{2+}, Cu^{2+}, and Zn^{2+}),[9-13]

pharmaceuticals (e.g. Zn^{2+}, Pt^{2+}, and Ru^{3+}),[14-16] or the decomposition of metal-containing implants (e.g. Co^{3+}, Cr^{3+}, Mn^{2+}, Ni^{2+}, and Ti^{4+}).[17, 18]

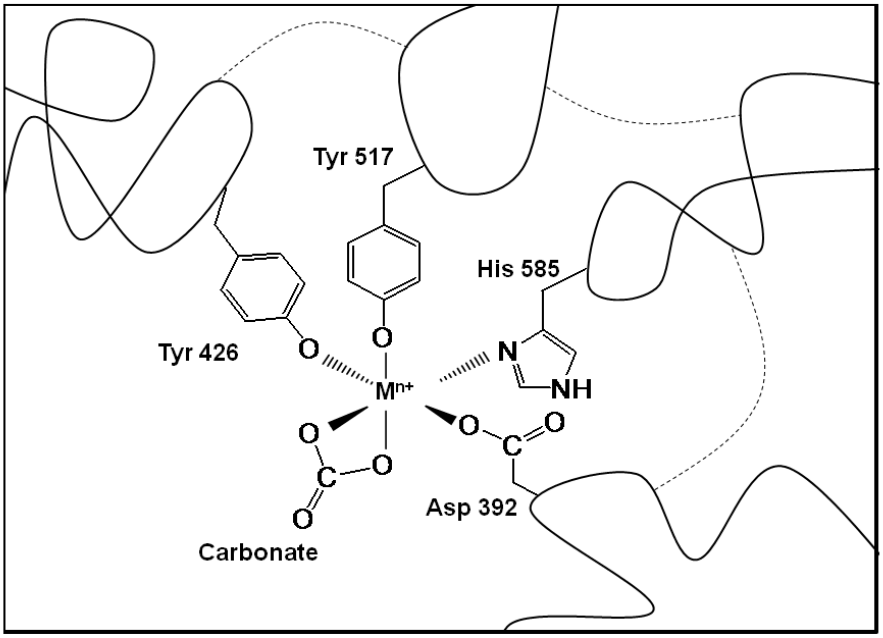

Figure A.1 Representation of the binding pocket in Tf.

Presented here is an investigation of the effects of sample manipulation and solvent conditions on Fe^{3+} retention percentages in Tf as monitored by UV-VIS absorbance spectroscopy. Using a simple UV-VIS absorbance method allows for monitoring of Fe^{3+} retention in Tf under various sample preparation conditions. The amount of Tf denaturing due to changes in ionic strength (guanidinium) and hydrophobicity (urea) were monitored by UV-VIS absorbance to determine the amount of Fe^{3+} retained in the Tf binding pocket. Circular dichroism (CD) spectroscopy was also used to monitor changes in optical activity at ~ 240 nm; reduction in signals in this region corresponds to the cleavage of

disulfide bonds that hold Tf in its native, folded state.[19] Using both spectroscopic techniques will provide a better understanding of the relationship between denaturing of the Tf complex and the retention of Fe^{3+} in the binding site. This study demonstrates how solvent composition affects metal-binding proteins and gives insight into the precautions that must be taken with metalloproteins to ensure that metal ions are not lost during chromatographic separations. Appendix A will be submitted for publication in *Metallomics.*

EXPERIMENTAL

Solvent Composition and Sample Preparation

High-purity water (18.2 MΩ-cm, Barnstead Nanopure, Dubuque, IA), methanol (EMD Chemicals, Cincinnati, OH), acetonitrile (EMD Chemicals, Cincinnati, OH), and Tris buffer (20 mM, TEKnova, Hollister, CA), were used as solvents. Trifluoroacetic acid (TFA, Sigma-Aldrich, Milwaukee, WI, USA) was added to simulate the addition of an ion paring agent that may be used during reversed-phase separations. Guanidinium (Sigma Aldrich, St. Louis, MO) and urea (Sigma Aldrich) were added to the Tf solutions to change the ionic interactions and hydrophobicity of Tf. Samples were prepared in 15 mL centrifuge tubes that had been washed with 1M HCl, thoroughly rinsed, and dried to remove residual metals. Stock solutions of human holo- and apo-transferrin (50 µM, Sigma-Aldrich) with sodium carbonate (20 mM, Sigma-Aldrich) were prepared separately in water, methanol, acetonitrile, and 20 mM Tris buffer.

pH Measurements

The pH values of the Tf solutions were measured with an Accumet Research (Fisher Scientific, Pittsburgh, PA) AR 10 pH meter with an Accumet (Fisher Scientific) double junction Ag/AgCl pH probe. Adjustments to pH were made by addition of hydrochloric acid (6.0 M, Sigma-Aldrich) or sodium hydroxide (2.0 M, Sigma-Aldrich).

UV-VIS Absorbance Spectroscopy

All absorbance measurements were performed with a Genesys 10-S UV-VIS spectrometer (Thermo Electron Corporation, Waltham, MA). The concentration of Tf was determined by measuring the absorbance at 280 nm, using an extinction coefficient of 87,200 M^{-1} cm^{-1}.[20] The concentration of Fe^{3+} loaded into Tf was determined by measuring the absorbance at 470 nm, using an extinction coefficient of 4,860 M^{-1} cm^{-1} (determined in 20 mM Tris buffer).[20] This same extinction coefficient was used under all solvent conditions, since solvents other than buffers may cause release of the Fe^{3+} from Tf which would give inaccurate extinction coefficients. Fe^{3+}-Tf absorbance spectra were background-corrected using an apo-transferrin solution (no loaded metal ion) as the blank. The changes in solvent were negligible for the absorbance spectra representing metal retention, thus apo-Tf in Tris buffer was used as the blank solvent for all samples. All loading percentages were calculated based on the assumption that 2 molar equivalents of metal ions can be loaded into transferrin, meaning a 2 Fe:1 Tf molar ratio equates to 100% loading.

Circular Dichroism Spectroscopy

All optical activity measurements were performed with a J-810-150S spectropolarimeter (Jasco, Easton, MD). A cuvette with a 1 cm path length, which holds 2 mL of sample, was used for the Fe^{3+}-Tf measurements. Samples were background-corrected using the solvent as the blank. All optical measurements are the average of 5 scans.

RESULTS AND DISCUSSION

Typically, chemical analysis requires that the sample be in a particular solvent that is adequate for the type of separation/detection instrumentation being employed. To study metal-binding in metalloproteins, it is vital to keep the metal-protein complex intact and in its native physiological confirmation. Changing solution conditions may cause the metal to be released or displaced by other ions. Subsequent sections of this work will focus on the effects of various solvent (acetonitrile, methanol, water, urea, guanidine, TFA) and pH (2 – 12) conditions on Fe^{3+} retention in Tf.

Reversed-Phase Conditions

Reversed-Phased (RP) chromatography is often used to separate proteins and is typically performed using predominately organic solvents (e.g. methanol or acetonitrile) and water as the mobile phases for the separation. Figure 2 represents the UV-VIS absorbance spectra of 50 μM holo-Tf (initially 100% Fe^{3+} loaded Tf, 20 mM sodium carbonate) that were prepared in 20 mM

Tris buffer, deionized-water (DI-H_2O), acetonitrile, methanol, and 0.1 % trifluoroacetic acid (TFA), typical of solvents used in RP chromatography. Holo-Tf is not soluble in methanol or acetonitrile (ACN) at pH 7.4, so 50:50 mixtures were made with water, this is also a common mixture at which protein are eluted off the column in many RP chromatographic conditions.[21] Absorbance spectra were recorded immediately after sample preparation (t=0, Fig. 2). The absorbance band at 470 nm is indicative of a ligand-to-metal charge transfer (LMCT) for Fe^{3+} bound in Tf. No change was observed in the percentage of Fe^{3+} retained in Tf after 1 h (data not shown). As can be seen in Fig. 2, the solvents that use the ion pairing agent TFA show no LMCT absorbance band at 470 nm, indicating that Fe^{3+} has been released from Tf and suggesting that the protein has been denatured. The LMCT band at ~ 305 nm is the result of non-specific metal-binding to the Tf pocket, and can represent the binding of any metal ion, so no quantitative data was obtained from this region to ensure that only Fe^{3+} bound to Tf is being quantified. Table 1 presents the determined loading percentages for each of the solvent conditions tested. Holo-Tf in Tris buffer is used as the control for these experiments, having an iron-loading percentage of 96 ± 1 %. For acetonitrile, water, and methanol the loading percentages ranged from 64 to 77 % Fe^{3+} retained in Tf. As seen in Fig. 2, all solvents with TFA added (pH = 1.8) resulted in complete loss of Fe^{3+}. To determine if iron loss was a result of TFA addition or simply the lower pH, two methanol:water solutions (50:50) containing 0.1 % TFA were adjusted to pH 7.4 and pH 1.8, respectively. The data in Table 1 indicating that it is indeed the pH of the solution and not the ion

pairing agent that causes iron loss, although the introduction of TFA at pH 7.4 in methanol/water did decrease the percentage of iron retained by ~ 9 % as compared to methanol/water sample without TFA (77 %). Sample preparation of holo-Tf in aqueous/organic (methanol or acetonitrile) or pure DI-H_2O at physiological pH conditions (7.4) resulted in a release of 20 – 30 % of the Fe^{3+} from the Tf binding pocket. Griebenow and Klibanov have shown that pure organic solvents showed less denaturing of secondary structures of proteins as compared to aqueous-organic mixtures at acidic pH (1.9).[22] As indicated in Table 1, at physiological pH (7.4), the methanol:water mixture causes the least amount of iron release from holo-Tf (23 % Fe^{3+} lost), followed by water (29 % Fe^{3+} lost), with the water:acetonitrile mixture causing the most iron release (36 %

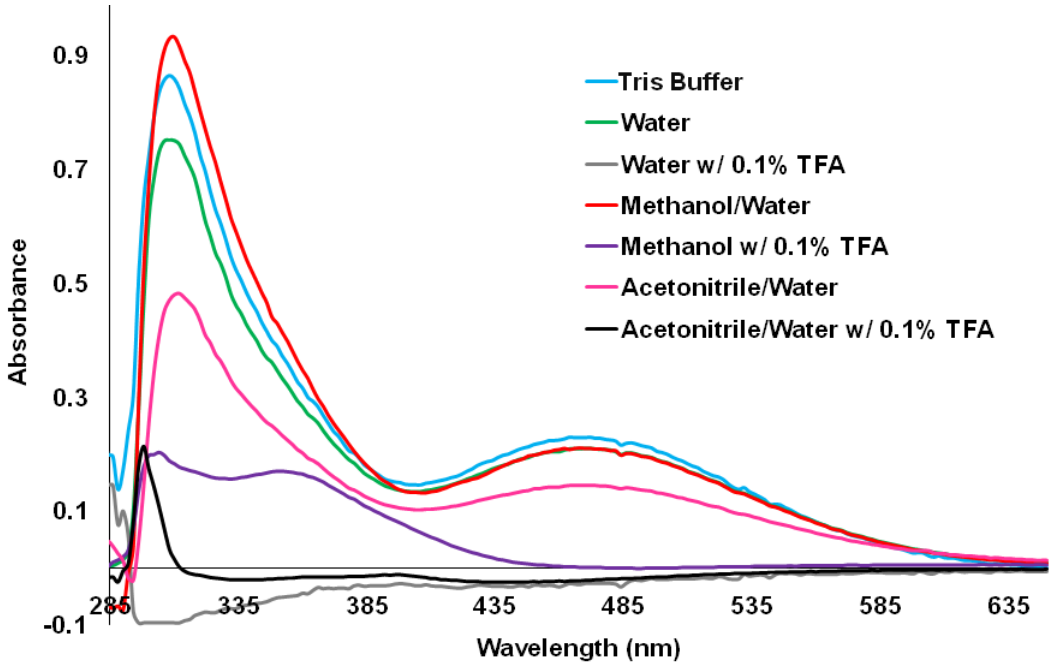

Figure A.2 UV-VIS absorbance spectrum displaying the changes in LMCT bands at 470 nm due to the affect of solvent on Fe^{3+} retention in holo-Tf.

Table A.1 Effect of solvent composition on Fe^{3+} retention in Tf (% Fe^{3+} retained in Tf is a result of triplicate absorbance measurements with calculated standard deviations)

Solvent	pH	% Fe^{3+} Retained
Tris Buffer	7.4	96 ± 1
Water	7.4	71 ± 2
Water + 0.1 % TFA	1.8	0
Acetonitrile:Water	7.4	64 ± 2
Acetonitrile:Water + 0.1 % TFA	1.8	0
Methanol + 0.1 % TFA	1.8	0
Methanol:Water	7.4	77 ± 2
Methanol:Water + 0.1 % TFA	1.8	0
Methanol:Water + 0.1 % TFA	7.4	67 ± 1

Fe^{3+} lost). Therefore it has been demonstrated that RP conditions involving organic solvents and/or DI-H_2O are destructive to metal retention and should not be considered an option for the analysis of metal-binding proteins when metal identity or quantification is the primary interest.

After Tf is transported into the cell via endocytosis, the pH is lowered from 7.4 to ~ 5.5 in the endosome, causing Fe^{3+} to be released from Tf.[6] In vitro, iron release differs for the *C*- (pH = 4.8) and *N*-lobes (pH = 5.7) of Tf.[23, 24] The iron release from the two lobes was achieved in those studies in the presence of EDTA to accelerate iron removal. Figure 3a is a plot of the iron loading percentages for holo-Tf in 20 mM Tris buffer over a pH range of 2.0 – 12.0, in the absence of a chelating ligand to help remove iron from Tf, as the goal in this study is to determine iron loss due to solely pH changes. The results show that at pH 2.0 and 12.0, Fe^{3+} is completely released from Tf due to the extreme pH of

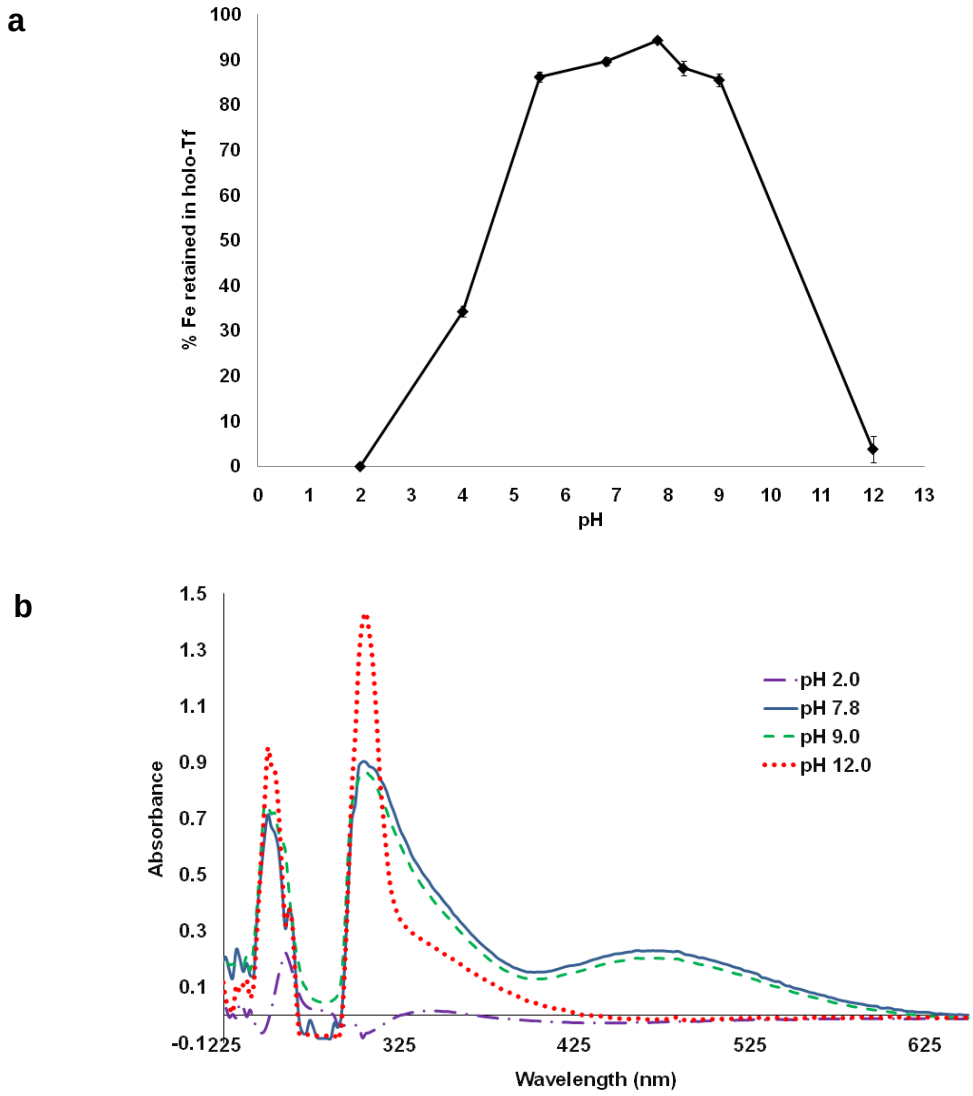

Figure A.3 Affect of pH on Fe^{3+} retention within holo-Tf **a)** Loading percentages determined by UV-VIS absorbance measurements **b)** UV-VIS absorbance spectrum.

the solution. Under pH conditions that range from 5.5 to 9.0 at least 85 % of Fe^{3+} is retained in Tf. At pH 4.0, 34 % of Fe^{3+} remains loaded into Tf, this is was unexpected as most if not all Fe^{3+} should have be released, and is most likely due to the lack of a chelating ligand in solution that would help remove loosely bound iron from Tf. Figure 3b presents the UV-VIS spectra of holo-Tf for pH 2.0,

7.8, 9.0, and 12.0. For pH 2.0 and 12.0 it is clear there is no Fe^{3+} binding to Tf due to the absence of the LMCT absorbance at 470 nm. Interestingly, there is a large peak at ~ 305 nm for pH 12.0 that is most likely due to deprotonation of the two tyrosine (pKa ~ 10.0) residues in the binding pockets causes a distinct change in absorbance.

Role of Ionic Strength

Size exclusion should be the most effective chromatographic process for retention of Fe^{3+} in the binding pocket of Tf, since the eluting solvent is typically a buffered solution (i.e. Tris buffer) and does not require changes to the solution environment (i.e. solvent or salt content). The only drawback with this type of chromatography is that it is based on size, such that when analytes of similar size are in the same solution complete resolution of analytes is not always feasible. So another approach to physiological-condition chromatography involves ion exchange chromatography (IEC), however the high salt content required for this separation method may change the metal loading in metalloproteins. Hamilton and co-workers have reported that changes to the concentration of salts interacting with holo-Tf can affect the iron loading, by disrupting the metal-binding capabilities of the protein complex.[5] Table 2 displays the percentages of Fe^{3+} retained in holo-Tf under various IEC conditions at constant pH, 7.4. Addition of increasing concentrations of NaCl to Tris buffer, typical conditions for IEC, had minimal effects on Fe^{3+} retention in holo-Tf. Addition of NH_4^+ as the cation caused more Fe^{3+} to be released as compared to

Na^+ and K^+. Richardson and Baker reported that the presence of ammonium caused a decrease in iron uptake into Tf.[25] While the uptake of iron is not being studied here it is reasonable to assume that ammonium may be displacing some Fe^{3+} from the binding pocket. The most drastic release of Fe^{3+} under IEC conditions was seen when CH_3COO^- was the anion. Non-synergistic anions can affect the thermodynamic stability of the Fe^{3+}-Tf complex, while synergistic anions can interfere with carbonate for metal binding, thereby disrupting the Fe^{3+} loading.[6] The results in Table 2 indicate that IEC conditions are significantly less destructive to the Fe^{3+}-Tf binding compared to typical RP conditions seen in Table 1. Although, small losses of Fe^{3+} from Tf was observed under typical IEC conditions, it is minimal and this method may be the best option for physiological-condition chromatographic separations involving metal-binding proteins.

Table 2. Effect of Ion exchange conditions on Fe^{3+} retention in holo-Tf, pH 7.4

Holo-Tf in Tris Buffer	**% Fe^{3+} Retained**
Control (Tris buffer only)	94 ± 1
+ 0.1 M NaCl	92.4 ± 0.7
+ 0.25 M NaCl	91.3 ± 0.9
+ 0.5 M NaCl	92 ± 1
+ 1.0 M NaCl	91.6 ± 0.6
+ 1.0 M KCl	90.2 ± 0.8
+ 1.0 M NH_4Cl	87.9 ± 0.5
+ 1.0 M $NaOOCCH_3$	85.3 ± 0.4
+ 1.0 M Na_2SO_4	91.6 ± 0.9
+ 1.0 M Na_2HPO_4	92 ± 1

The addition of salts typical for IEC conditions had minimal effect on iron retention. Compounds such as guanidinium have a greater effect on the ionic nature of proteins; therefore the addition of guanidinium was used to disrupt the native state of Tf. The addition of guanidinium will cleave the disulfide bonds that hold protein structures in their native folded state.[26] Figure 4 presents the UV-VIS spectra of holo-Tf with increasing concentrations of guanidinium at physiological pH 7.4. Addition of guanidinium changes the ionic interactions (disulfide bonds) of holo-Tf that hold the protein in its native folded state, thus resulting in a diminished LMCT band at 470 nm corresponding to iron release as the guanidinium concentration is increased. Additions of ≥ 6 M guanidinium cause complete iron loss from Tf, almost instantaneously. Figure 5 is the measured iron retention over time as a result of guanidinium addition, it can be seen that the initial (1 min) addition of 1- 5 M guanidinium did not cause

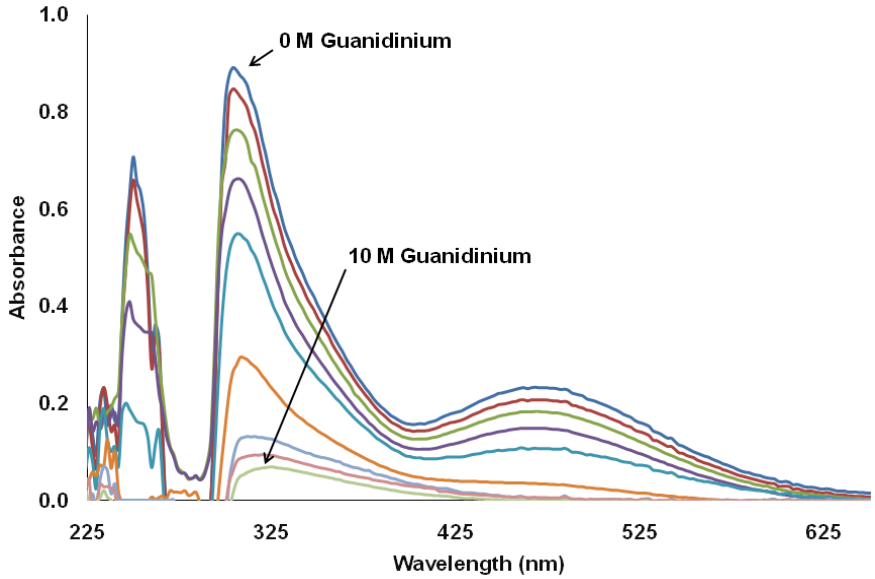

Figure A.4 UV-VIS absorbance spectrum showing the affect of 0 – 10 M guanidine additions on 50 µM holo-Tf.

complete loss of Fe^{3+} from the Tf complex. However, changes in ionic interactions are time sensitive and continue to cause Fe^{3+} release from Tf. Addition of 1 M guanidinium caused no change in Fe^{3+} loading (86 %) after 48 h, very similar to results observed after addition of 1 M salts (92 – 85 % retained; Table 2). However, increasing the guanidinium concentration (≥ 2 M) resulted in larger decreases of Fe^{3+} retention. The addition of 3 M guanidinium to holo-Tf resulted in 60 % retention (t=0) of the Fe^{3+}, but after 48 h only 9 % of the Fe^{3+} was retained in Tf. For 4 and 5 M guanidinium additions, it took 12 h and 30 min, respectively for complete loss of Fe^{3+} from the Tf binding pocket. The addition of guanidinium, which causes the cleavage of disulfide bonds that hold Tf in its native conformation to break, has a direct effect on Fe^{3+} retention in holo-Tf.

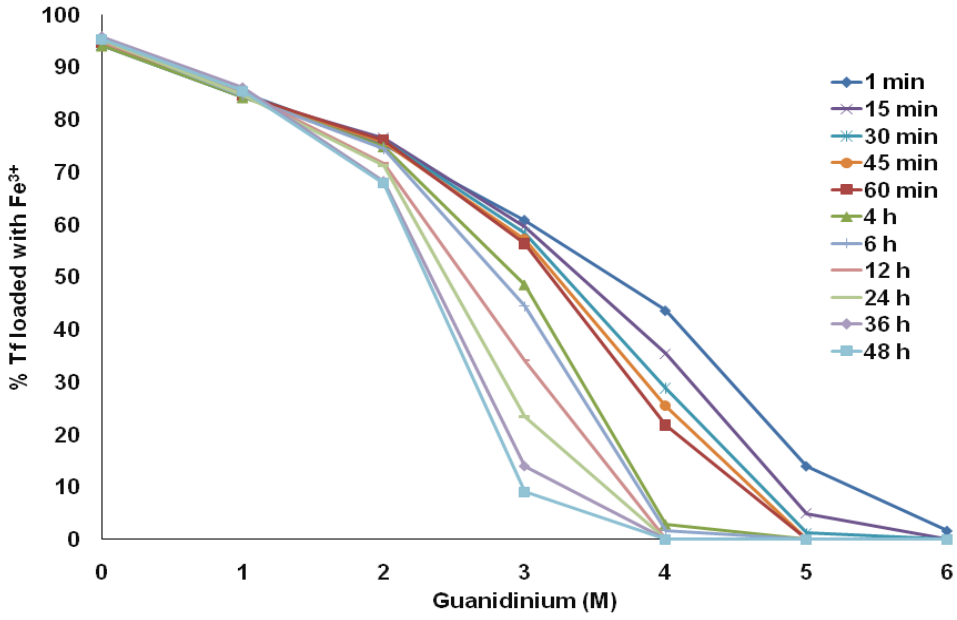

Figure A.5 Percentage of Fe^{3+} retained in holo-Tf after addition of 0 – 6 M Guanidine over 48 h.

Gel Chromatography/Electrophoresis

Urea (6 M) gels (with EDTA) have been used for ~ 30 years to distinguish iron loading in the *N*- or *C*-lobe of Tf.[3, 5] The urea gels (6 M) work by denaturing Tf at different rates, corresponding to the apo-, mono-, and holo-forms.[5] Figure 6 presents the UV-VIS absorbance spectra of holo-Tf under increasing concentrations of urea. Addition of urea changes the hydrophobic interactions of the Tf complex resulting in a decrease in the band at 470 nm, corresponding to a decrease in Fe^{3+} Tf binding. Additions of urea decrease the loading percentages of Fe^{3+} bound in Tf from ~ 91 % (holo-Tf, no urea) to ~ 50 % (holo-Tf and 14 M urea). Addition of 6 M urea caused a ~ 21 % decrease in Fe^{3+} retained from the holo-Tf complex from its original loading of 91% Fe^{3+} loaded Tf. Table 3 presents the influence of urea on the loading percentages of Fe^{3+} in Tf with respect to time. As can be seen, there is statistically no change in the loading percentage of Fe^{3+} in Tf at t = 0 or 3 h time period.

Changing the ionic interactions and hydrophobicity has differing effects on holo-Tf. The addition of guanidinium causes a more dramatic release of Fe^{3+} from Tf at similar concentrations compared to urea. The release of Fe^{3+} to changing the ionic interactions of Tf is not an instantaneous process, as evident in the retention data provided in Fig. 5. On the other hand, changing the hydrophobicity of the Tf complex has an immediate effect, since no further loss of Fe^{3+} from the Tf complex occurs over time (Table 3). These results imply that any chromatographic method that changes either the ionic strength or

hydrophobicity of Tf will affect the observed iron loading. The metal retention in Tf resulting from gel chromatography/electrophoresis conditions (6 M urea

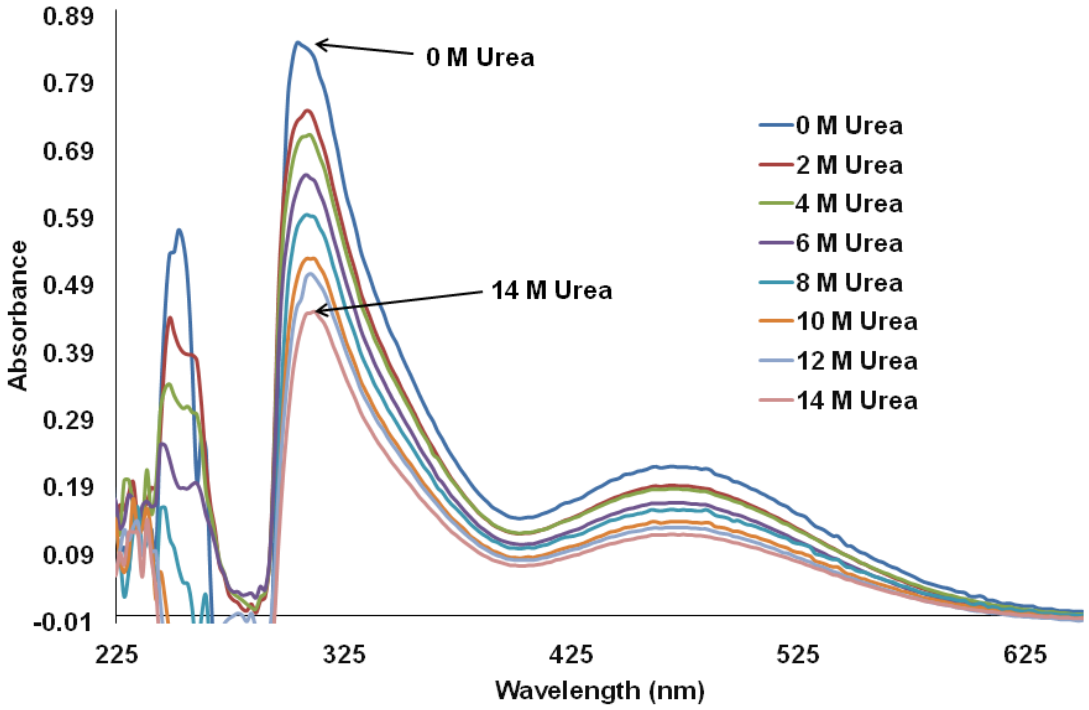

Figure A.6 UV-VIS absorbance spectrum showing the affect of 0 – 14 M urea additions on 50 µM holo-Tf.

Table A.3 Urea denaturation and metal loss

Urea (M)	% Fe^{3+} Retained at t = 0	% Fe^{3+} Retained at t = 3 h
0	91 ± 1	91 ± 1
2	80 ± 2	79 ± 3
4	78.8 ± 0.9	77 ± 1
6	69.1 ± 0.5	70 ± 1
8	65 ± 2	64.9 ± 0.7
10	57 ± 2	57 ± 1

~ 69 %) is comparable to that of RP chromatographic conditions (50:50 methanol:water ~ 77 %), while both chromatographic conditions were found to have lower iron retention in Tf than typical IEC conditions (1 M NaCl ~ 92 %). It must be made clear that by no means are we suggesting that these chromatographic methods should not be used, but instead want to draw attention to potential problems that result in inaccurate data reporting of metal-binding percentages.

Relationship Between Metal Retention and Tf Denaturation

During any type of chromatographic separation the protein is always susceptible to being denatured on column. It is important to understand the relationship between metal retention and Tf denaturation. Circular Dichroism (CD) spectroscopy was used to measure the amount of denaturing that occurs from additions of urea or guanidinium to the holo-Tf complex. The CD spectral region at ~ 240 nm corresponds to optical activity associated with the dihedral angle of the disulfide bonds in Tf.[19] Changes in optical activity at ~ 240 nm correspond to cleavage of the disulfide bonds in the protein, which result in Tf denaturation. Figure 7 depicts the CD spectra of apo-Tf, holo-Tf, holo-Tf + 6 M urea, and holo-Tf + 6 M guanidinium measured within 2 minutes of preparation. Only the 6 M guanidinium immediately cleaves the disulfide bonds in Tf, with only a slight change in optical activity seen for addition of 6 M urea to holo-Tf. The spectra reveal that apo-Tf and holo-Tf have the same optical activity, indicating that changes in lobal confirmation have no influence on optical activity in this

region of the spectra. Only the addition of guanidinium caused increased denaturation to Tf over time and all other samples (apo-Tf, holo-Tf, and addition of urea to holo-Tf) showed no further denaturation after initial sample preparation. Figure 8 presents the CD spectra of holo-Tf with increasing concentrations of guanidinium (t = 0). Increasing concentrations of guanidinium increase the denaturing of Tf. Although not shown here, addition of urea (increasing concentrations) to holo-Tf shows minimal to no change in optical activity, suggesting that urea addition does not cause disulfide bond cleavage. This suggests that any denaturing of Tf from urea is occurring to the surface of the protein and not the disulfide bonds holding Tf in its folded native state.

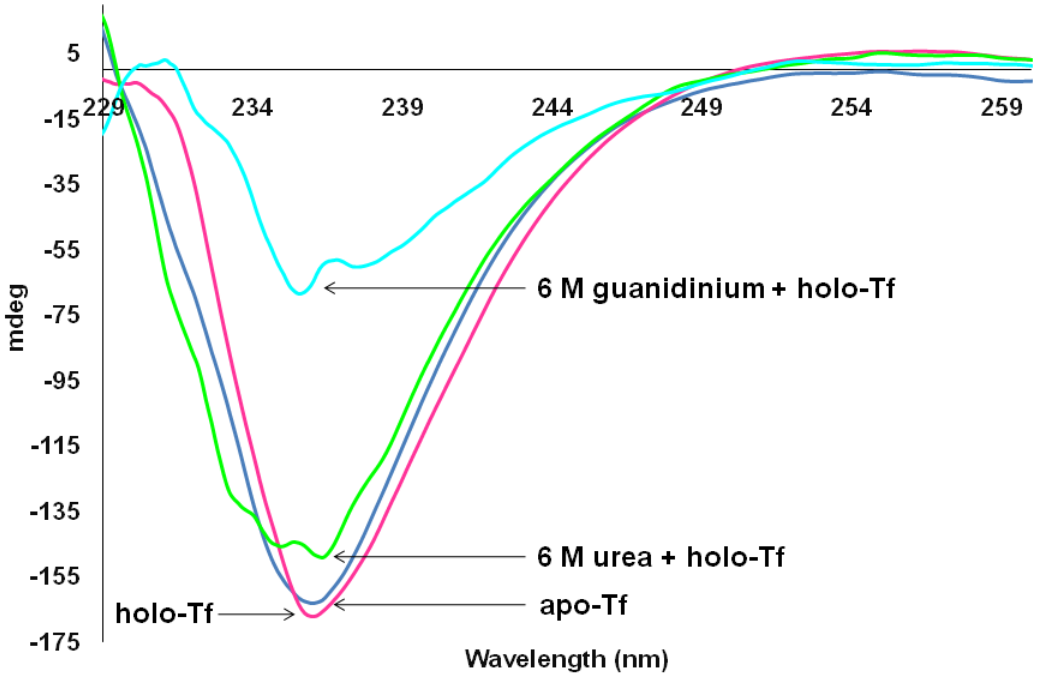

Figure A.7 CD spectra displaying the change in optical activity due to breakage of disulfide bonds. Apo-Tf and holo-Tf are used as the control.

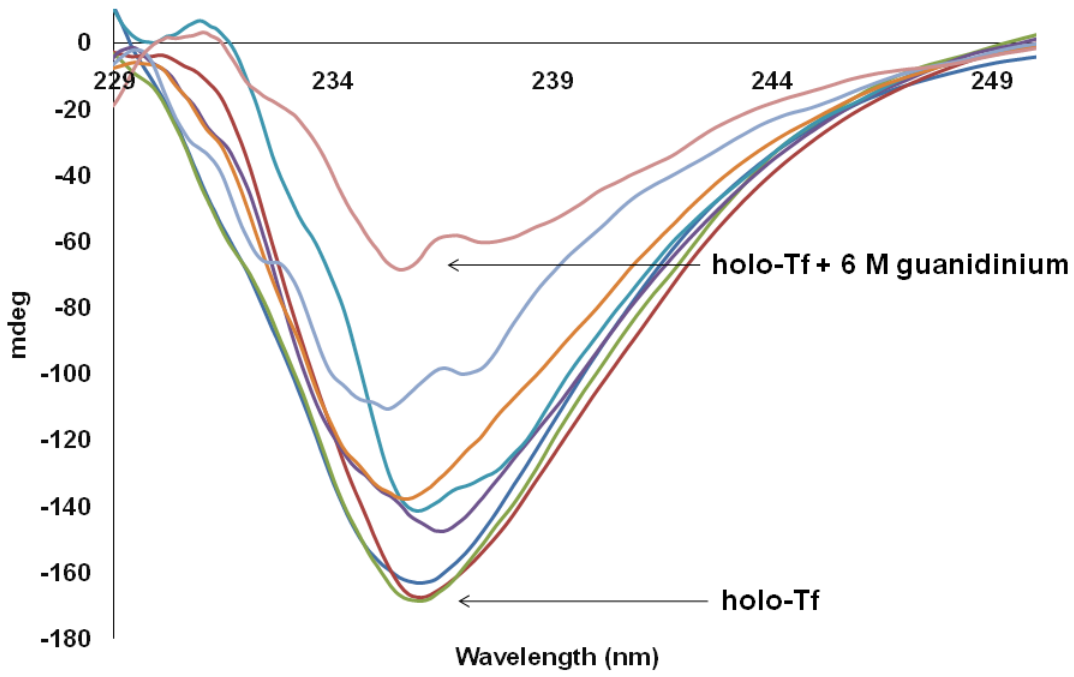

Figure A.8 CD spectra displaying the change in optical activity due to additions of 0 – 6 M guanidine. Apo-Tf and holo-Tf are used as the control.

Figure 9 depicts the percentages of Fe^{3+} lost from Tf along with the amounts of Tf denatured as a function of guanidinium added (t = 0). The changes in the percentage of iron lost and the amount of S-S bond cleavage occurring to Tf parallel each other, suggesting there is a distinct relationship between the unfolding of Tf and the loss of Fe^{3+}. The percentage of Fe^{3+} lost from Tf and the percentage of Tf that was denatured due to 4 M guanidinium as a function of time (data not shown here) shows a direct correlation between the unfolding of Tf and the loss of Fe^{3+} from Tf. These studies show that changing the ionic interactions by addition of guanidinium denatures the Tf complex and is the likely cause for the drastic difference seen in loading percentages of Fe^{3+} in

Tf due to guanidinium. On the other hand, the non-denaturing effect of urea causes only a partial unloading of Fe^{3+} from Tf.

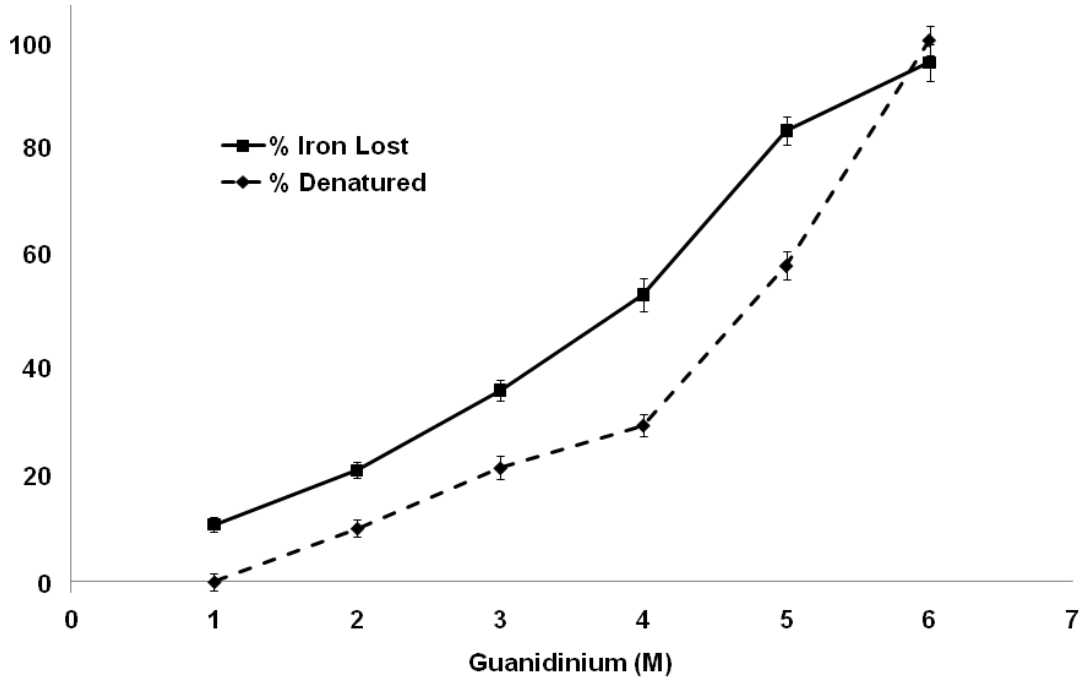

Figure A.9 Percentage of iron lost and denaturation due to 1 – 6 M additions of guanidine to 50 µM holo-Tf.

The aforementioned studies have demonstrated that changing polarity, pH, ionic strength, and the ionic and hydrophobic nature of the protein have a direct effect on metal retention in Tf. These results should be very similar for other metal-binding transport proteins, while metalloproteins that contain a metal co-factor (e.g. hemoglobin) will be more stable under these types of conditions. These results are the first to explore the potential pitfalls that may arise in sample preparation for analytical measurements to determine metal-binding percentages involving Tf.

CONCLUSION

The sample manipulation should be considered carefully when analyzing metal binding proteins such as Tf. Disturbing the physiological environment of Tf disrupts the metal binding abilities and ultimately changes the metal loading properties. If metal binding studies are to be performed on Tf (or any metal binding protein) the solvent system needs to be non-denaturing and the pH needs to be kept at the optimal physiological range. Organic and aqueous solutions at pH 7.4 are not completely detrimental to the Tf-iron binding, but they do not provide ideal environments for keeping Fe^{3+} retained in Tf. Salts that are typically used in IEC conditions had the most promise in keeping the metal-binding pocket of Tf intact. Furthermore, changes in ionic interactions from guanidinium additions are far more destructive to Tf resulting in denaturing and loss of Fe^{3+} binding pocket as compared to that of the hydrophobic changes that result from urea additions. Changing the hydrophobic interactions of Tf, results in partial Fe^{3+} loss and little to no denaturation occurring. Further investigation needs to be undertaken to understand how metal binding proteins are affected by the stationary phase during chromatographic separations. When introducing metal binding proteins into an ICP-MS or ESI-MS, extreme caution should be taken in order to keep the metal binding complex in its native state. These results have brought awareness to potential problems that can arise in sample preparation of metal-binding proteins that may lead to inaccurate data reporting.

REFERENCES

1. J. A. Tainer, V. A. Roberts and E. D. Getzoff, *Cur. Opin. Biotech.*, 1991, **2**, 582-591.

2. S. Mounicou, J. Szpunar and R. Lobinski, *Chem. Soc. Rev.*, 2009, **38**, 1119-1138.

3. R. W. Evans and J. Willliams, *Biochem. J.*, 1980, **189**, 541-546

4. W. W. Fish, J. A. Reynolds and C. Tanford, *J. Biol. Chem.*, 1970, **245**, 5166-5168.

5. D. H. Hamilton, I. Turcot, A. Stintzi and K. N. Raymond, *J. Biol. Inorg. Chem.*, 2004, **9**, 936-944.

6. H. Sun, H. Li and P. J. Sadler, *Chem. Rev.*, 1999, **99**, 2817-2842.

7. A. C. G. Chua and R. M. Graham, *Crit. Rev. Clin. Lab. Sci.*, 2007, **44**, 413-459.

8. J. Williams and K. Moreton, *Biochem. J.*, 1980, **185**, 483-488.

9. D. H. Baker, *J. Nutr.*, 1999, **129**, 2278-2279.

10. E. J. Baran, *Mini-Rev. Med. Chem.*, 2004, **4**, 1-9.

11. J. J. Fickel, J. H. Freeland-Graves and M. J. Roby, *Am. J. Clin. Nutr.*, 1986, **43**, 47-58.

12. H. C. Lukaski, W. A. Siders and J. G. Penland, *Nutr.*, 2007, **23**, 187-195.

13. A. Nischwitz, A. Berthele and B. Michalke, *Anal. Chim. Acta* 2008, **627**, 258-269.

14. W. H. Ang and P. J. Dyson, *Eur. J. Inorg. Chem.*, 2006, **2006**, 4003-4018.

15. G. J. Brewer, *Exp. Opin. Pharmacother.*, 2001, **2**, 1473-1477.

16. D. Esteban-Fernandez, M. Montes-Bayon, E. B. Gonzalez, M. M. Gomez Gomez, M. A. Palacios and A. Sanz-Medal, *J. Anal. At. Spectrom.*, 2008, 378-384.

17. N. J. Hallab, A. Skipor and J. J. Jacobs, *J. Biomed. Mater. Res.*, 2003, **65A**, 311-318.

18. Y. Okazaki and E. Gotoh, *Corrosion Sci.*, 2008, **50**, 3429-3438.

19. S. M. Kelly and N. C. Price, *Biochim. Biophys. Acta*, 1997, **1338**, 161-185.

20. E. E. Battin, A. Lawhon, D. H. Hamilton and J. L. Brumaghim, *J. Chem. Educ.*, 2009, **86**, 969-972.

21. D. M. Nelson and R. K. Marcus, *Protein and Peptide Letters*, 2006, **13**, 95-99.

22. K. Griebenow and A. M. Klibanov, *J. Am. Chem. Soc.*, 1996, **118**, 11695-11700.

23. D. A. Baldwin, D. M. R. De Sousa and R. M. A. Von Wandruszka, *Biochim. Biophys. Acta*, 1982, **719**, 140-146.

24. J. V. Princiotto and E. J. Zapolski, *Nature*, 1975, **255**, 87-88.

25. D. Richardson and E. Baker, *J. Biol. Chem.*, 1992, **267**, 13972-13979.

26. A. Bezkorovainy and D. Grohlich, *Biochem. Biophys. Acta*, 1967, **147**, 497-510.